5-2014

An assessment of the frequency and cause of concentrated flow on agricultural fields in the Virginia Coastal Plain portion of the Chesapeake Bay watershed

Monica H. Stone
College of William and Mary

An assessment of the frequency and cause of concentrated flow on agricultural fields in the Virginia Coastal Plain portion of the Chesapeake Bay watershed

A thesis submitted in partial fulfillment of the requirements
for the degree of Bachelor of Science in Environmental Geology from
The College of William and Mary in Virginia

by

Monica Stone

Accepted for _____
(Honors, High Honors)

_____
Dr. Gregory Hancock, Director

_____
Dr. Stuart Hamilton

_____
Dr. James Kaste

Williamsburg, Virginia
May 28, 2014

Table of Contents

Abstract 8

Introduction 9

Previous Research 17

Study Area 22

Methods 24

- Field Selection 24
- Field Digital Terrain Model (DTM) Creation 25
- Determination of Field-level Watersheds 27
- Model Compilation 31
- Validation of Model on Study Fields 31
- Field Index Calculations 33
- Principle Component Analysis 36

Results 37

- Extent of Flow Concentration 37
- Wetness Index 38
- Topographic Index 41
- Water Retention Index 41
- Sediment Transport Index 42
- Principle Component Analysis 42

Discussion 48

Conclusions 68

References 69

Appendix A: Using the Agricultural Runoff Flow Concentration ArcGIS Toolbox Models 72

Appendix B: Wetness Index Model 89

Appendix C: Topographic Index Model 91

Appendix D: Water Retention Index Model 95

Appendix E: Sediment Transport Index Model 99

Appendix F: Principle Component Analysis Methodology 101

Appendix G: Tests of Normality for Index Variables 103

List of Figures

Figure 1. Schematic of a forested riparian buffer 11

Figure 2. Nitrogen loads delivered to Chesapeake Bay from 1990-2013 14

Figure 3. Phosphorous loads delivered to Chesapeake Bay from 1990-2013 15

Figure 4. Sediment loads delivered to Chesapeake Bay from 1990-2013 16

Figure 5. Relationship between buffer-area ratio and sediment trapping efficiency . . . 20

Figure 6. Diagram showing the relationship between gross and effective riparian buffer area 20

Figure 7. Study Area 23

Figure 8. Examples of a correct field margin digitization and 2 incorrect field margin digitizations 29

Figure 9. Watersheds for the top 10 points of highest flow accumulation off the field for 4 example fields 30

Figure 10. Schematic of the model used to determine elevation, flow accumulation, flow direction, slope, and the top 10 field-level watersheds for each of the 74 fields 32

Figure 11. Extent of Flow Concentration Along Field Margins 39

Figure 12. Comparison of predicted areas of concentrated flow based on modeling and actual evidence of concentrated flow for five of the study fields 40

Figure 13. Wetness Index 43

Figure 14. Topographic Index 44

Figure 15. Water Retention Index 45

Figure 16. Sediment Retention Index 46

Figure 17. Mean Specific Catchment Area Vs. Flow Concentration Linear Regression 49

Figure 18. Mean Runoff Source Area Vs. Flow Concentration Linear Regression 50

Figure 19. Mean Slope Vs. Flow Concentration Linear Regression 51

Figure 20. Mean K_{sat} Vs. Flow Concentration Linear Regression 52

Figure 21. Mean D Vs. Flow Concentration Linear Regression 53

Figure 22. Mean R Vs. Flow Concentration Linear Regression 54

Figure 23. Principle Component Analysis Scree Plot 56

Figure 24. Component 1 Vs. Flow Concentration Linear Regression 57

Figure 25. Component 2 Vs. Flow Concentration Linear Regression 58

Figure 26. Variable-width Buffer Design 63

Figure 27. Areas of concentrated flow on an example field that might be required to have a buffer 65

Figure 28. Example modification of flow patterns on a field 66

A1. Example field shapefile and tiled file 73

A2. Example use of the Identify tool to download DEMs 74

A3. Downloaded DEMs in ArcMap 75

A4. Creating file geodatabases in ArcMap 76

A5. Part 1 of the Agricultural Runoff Flow Concentration Model input-output specification window 76

A6. Schematic of Part 1 of the Agricultural Runoff Flow Concentration Model 77

A7. Section of Part 1 of the Agricultural Runoff Flow Concentration Model showing the mosaic, reprojection, and conversion of elevation data to meters steps 78

A8. Section of Part 1 of the Agricultural Runoff Flow Concentration Model showing the raster to point, and adding XY data steps 78

A9. Checking the projection in ArcMap 79

A10. Creating the field margin layer 80

A11. Importing the coordinate system 80

A12. Setting the symbology for the flow accumulation layer 81

A13. Field digitization example showing the starting point 82

A14. Example of correct field digitization 83

A15. Example showing the deletion of one vertex at the starting point of digitization . . 84

A16. Part 2 of the Agricultural Runoff Flow Concentration Model input-output specification window 85

A17. Schematic of Part 2 of the Agricultural Runoff Flow Concentration Model 86

A18. Section of Part 2 of the Agricultural Runoff Flow Concentration Model showing the polyline to point and sampling steps 87

A19. Clipped field-level watersheds for an example field in ArcMap 88

B1. Wetness Index Model 90

C1. Topographic Index Model 94

D1. Water Retention Index Model 98

E1. Sediment Transport Index Model 100

G1. Distribution of Mean Specific Catchment Area 103

G2. Distribution of Transformed Mean Specific Catchment Area 103

G3. Distribution of Mean Runoff Source Area 104

G4. Distribution of Transformed Mean Runoff Source Area 104

G5. Distribution of Mean Slope 105

G6. Distribution of Mean Ksat 105

G7. Distribution of Mean D 106

G8. Distribution of Mean R 106

List of Tables

Table 1. Principle Component Analysis Total Variance 55

Table 2. Principle Component Analysis Component Matrix 56

Abstract

Agricultural lands are the largest non-point source of nitrogen, phosphorous, and sediment that is delivered to Chesapeake Bay. There has been an increase in the amount of these nutrients and sediment being delivered to the Bay over the last century, which has caused extensive eutrophication and subsequent anoxic zones in the Bay. The Chesapeake Bay Act attempted to mitigate this problem by mandating 100-foot riparian buffer zones between agricultural fields and perennial streams in the Coastal Plain region of Virginia. Previous studies have shown that riparian buffers increase infiltration of runoff into the groundwater system, where nutrients and sediment can be removed from the water before it discharges into perennial streams. However, riparian buffers require flow to be widely disseminated throughout the buffer area in order for them to be effective. No declining trends have been noted in the amounts of nutrients and sediment being delivered to Chesapeake Bay since 1990, when buffers were required to be maintained in the Coastal Plain region of Virginia. I hypothesized that flow concentration, which can promote channel incision and allow agricultural runoff to bypass riparian buffers, is widespread in the Coastal Plain region of Virginia and may be one reason why reductions of nutrients and sediment in Bay waters have not been as great as expected. Geographic Information Systems (GIS) was used to determine flow accumulation patterns across 74 agricultural fields in the Coastal Plain region of Virginia. The percentage of each field drained by the 5 field margin points of greatest flow accumulation area was used as a proxy for measuring flow concentration. The cell size for points along each field margin was 3 m by 3 m. Further, 4 field indexes that related topographic and soil parameters on a field (wetness index, topographic index, water retention index, sediment transport index) were calculated for each field. These indexes were analyzed to determine if any were correlated with and could be used to easily predict places of flow concentration over a large geographic area, such as the Coastal Plain region of Virginia. Flow concentration occurred on all 74 study fields. On average, 70% of a field was drained through just 5 points along its field margin. The strongest field index relationship existed between the Wetness Index and flow concentration (R^2 = 0.323). The field indexes were not good predictors of areas of high flow concentration because for any given value of an index, there was a large range of possible flow concentrations. Of the 6 topographic/soil property characteristics analyzed by these 4 field indexes (specific catchment area, runoff source area, slope, saturated hydraulic conductivity, depth to impermeable subsurface layer, and rainfall erosivity), the field slope showed the strongest relationship with flow concentration (R^2 = 0.270). Principle component analysis on these 6 topographic/soil property characteristics had a first component that described 47% of the variance among these 6 variables and displayed the strongest relationship with flow concentration (R^2 = 0.403). Rather than being attributable to characteristics of the topography or soil that vary from place to place, flow concentration seems to be a phenomenon that is of widespread occurrence in all areas of the Coastal Plain region of Virginia. I recommend requiring farmers to maintain riparian buffers on their land yearly. Future research should focus on determining how to reduce flow concentration through and increase the effectiveness of riparian buffers in the Coastal Plain region of Virginia.

Introduction

Agricultural lands are the single largest non-point source of nitrogen, phosphorous, and sediment in the Chesapeake Bay watershed, accounting for 42% of the nitrogen, 58% of the phosphorous, and 58% of the sediment delivered to the Bay annually (Chesapeake Bay Program, 2012). Agricultural lands occupy ~22% of the watershed land area, and fertilizer application, tilling, and applying animal manure to agricultural fields are the primary origins of the nutrients and sediment. Nutrient and sediment loads from agricultural runoff have increased over the last century (Kemp *et al*., 2005), contributing to enhanced primary productivity and subsequent eutrophication in Chesapeake Bay, and an increase in the size and duration of annual anoxic zones within Bay waters (Boesch *et al*., 2001). The anoxic zones have resulted in a sharp decline over the last several decades in the populations of benthic aquatic species (e.g. oysters, crabs, striped bass, and sturgeon) (Kemp *et al*., 2005). Reduced water clarity associated with eutrophication and suspended sediment has substantially reduced sea grass coverage (Kemp *et al*., 2005) and degraded the quality of water in the Bay that is used for human recreation, and there has been an increase the occurrence of toxic algal blooms that are detrimental to human health (Kleinman *et al*., 2011).

In 1987, the states in the Chesapeake Bay watershed agreed to reduce controllable sources of nitrogen and phosphorous by 40% by the year 2000 in an effort to restore the Bay's health (Boesch *et al*., 2001; Lowrance *et al*., 1997). Known as the Chesapeake Bay Agreement (CBA) of 1987, this agreement mandated practices to decrease the amount of nutrients and sediment being delivered to the Bay in an effort to reduce the amount of subsequent eutrophication. As part of this effort, the Chesapeake Bay

Protection Act (CBPA), incorporated into the Virginia Administrative Code, requires the designation of Resource Protected Areas (RPAs) in the Coastal Plain region of the Bay's watershed in Virginia to "lands adjacent to water bodies with perennial flow that have an intrinsic water quality value due to the ecological and biological processes they perform or [to those that] are sensitive to impacts which may cause significant degradation to the quality of state waters" (CBPADMR, 2012). Lands adjacent to RPAs are required to have "a buffer area not less than 100 feet in width located adjacent to and landward of [RPAs], and along both sides of any water body with perennial flow" (CBPADMR, 2012). The buffer required by this law is generally a forested riparian buffer (Lowrance *et al*., 1984, Lowrance *et al*., 1997).

Forested riparian buffers (*Fig. 1*) are streamside ecosystems that improve stream water quality by removing nutrients and sediment from runoff that passes through them before entering adjacent streams (Lowrance *et al.*, 1997). Riparian vegetative cover on the land surface slows the movement of overland flow, traps sediment, and increases infiltration of flow to the subsurface root system where absorption of nutrients can occur (Tomer *et al.*, 2009). The root systems of riparian vegetation directly uptake nutrients and some heavy metals from shallow subsurface flow passing through them, promote denitrification, and stabilize stream banks – helping to prevent erosion (Dosskey *et al.*, 2010). Riparian buffer systems are generally very efficient at removing nitrogen from runoff (up to 90%), but are only effective at removing sediment-bound phosphorous; they remove very little phosphorous that is dissolved in runoff (Lowrance *et al.*, 1997). Vegetation requires more nitrogen than phosphorous and consequently absorbs less phosphorous, thus most of the phosphorous that riparian buffers remove is that bound to

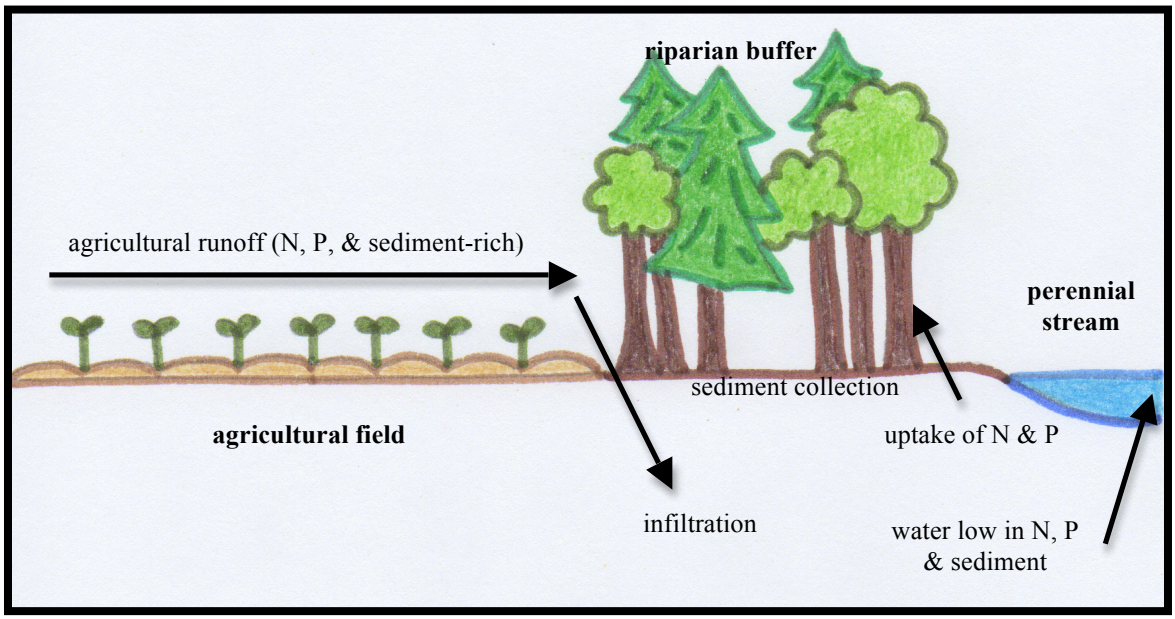

Figure 1. Schematic of a forested riparian buffer.

sediment when runoff flow is slowed and the sediment settles out (Dosskey *et al*., 2010). This is significant because dissolved phosphorous is a biologically available form of phosphorous, and thus is immediately taken-up by organisms when delivered to water bodies, leading to harmful eutrophication effects (Kleinman *et al*., 2011).

In the Coastal Plain of the eastern U.S., where this study is focused, forested riparian buffers have been shown to be effective at reducing nutrient and sediment loads in runoff from agricultural fields. Relying on a compilation of studies in the Coastal Plain, Lowrance *et al*. (1997) suggest that forested riparian buffers may accomplish nitrogen, phosphorous, and sediment reductions of ~75%, ~77%, and ~96% respectively, for a contributing area:buffer area ratio of ~2:1. Observed reductions of total nitrogen and phosphorous range from 67% to 89% and 24% to 81% respectively (Lowrance *et al*., 1984).

Maximum nutrient and sediment trapping efficiency for riparian buffers requires runoff to be uniformly disseminated across the entire buffer (Knight *et al*., 2010). However, concentrated flow may be a common occurrence on agricultural fields, generated by natural field topography, furrow orientation, and surface topography modifications (Dosskey *et al*., 2002). A limitation to most of the existing Coastal Plain studies is that the estimates of nutrient and sediment reduction cited above assume that concentrated and channelized surface flow within the buffers does not occur (Lowrance *et al*., 1997). Flow concentration reduces the efficiency of nutrient and sediment removal by buffers (Knight *et al*., 2010), in part because flow concentration may substantially increase the contributing area:buffer area ratio, thus reducing the buffer area utilized for nutrient and sediment trapping (Dosskey *et al*., 2002). Concentrated flow also may

promote channel incision and growth within forested buffers, allowing water to effectively bypass buffers with little to no trapping of sediments or absorption of nutrients (Dosskey *et al*., 2002; Knight *et al*., 2010).

In spite of the implementation of the CBPA, reduction of non-point sources of nutrients and sediment, such as agricultural runoff, has lagged behind that of point source reduction, and the goal for 40% reduction has still not been met as of 2011 (NRC, 2011). The amounts of nitrogen, phosphorous, and sediment being delivered to the Bay have been monitored on a yearly basis since 1990. Nitrogen, phosphorous, and sediment loads delivered to the Bay have fluctuated from year to year since 1990, however no prominent declining trends have been seen (*Figs*. *2-4*) (Chesapeake Bay Program, n.d.).

I propose that the occurrence of concentrated flow across agricultural fields and through their bordering riparian buffers is widespread in the Virginia Coastal Plain portion of the Chesapeake Bay watershed, and that the associated reduction of buffer effectiveness due to flow concentration could partially explain the inability to meet the CBPA goals. This study used Geographic Information Systems (GIS) to evaluate the potential for flow concentration across agricultural fields in the Virginia Coastal Plain that are adjacent to perennial streams, where forested riparian buffers are required by law. This was done through the use of lidar data, allowing for high-resolution determination of flow pathways at the agricultural field-scale. Further, this study sought to determine an easy metric that could be used to predict areas where flow concentration occurs. Currently, agricultural fields in the Coastal Plain region of Virginia must be analyzed individually for flow concentration. It was the goal of this study to determine if any easily calculable topographic metric was correlated with flow concentration. Such a

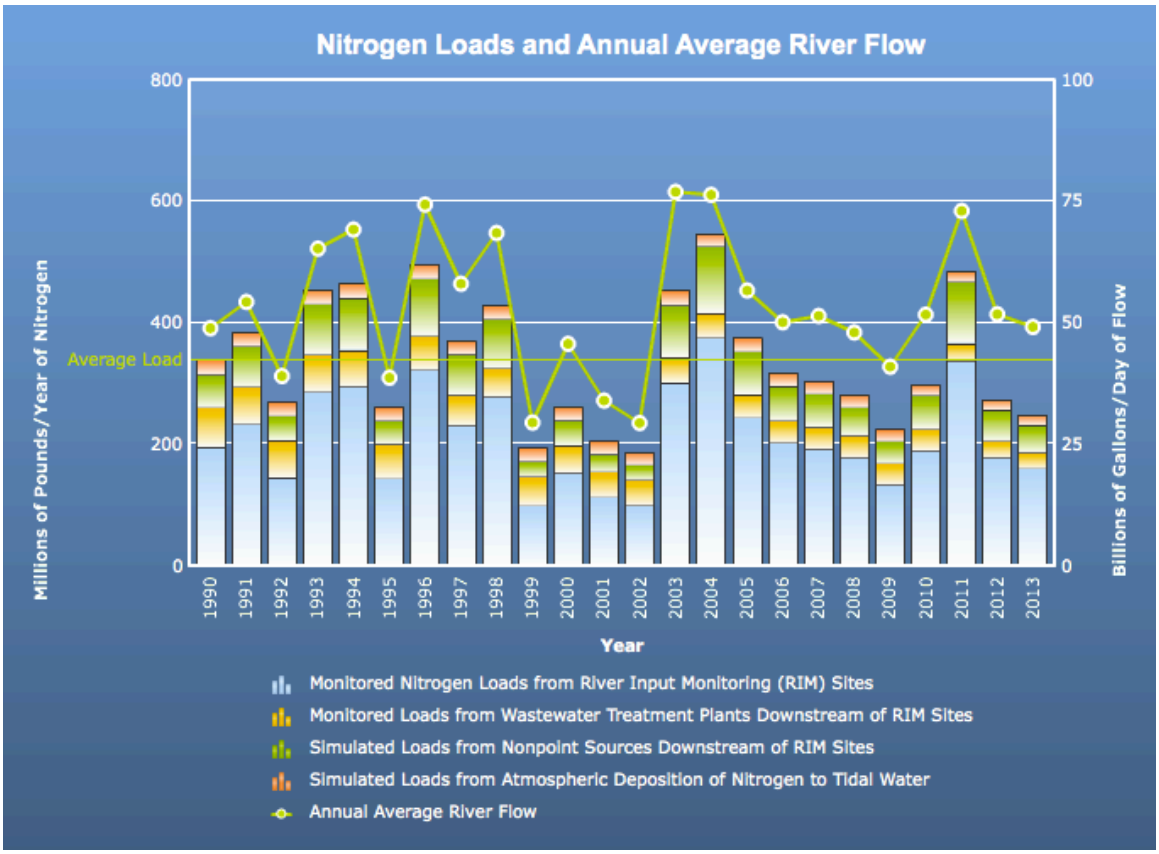

Figure 2. Nitrogen loads being delivered to Chesapeake Bay from 1990-2013 (Chesapeake Bay Program, n.d.).

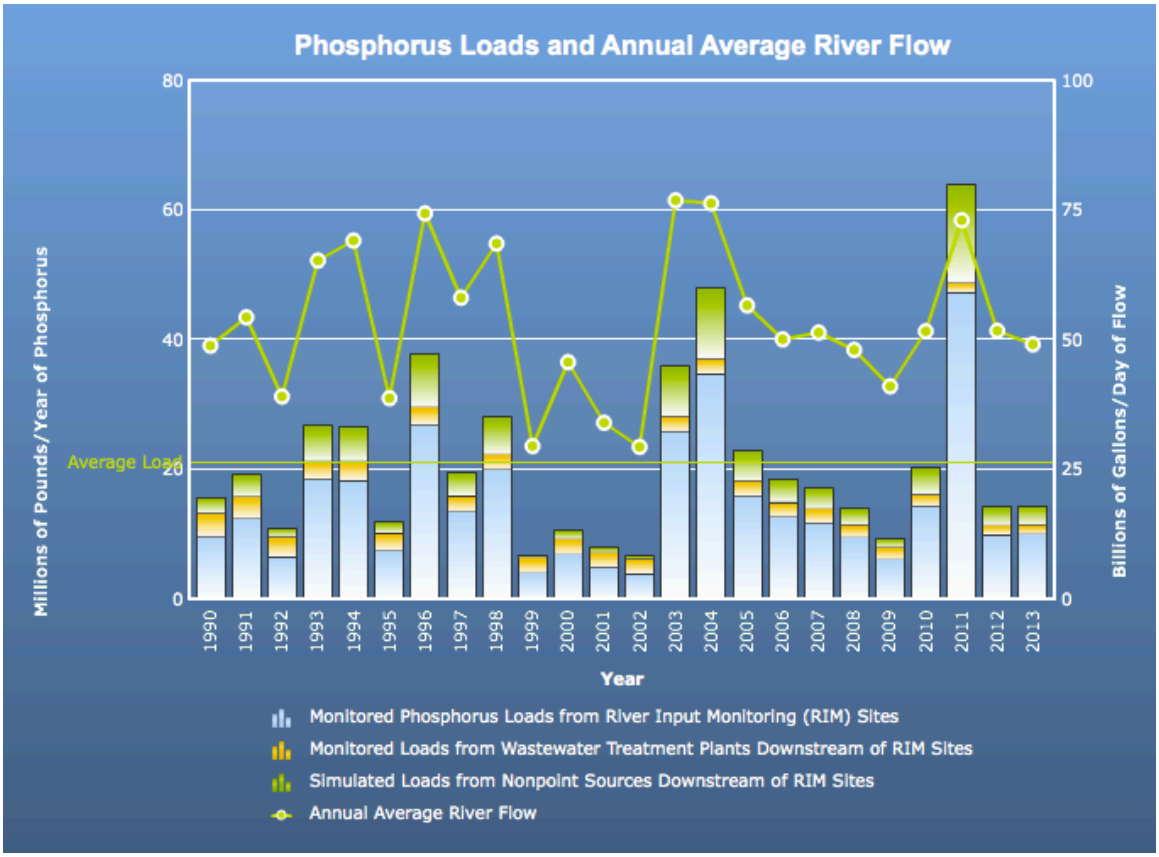

Figure 3. Phosphorous loads being delivered to Chesapeake Bay from 1990-2013 (Chesapeake Bay Program, n.d.).

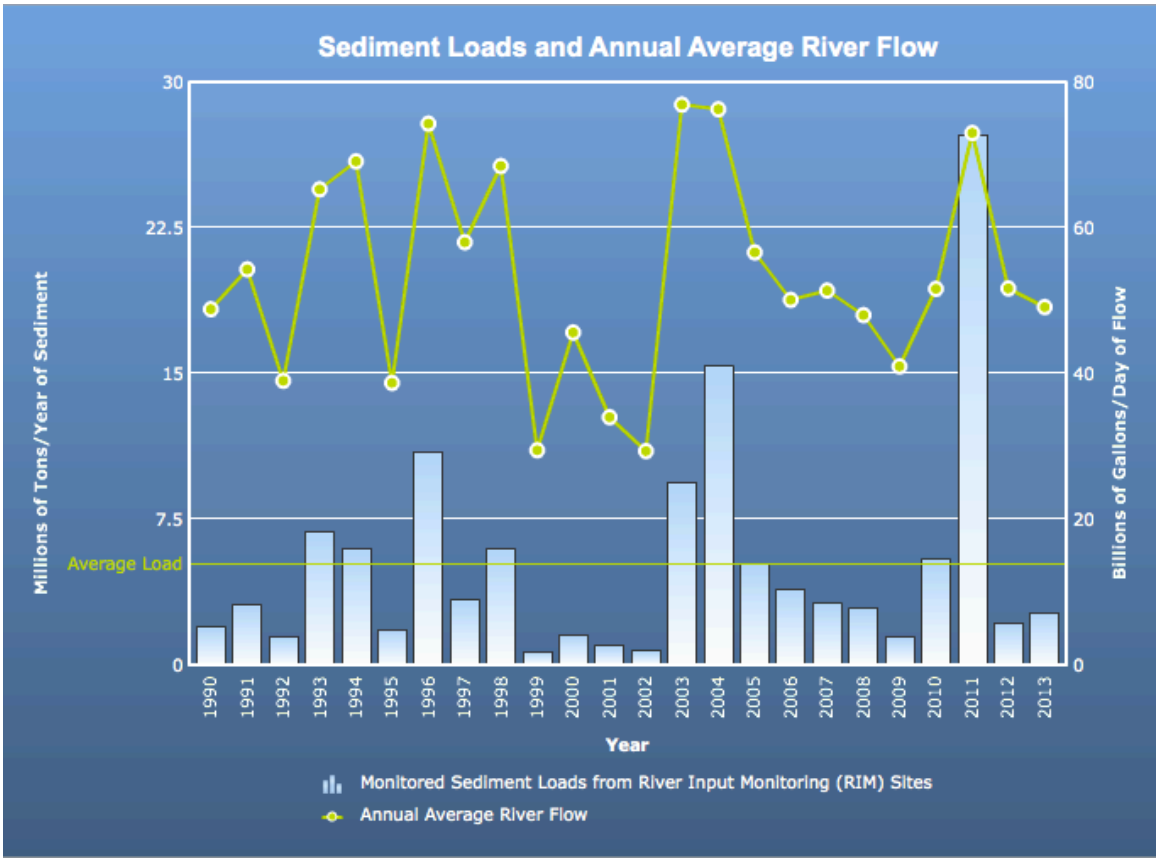

Figure 4. Sediment loads being delivered to Chesapeake Bay from 1990-2013 (Chesapeake Bay Program, n.d.).

metric could then be calculated across the entire Coastal Plain of Virginia to determine where flow concentration occurs across this large geographic area without having to analyze individual agricultural fields. Four topography-based indexes were calculated for each field and analyzed to determine if any are correlated with and could be used to predict the presence of concentrated flow. Linear regression and principle component analysis of 3 topographic and 3 soil property characteristics of agricultural fields was used to determine which, if any, contribute to flow concentration. Lastly, this study seeks to propose alternatives to riparian buffer rules, as they exist currently in the Virginia Administrative Code, that would not only increase buffer effectiveness and reduce the loads of nitrogen, phosphorous, and sediment delivered to Chesapeake Bay, but that are also economically feasible and beneficial for farmers.

Previous Research

Previous studies have shown that the best places to establish and manage riparian buffers are in areas where the slope and soil conditions promote sediment-rich runoff and that are located along first order streams (Tomer *et al.*, 2009). Buffers along first-order streams have a greater ability to intercept and filter out nutrients and sediment in water draining to them because most of the water entering first-order streams comes from overland runoff draining from nearby catchment areas. Larger rivers receive a significant amount of water from tributaries, and thus, most of the water entering larger water bodies does not pass through their buffer systems (Burkart *et al.*, 2004). Further, Lowrance *et al*. (1997) noted that riparian buffers are more effective in the Coastal Plain region, compared to the Piedmont and Valley and Ridge regions, because water in the Coastal

Plain is restricted to overland flow or shallow subsurface flow at depths within the range of buffer root systems. The presence of deep regional aquifers in the Piedmont and Valley and Ridge regions draws water away from the land surface, allowing it to bypass buffer root systems before entering water bodies (Lowrance *et al.*, 1997). Burkart *et al*. (2004) concluded that riparian buffers are most effective in areas with near-surface water tables and that have slower overland flow velocities. Near-surface water tables allow the root systems of riparian vegetation to more easily reach subsurface flow and uptake dissolved nutrients. When overland flow velocity is slowed, the load of suspended sediment it is capable of transporting decreases; thus, areas with slower overland flow velocities promote sediment removal from runoff, through the settling out of sediment. Also, infiltration is often greater in areas where overland flow velocity is slower, and thus such areas would deliver more flow to the shallow subsurface for "cleansing" by riparian vegetation root systems (Burkart *et al*., 2004).

An example of the importance of riparian buffer systems for water quality in agricultural watersheds is the study by Lowrance *et al*. (1984) on Watershed N of the Little River in Georgia. Watershed N is located in a dominantly agricultural area that receives extensive fertilization and that has riparian buffers along perennial streams. Lowrance *et al*. (1984) calculated the nutrient budget for this watershed based on inputs of nutrients from precipitation, subsurface flow, and nitrogen-fixation, and outputs of nutrients to streams and denitrification. They concluded that nutrient inputs were greater than nutrient outputs, and thus that the riparian buffers were retaining some nutrients. Nitrogen had the highest retention rate, 68%, but calcium, chlorine, magnesium, phosphorous, and potassium nutrients were also retained (Lowrance *et al*., 1984).

A later study done by Lowrance *et al*. (1997) analyzed riparian buffer functions in the Chesapeake Bay Watershed. This study found that riparian buffers in the Coastal Plain region of the Chesapeake Bay Watershed could remove 90% of the sediment, 75% of the nitrogen, and 77% of the phosphorous in agricultural runoff passing through them when the runoff contributing area to riparian buffer area ratio was 2:1. These results were based on the assumption of non-channelized flow through the buffers, and that the buffers were properly managed (continuously replanted to maintain the 2:1 contributing area to buffer area ratio) (Lowrance *et al*., 1997).

Agricultural field runoff is not always uniform; it is greater on some areas of a field than others (Dosskey *et al*., 2005). A study done by Dosskey *et al*. (2002) on 4 farms in southeastern Nebraska found that the sediment trapping efficiency of a riparian buffer increases as the buffer-to-field-area ratio increases (*Fig. 5*). However, if flow across an agricultural field is concentrated, certain portions of the buffer along the field margin will have no flow passing through them, reducing the effect buffer area (*Fig. 6*). Dosskey *et al*. (2002) found flow concentration reduced the effective buffer area on the 4 fields they studied to 6% to 81% of the total buffer area, increasing the contributing area:effective buffer area ratio to between 30:1 and 100:1. In addition, 27% to 71% of the buffer area was drained by gullies feeding directly into receiving streams. Modeling of sediment trapping by Dosskey *et al*. (2002) on these fields suggests that flow concentration reduces the sediment trapping efficiency of buffers by 7% to 56%. The variable-width buffer design is a method for riparian buffer installation that addresses this problem in order to increase the sediment trapping efficiency, where more buffer is placed along agricultural field margins in areas where there is more runoff and less buffer

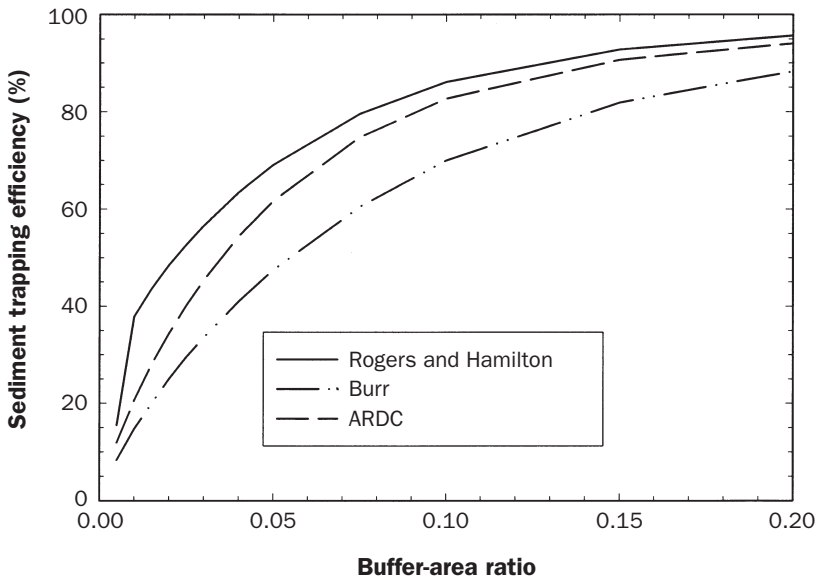

Figure 5. Relationship between buffer-area ratio and sediment trapping efficiency for four farms in southeastern Nebraska (Rogers, Hamilton, Burr, and ARDC). Buffer-area ratio = (buffer area / field runoff area) (Dosskey *et al*., 2002).

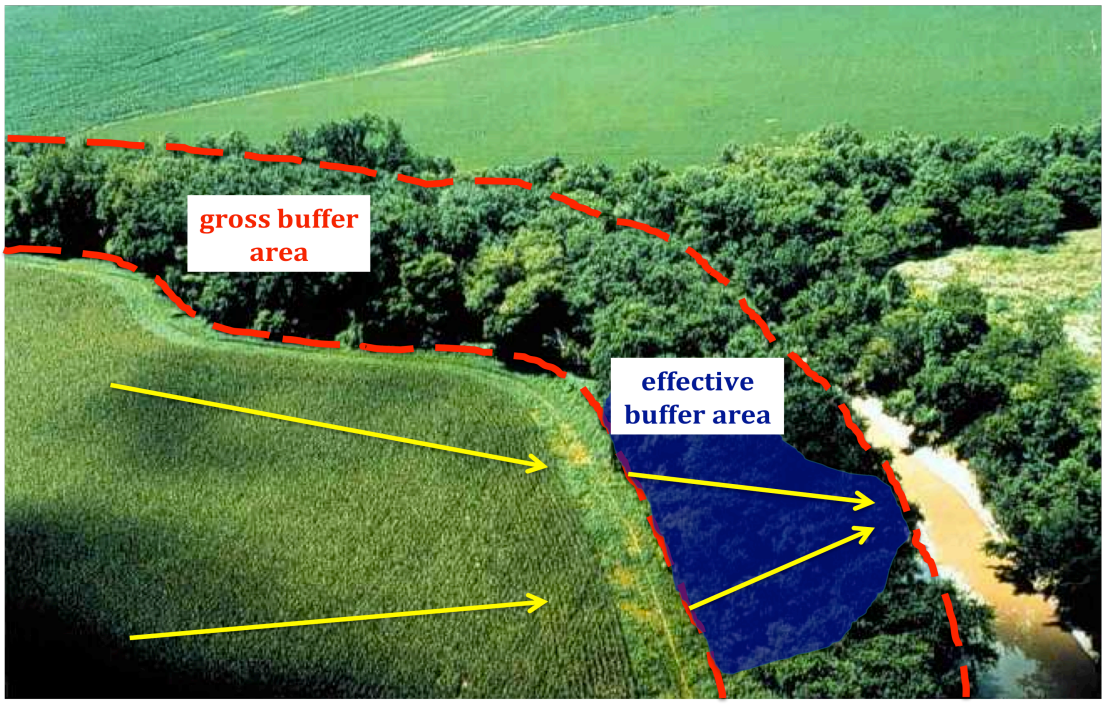

Figure 6. Diagram showing the relationship between gross and effective riparian buffer area. Water flows off the agricultural field following the yellow arrows. Gross area (outlined by red dashes) is the entire area of the riparian buffer; effective area (shaded blue) is just that area of the riparian buffer that runoff passes through (based on Dosskey *et al*., 2002).

is placed along areas with little runoff. This method utilizes information about the topography, soil, stream locations, and farming practices to determine where runoff would be greatest for each agricultural field (Dosskey *et al*., 2005).

A study conducted by Verstraeten *et al*. (2006) in Belgium further supports the conclusions of Dosskey *et al*. (2002). This study used a spatially distributed soil erosion and sediment delivery model to simulate the ability of riparian buffers to reduce the amount of sediment delivered from cultivated land to adjacent water bodies. Verstraeten *et al*. (2006) determined the amount of sediment coming off of agricultural fields, as well as the sediment trapping efficiency of the riparian buffers intercepting the runoff from the fields. They found that riparian buffers could only reduce the amount of sediment delivered to rivers by 17% on average across their study area, Flanders, Belgium. Further, they noted that most of the sediment that was removed from runoff was deposited in floodplain swamps on the riverside of the buffers, not the more forested side along the agricultural field margins. The relative inefficiency of riparian buffers in this study was found to be due to flow convergence over the rather large-scale, ~13,600 km^2, study area, especially in areas with higher slopes, as higher slopes make channelization easier and increase the likelihood of flow concentration (Verstraeten *et al*., 2006).

Funkhouser (2011) and Young (2013) have researched flow across agricultural fields in the Virginia Costal Plain region of the Chesapeake Bay watershed. The study conducted by Funkhouser (2011) found that at least 50% of the flow on the agricultural fields analyzed exited the fields through ten or less points along the field margin. These ten points of highest flow accumulation along the field margins were found to represent only between 0.25% and 0.8% of the total field margin length, and were an indication of

concentrated flow (Funkhouser, 2011). Young (2013) continued the study done by Funkhouser (2011) on agricultural fields in the Virginia Coastal Plain region of the Chesapeake Bay watershed and found that the point along the field margin with the most flow exiting ranges from 8% to 83% of the flow across the field, and that the area of a field drained by the five points of highest accumulation along the field margin ranges from 30% to 95%, again an indication of flow concentration (Young, 2013). My research continues the work started by Funkhouser (2011) and Young (2013) in order to further analyze the extent to which flow is concentrated across agricultural fields in the Virginia Coastal Plain region of the Chesapeake Bay watershed, but also investigates what topographic metrics, if any, are correlated with and could be used to more easily predict where flow concentration will occur, as well as how riparian buffer rules could be modified to better address the reduction in buffer effectiveness in areas with concentrated flow.

Study Area

The study area was all 46 counties and cities located in the Coastal Plain region of Virginia that are statutorily delineated by the Chesapeake Bay Act (CBPADMR, 2012) (*Fig. 7*). All counties and cities in the Coastal Plain region of Virginia are wholly contained within the Chesapeake Bay watershed. All agricultural fields within these counties and cities are therefore covered under the Resource Protection Area (RPA) requirement of the Chesapeake Bay Act (CBPADMR, 2012).

The study area was further restricted to areas with lidar data available with the point-spacing required to create field-level terrain models within the aforementioned

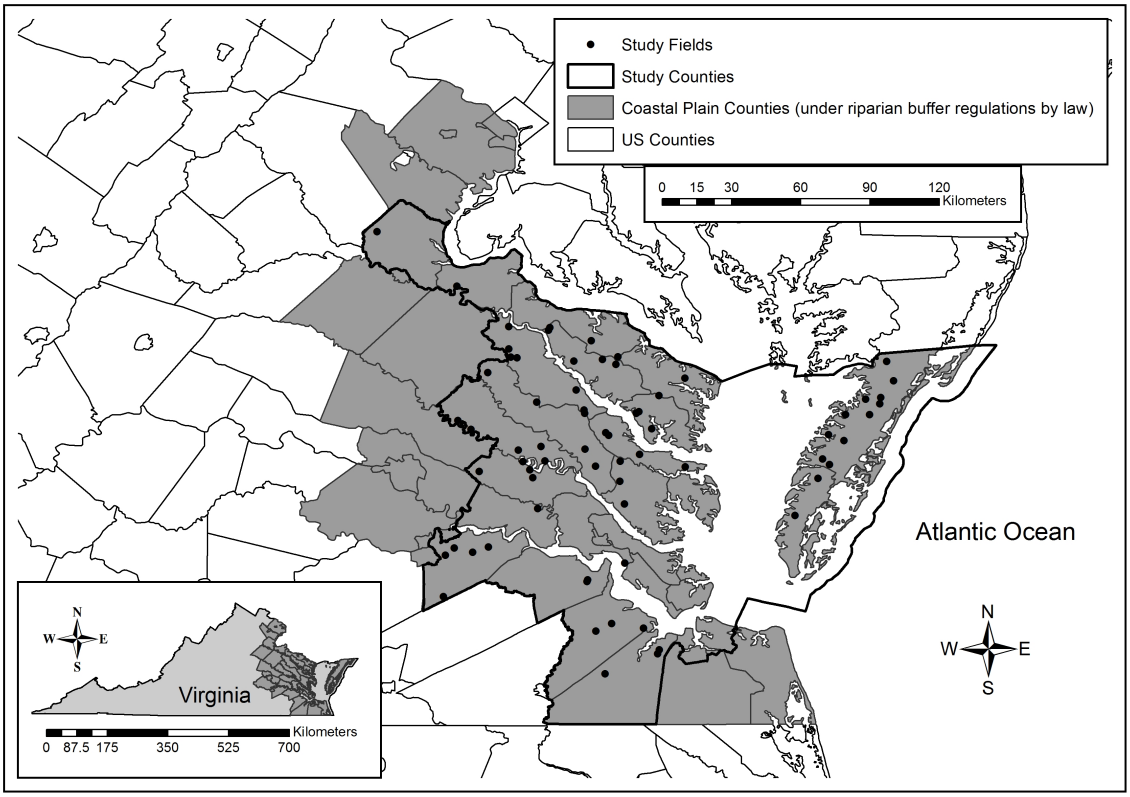

Figure 7. Study Area

municipalities. The final study area therefore is all terrestrial land within the area of the Coastal Plain region of Virginia with available lidar data with a horizontal point spacing density of more than one point per square meter. This resulted in a study area consisting of 25 counties and cities (*Fig. 4*), with an area of 20,456 km^2 and a total 2010 census population of 1,342,860. Although these cities and counties are all included as potential sites for analyses, study sites were selected randomly from within this set of localities. To protect the privacy of individual property owners, exact coordinates for the field sites analyzed are not included.

Methods

Field Selection

Within the study area (*Fig. 7*), the 2006 National Land Cover Database (NLCD) was queried to return all cells classified as cultivated crops. This resulted in 2,182,052 nine-hundred square meter cells, or 1,964 km^2. Each cell was given a unique identifier and then a singular random value between 1 and 2,182,052 was generated. The field containing this random cell was rejected or accepted based on the five criteria below.

The first rejection of a random cell was if a randomly selected value occurred twice, however this never happened. The second rejection of a random cell occurred when a cell selected was within 1 km of a previously selected cell or if a cell was clearly on a field that had already been selected, again this never occurred. The reason for this rejection is that the process of turning cells into larger fields has the potential for two or more random cells to exist on the same field and the same field to be selected twice. The third rejection criterion is based on NLCD misclassification. The NLCD data does not

represent the present and it misidentified some large rural lawns as cultivated crops. Misclassified cells were identified by analyzing color aerial photography collected in 2006/2007 – to coincide with the NLCD timeframe – and 2011 – to coincide with the lidar data timeframe – both validation datasets were provided by Virginia Geospatial Archive Resource and Data Exchange Network (VA GARDEN). This misclassification criterion based on aerial photography resulted in the rejection of ten fields. The fourth rejection reason is the lack of a nearby river or stream. Because the focus of this study is on the effectiveness of riparian buffers, a field was rejected if it was not within 1 km of a perennial stream requiring a buffer. Finally, cells that drained directly into tidal waters rather than perennial streams were also rejected, as they are not required to have a riparian buffer.

This selection process was repeated iteratively until 69 random cells, and the fields containing them, had been accepted. Additionally, 5 fields were added to the sample set for which visitation and in-situ field testing was possible. This resulted in 74 fields of which 69 are randomly sampled and 5 are systematically selected. The 74 figure was based purely on available resources to manually digitize field margins.

Field Digital Terrain Model (DTM) Creation

Lidar data was obtained from the Virginia State lidar clearinghouse operated by The College of William and Mary (http://www.wm.edu/as/cga/VALIDAR/) collected between 2010 and 2011 in early spring leaf-off conditions flown by two commercial vendors. Both venders used the Optech ALTM 3100EA lidar system. Point densities varied across the study area from a high of one point per 0.5 m^2 to a low of one point per

0.7 m^2. From the three-dimensional multi-return lidar data cloud, ground points were extracted by the vendors using a proprietary Terrascan algorithm combined with human-based three-dimensional visualization techniques. This combined with stereo-derived breakline features allows for the creation of a highly-accurate DTM. All DTMs were delivered with horizontal coordinates in the Virginia State Plane South (NAD 1983, NSRS2007 adjustment) coordinate system with the linear unit of US survey feet. The vertical coordinate system utilized was the NAVD 1988 with vertical units in feet and tenths. The horizontal coordinates were reprojected to UTM Zone 18N (NAD 1983, NSRS2007 adjustment) with a horizontal unit of meters, and the vertical coordinates were kept in the NAVD 1988 coordinate system, but adjusted to a vertical unit of meters. Field verification of point data by the vendor resulted in the root mean squared error varying between a low of 0.09 m to a high of 0.22 m at the 95% confidence level. During reprojection, the lidar data was resampled to obtain a 3-meter grid spacing for the DTM. Zhang and Montgomery (1994) have shown that DTM grid size affects hydrologic modeling. Larger grid sizes increase estimated contributing area in hydrologic modeling. Further, runoff processes are best modeled at an intermediate scale of the topography (Zhang and Montgomery, 1994). A 3-meter grid size was selected because it was a fine enough scale to represent elevation and slope across the agricultural fields studied, and also minimized overestimation of catchment area. No concentrated flow leaving the 5 agricultural fields that were visited to validate the model used in this study had a width exceeding 3 meters. A 3-meter grid size ensured that there would be at least 1 lidar point per m^2, and also that there would be minimal exaggeration in the spatial extent of concentrated flow areas.

Portions of the raster DTM were then extracted that corresponded to each field location with a buffer of 2 km around the selected cells to capture flow accumulation from off of the field. The buffered area was then preprocessed using the D8 algorithm to fill spurious sinks within the DTM and to generate a flow direction raster from the filled DTM (Jensen and Domingue, 1988). The flow direction grid was then processed into a flow accumulation raster with each cell value being the cumulative network flow from upstream cells into the object cell.

Determination of Field-level Watersheds

Following calculation of flow accumulation, field margins were manually digitized using heads-up digitization from 1 m resolution aerial imagery flown in 2011. Field margins were defined as being the furthest extent to which crops were planted on a field. While being digitized, field margin points were snapped to the center of the nearest flow accumulation cell. A 4-neighbor digitizing strategy was used to ensure that opposing angular flows also would be captured at the field margin. That is, no flow can bypass a field-margin point regardless of the angle of flow. Utilizing this method minimizes the potential of missing points of significant flow accumulation crossing the field margin. For example, if at a field margin point the flow direction was NE – SE, whereas the field margin at the same point was NW – SW, then it would be possible to miss the flow with an 8-neighbor approach to field construction, but by ensuring that the field margin connectivity was restrained to only one of the 4 cardinal directions this potential for lost flow was mitigated (*Fig. 8*). In locations where flow directions were parallel to the edge of fields, the digitized field margin was moved a few cells in either

direction to prevent flow running directly on top of the digitized field margin, which would result in a single flow being counted multiple times along the field margin. Following the manual creation of the field margin, the flow accumulation and flow direction were sampled at each field margin point, providing the number of cells draining to each point on the field margin and the direction of flow at each point. Flow area was determined by multiplying the number of cells by 9 m^2 (i.e. 3 m x 3 m area represented by each cell).

The points along the digitized field margin were then ranked by the total area draining to each point. However, in many cases some drainage area came from flow onto the opposing side of a field that is then incorporated in the total area draining off the field at some other point on the field margin. To isolate drainage area from the field only, the 10 points along the margin with the greatest total flow accumulation were used as pour points to determine the total watershed at these points. Then, the watershed polygons were clipped using the field margin, leaving polygons incorporating only the area draining from the field to each pour point on the field margin (*Fig. 9*). Because the watershed size and rank were determined before clipping the polygons, the new polygon areas are reranked according to decreasing flow accumulation from the field. While 10 watersheds were created, only the top 5 were used for analysis. This allowed us to determine the percentage of each field area that was being drained through the 5 field margin points of greatest flow accumulation area. The user operating the model defined may alter these values to create more or less than 10 watersheds per field and more or less than 5 for analysis.

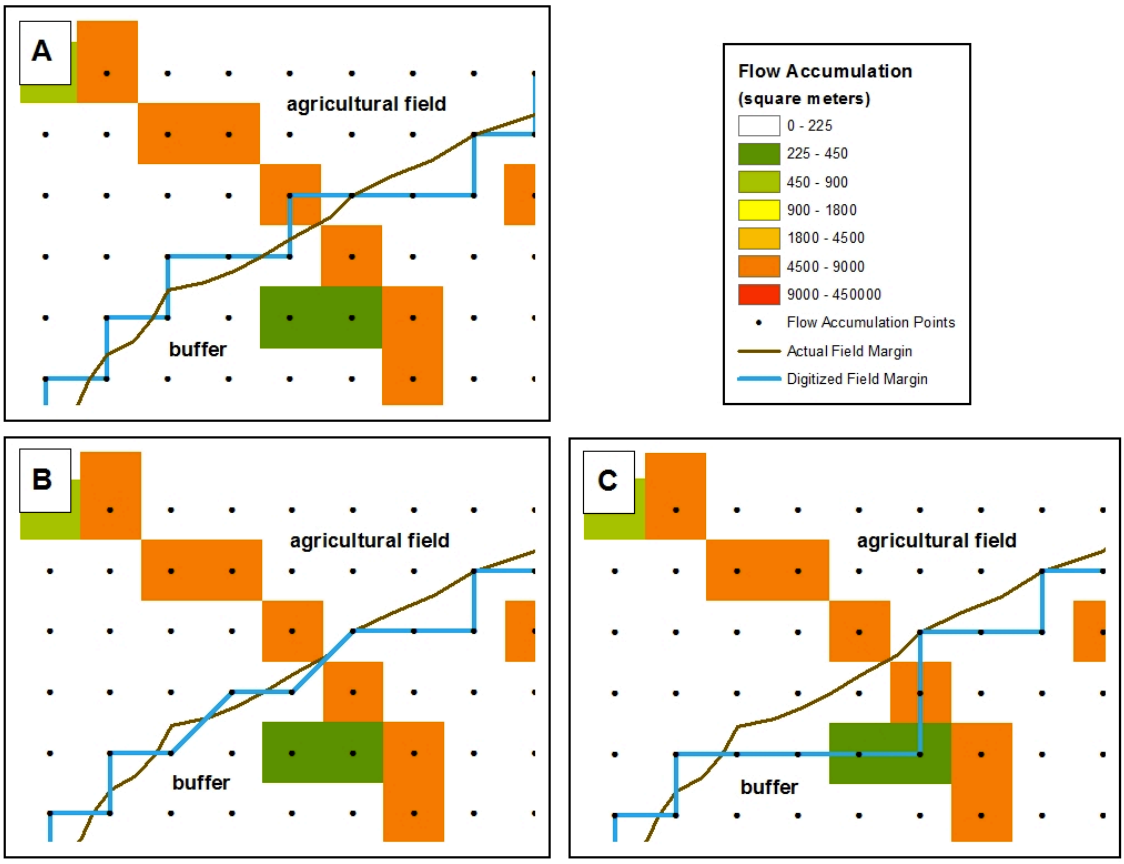

Figure 8. Examples of a correct field margin digitization (A) and 2 incorrect field margin digitizations (B and C). Field margins were digitized only in the directions of directly north, south, east, or west, as shown in the correctly digitized field (A). The digitization in B is incorrect because a major flow off the field is missed due to diagonal digitization. The digitization in C is incorrect because the digitization follows a flow path and counts the flow multiple times.

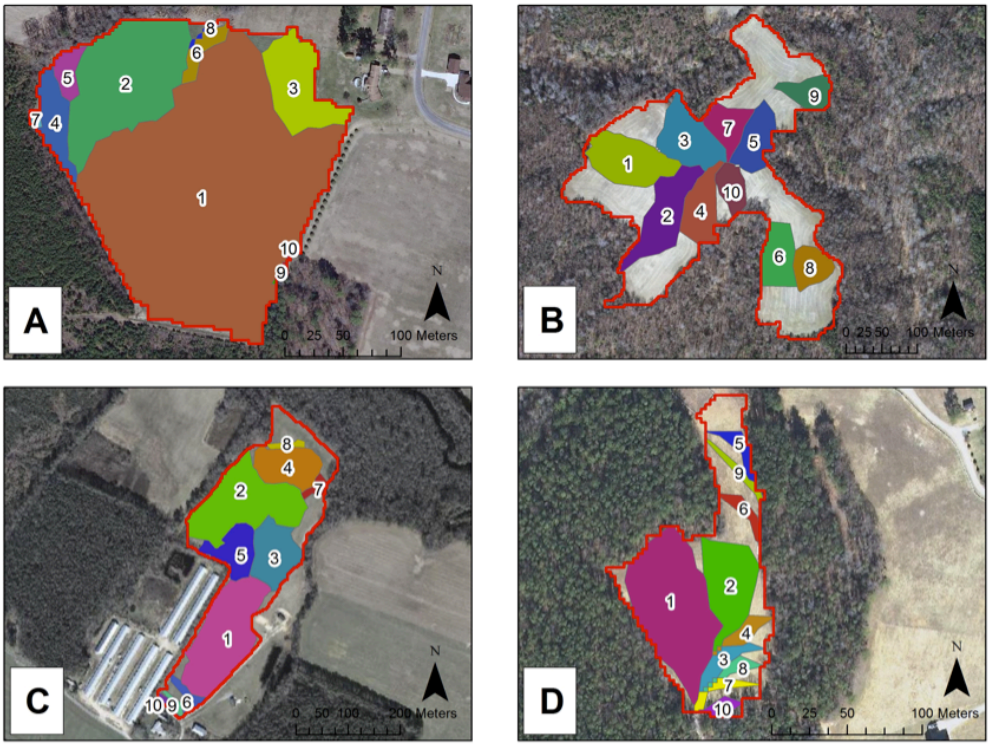

Figure 9. Watersheds for the top 10 points of highest flow accumulation off the field for: A) the field with the largest percent area (99.32%) drained by these 10 points, B) the field with the smallest percent area (40.65%) drained by these 10 points, C) the field with the median percent area (84.07%) by these 10 points, and D) the field with an average low percent area (69.38%) drained by these 10 points.

Model Compilation (See Appendix A)

ArcGIS model builder was utilized to create an automated model from which fields can be analyzed from lidar-derived digital elevation models (DEMs) as outlined in the above methodology. This model was created for three separate purposes: 1) to remove user errors and promote efficiency in the execution of field analysis, 2) to allow for repetition of these methods for validation within the study area, and 3) to allow for similar analyses in other study areas while maintaining the same methodology. This model contains 78 distinct steps, beginning with just one independent input variable and producing 16 output files. A simplified schematic of the model is shown in *Fig*. 10. User operation of the model consists of two parts. Part 1 of the model produces elevation, flow accumulation, flow direction, and slope outputs for each field. After utilizing Part 1 of the model, a heads-up digitization of the field margin is required using the 4-neighbor method previously described. After the digitization of the field margin, Part 2 of the model creates field-level watersheds. The automated steps of the model run in less than 1 minute on an off-the-shelf PC, and an experienced user can digitize an average of four fields in an hour, making for an efficient process. The output files for the 74 fields included in this analysis occupy approximately 9GB of compressed spatial storage space.

Validation of Model on Study Fields

In order to obtain a large enough sample size of agricultural fields to analyze flow concentration, DTMs were used to predict the flow patterns across these fields from lidar elevation data. However, predicting flow accumulation in GIS does not confirm that

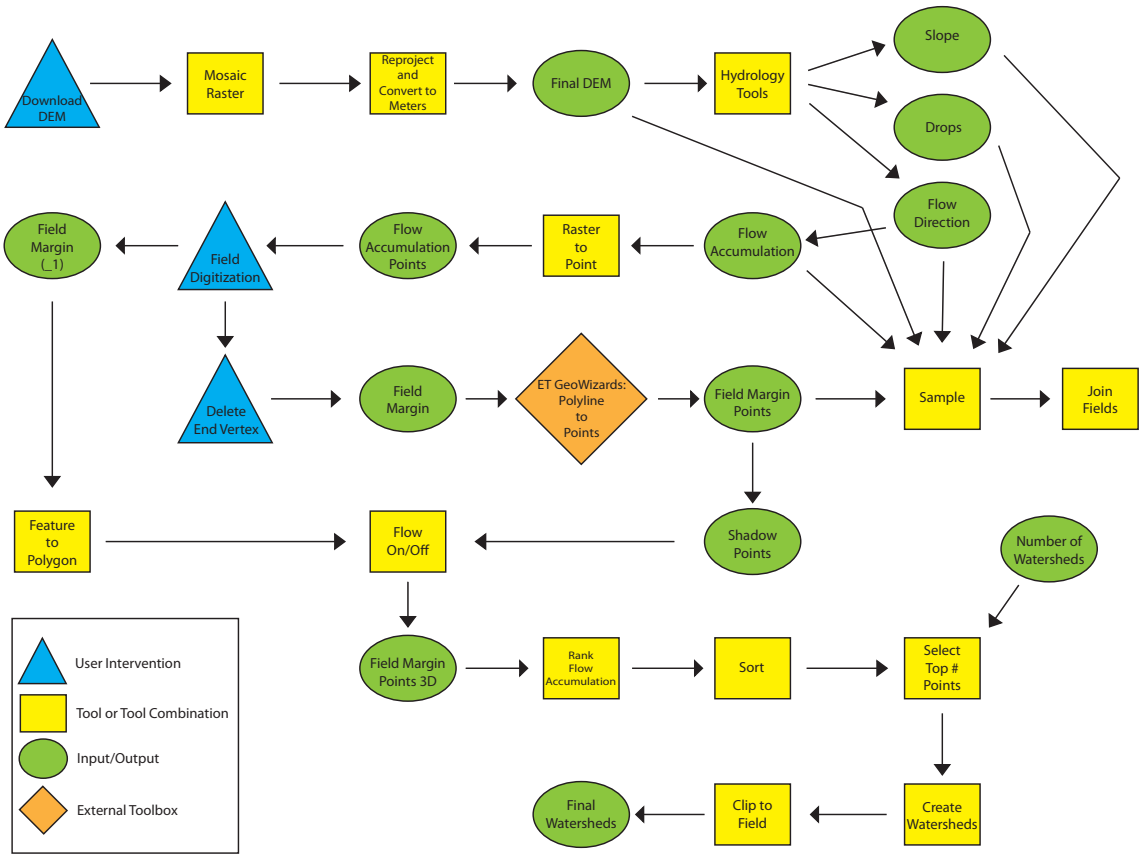

Figure 10. Schematic of model used to determine elevation, flow accumulation, flow direction, slope, and the top 10 field-level watersheds for each of the 74 fields (created by John Lovette).

flow actually occurs in those locations. To document evidence for flow along field margins, 5 fields were surveyed using GPS. The choice of fields was limited to those fields for which permission to enter was granted, and hence these were not randomly chosen. The well-defined margin of each of these fields was walked and the locations with evidence for concentrated flow moving off the field across the field margin were noted. Where noted, evidence for concentrated flow was categorized as dispersed (i.e. unchannelized) or channelized. Evidence noted included deposition or removal of sediment and organic material, bent plants oriented in a common direction, channels within the adjacent buffer, and channels extending directly off the field into the adjacent buffer. Where evidence for concentrated flow was noted, a Trimble GeoXT GPS unit connected to a Trimble Hurricane antenna was used to obtain the location. GPS point locations were differentially corrected in Pathfinder Office using base stations within < 25 km of the surveyed field. This resulted in sub-meter GPS locations each of which are located inside the 3 m analysis cells that contained modeled flow, allowing for comparison between predicted areas of flow concentration and actual areas with evidence for concentrated flow (Young, 2013).

Field Index Calculations

The complexity of the above methodology illustrates why being able to determine an easily calculable metric that is correlated with flow concentration would be preferable when analyzing where flow concentration is likely to occur across a large geographic area, like the Coastal Plain of Virginia. Many field indexes were used in this study to ascertain what, if any, metrics of agricultural fields are correlated with concentrated flow.

The wetness index and the topographic index, as presented by Dosskey *et al*. (2011a), were calculated for each of the study fields (see Appendix B and Appendix C respectively). The wetness index ($w = \ln (A_s/B)$), where A_s is the specific catchment area, and B is the slope, describes the propensity for soil saturation and generation of overland flow in a landscape. The value of the wetness index increases the closer the water table is to the surface (Burkart *et al*., 2004). It was hypothesized that higher values of the wetness index, indicating a higher potential for overland flow, would correspond with increased flow concentration. The wetness index was tested in a study carried out by Leh and Chaubey (2009) in Basin 1 of the Savoy Experimental Watershed in Arkansas, as a proxy for identifying areas of saturation excess and infiltration excess runoff, located using subsurface saturation and runoff sensors, in their study area. They found that 69.5% of the predictions made using the wetness index were correct. The topographic index ($TI = \ln (A_s/\tan B) – (K_{sat}D)$), where A_s is the specific catchment area, B is the slope, K_{sat} is the saturated hydraulic conductivity of the soil, and D is the depth above an impermeable subsurface rock or soil layer, takes into account the water storage capability in the subsurface of a landscape and indicates the risk of water table rising (Dosskey *et al*., 2011a). It was hypothesized that higher values of the topographic index would also correspond with increased flow concentration because as the likelihood of water table rising increases, saturation likelihood and the potential for overland flow increases.

Next, following a second study carried out by Dosskey *et al*. (2011b), the water retention index was calculated for each of the study fields to determine if this metric is correlated with concentrated flow (see Appendix D). The water retention index (WRI =

0.2805 $\log(AR^{0.5}K_{sat})$), where A is the size of the runoff source area in acres, R is the rainfall erosivity, and K_{sat} is the saturated hydraulic conductivity, describes the volume of water that can be retained by a riparian buffer and takes into account the varying sizes of runoff source area in different locations (Dosskey *et al*., 2011b). It was hypothesized that higher values of the water retention index would correspond with decreased flow concentration because the more water retained a riparian buffer, the less water there is as overland flow on the surface to become concentrated.

Lastly, the sediment transport index was calculated for each of the study fields, following the methods of Burkart *et al*. (2004), to determine if it is correlated with concentrated flow (see Appendix E). The sediment transport index ($t = (A_s/22.13)^{0.6}$ (sin $B/0.0896)^{1.3}$), where A_s is the specific catchment area, and B is the slope, describes the ability of flow moving across a landscape to transport sediment. Greater values of this index correspond with greater rates of erosion and higher overland flow velocities. It was hypothesized that higher values of the sediment transport index would correspond with increased flow concentration because higher overland flow velocities increase the likelihood of channelization and the concentration of flow.

The specific catchment area, A_s, for each cell on a field was determined by multiplying the cell's flow accumulation (in cells) by 9 m^2 (the area of each cell) and then dividing this by 3 m (the length of a cell). The slope, B, of each cell on a field was obtained from the slope raster of the field created in the model describe above. The saturated hydraulic conductivity, K_{sat}, for each cell on a field was obtained from the Web Soil Survey (http://websoilsurvey.sc.egov.usda.gov/App/HomePage.htm). The depth above an impermeable subsurface rock or soil layer, D, was the depth to an impermeable

soil layer in this study since the bedrock in the Coastal Plain of Virginia is not near the surface, but shallow impermeable sediment layers do exist. D for each cell on a field was also obtained from the Web Soil Survey. The runoff surface area, A, for each cell on a field was determined by multiplying its flow accumulation (in cells) by 9 m^2 (the area of each cell). The rainfall erosivity, R, was obtained from the Web Soil Survey using the T factor for the soil type of each cell on a field. Each of the 4 indexes described above were calculated for each cell on all 74 of the fields analyzed in this study, however the average value of each index across a field was used in analysis. Plots of average index value on a field versus the percentage of each field drained through the 5 field margin points of greatest flow accumulation area were made to determine if any correlation existed between these indexes and flow concentration.

Principle Component Analysis (See Appendix F)

IBM SPSS Statistics was used to perform principle component analysis in order to analyze variables individually to determine how much each contributes to flow concentration on the fields examined in this study. The variables analyzed using SPSS were the variables used to calculate the above indexes: specific catchment area, slope, saturated hydraulic conductivity, depth above impermeable subsurface layer, runoff source area, and rainfall erosivity. First, the distribution of each of these variables was analyzed and classified as normal or non-parametric. Then, linear regression was performed on each variable and its relationship to flow concentration, where the percentage of each field drained by the 5 field margin points of greatest flow accumulation was used as a proxy for flow concentration. A principle component

analysis was then completed using the six variables stated above, and the first 2 components for each field were taken. These components were plotted against the values of flow concentration on the study fields, and linear regression was performed to determine the relationship between the two principle components and flow concentration.

Results

Extent of Flow Concentration

The size of the 74 studied agricultural fields ranged from 0.01 to 0.71 km^2, with a combined area of 14 km^2 and a combined field margin length of 226 km. A 3 m cell size was used to create the DTMs in this study. Further, the total number of field margin points analyzed (one for each 3 m by 3 m cell along the field margin), or potential areas of flow off the field, was 75,420 points. The average mean slope of the 74 fields was 1.43 degrees with a standard deviation of 0.84 degrees.

The field margin point with the greatest flow accumulation area moving in a direction off the field captured 8% to 83% of the total accumulation area on the each field, with an average over all of the fields of 34%. The percentage of each field area that was drained through the 5, and 10, field margin points (3 m by 3 m cells) of greatest flow accumulation area was determined for all 74 fields. 29% to 100% of a field was drained through the top 5 points, and 41% to 100% was drained through the top 10 points, with an average over all the fields of 70% and 81% respectively. To place this in perspective, the 10 field margin points of greatest flow accumulation area combined from all fields (740 points) receive ~81% of the total field drainage leaving these fields on average, but account for only ~1% of all of the points (75,420) digitized along the field margins. For

63 of the 74 fields, 50% of the field drained through 5 or fewer points along the margin, and 36 of these required only 2 or less points to drain 50% of the field (*Fig. 11*). Further, for 33 of the 74 fields, 75% of the field drained through 5 or fewer points along the field margin, and 9 of these required only 2 or less points to drain 75% of the field (*Fig. 11*).

These results indicate that a large proportion of the agricultural fields analyzed are being drained through just a small proportion of the field margin. Even in the best case scenario, where 40.65% of the field was drained through 10 points, concentrated flow was evident. Thus, flow across agricultural fields within the study area is accumulating in distinct watersheds and exits at limited points.

The results of this study are based on modeled flow patterns, not actual flow, but indicate that the topography in this area tends to promote concentrated flow. Areas of predicted high flow accumulation area by the model used in this study corresponded with field evidence of flow concentration (*Fig. 12*). Field evidence included: directed movement of debris or cleared water pathways, small channel incision, and channelization. Thus, the methodology presented in this study is an adequate way to determine where flow concentration is likely to occur.

Wetness Index

The mean value of the wetness index for each field was compared to the extent of flow concentration on each field (*Fig. 13*). The percentage of field area drained through the 5 field margin points of greatest flow accumulation area was used as a proxy for flow concentration. Fields with greater concentration of flow will have a higher percentage of their overall area draining through these 5 points. The lowest value of the wetness index

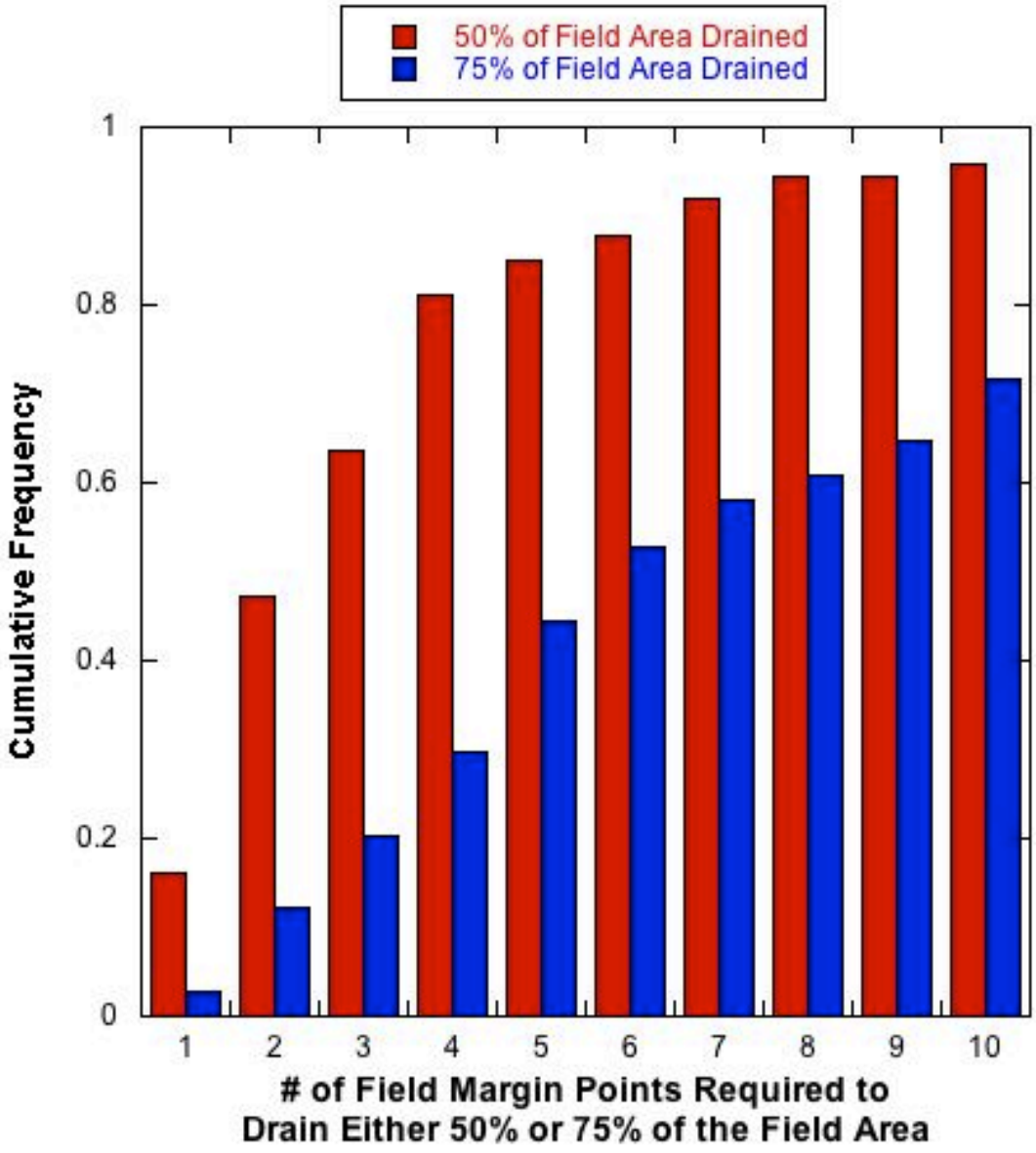

Figure 11. Evidence that flow concentration on agricultural fields is widespread in the Virginia Coastal Plain portion of the Chesapeake Bay watershed. ~95% of the fields analyzed needed 10 or less points along their margins to drain 50% of their total areas.

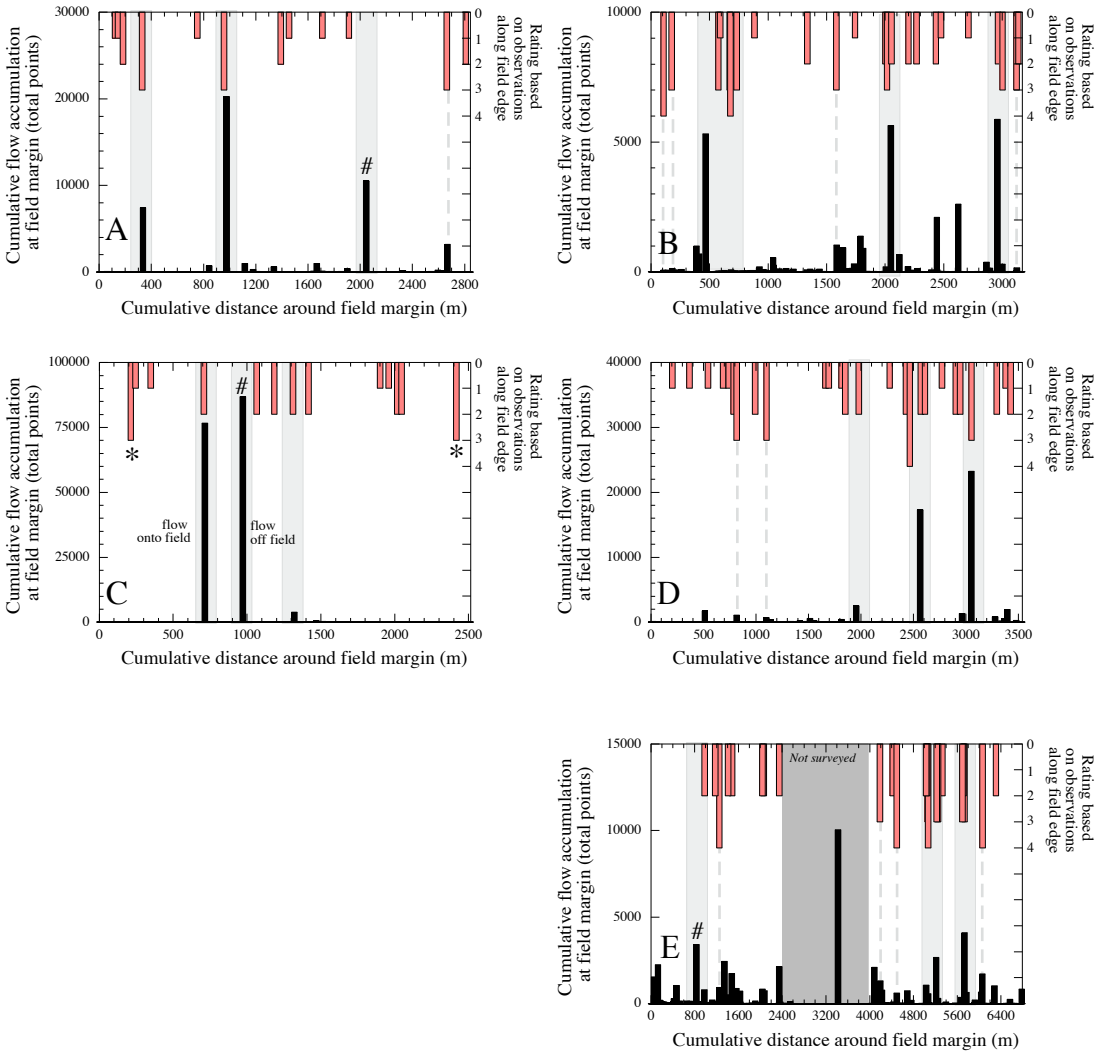

Figure 12. Comparison of predicted areas of concentrated flow based on modeling and actual evidence of concentrated flow for five of the study fields. Black bars represent flow accumulation area along the field margin, determined by the model used in this study. Pink bars represent locations along the field with evidence for flow concentration. Evidence was rated accordingly: 0=no evidence for concentrated flow, 1=evidence of water movement/overland flow, 2=directed movement of debris or clear water pathway, 3=small channel incision, and 4=large/extensive channelization. # indicates an area predicted by the model to have high flow accumulation area, but where no evidence for flow concentration was found. * indicates an area not predicted by the model to have high flow accumulation area, but where evidence for flow concentration was found. Most areas predicted to have very large flow accumulation areas also had evidence of flow concentration, typically of ranks 3 or 4 (analyzed by Dr. Gregory Hancock).

was 1.33 and corresponded to a field where ~60% of the field area is drained through 5 points along the field's margin. The highest value of the wetness index was 4.75 and corresponded to a field where ~79% of the field area is drained through 5 points along the field's margin. The median value of the wetness index was 3.08 and the mean value was 3.17. The wetness index displayed a positive correlation with flow concentration that was statistically significant with $R^2 = 0.32$ (*Fig. 13*).

Topographic Index

The mean value of the topographic index for each field was compared to flow concentration on each field (*Fig. 14*). Again, the percentage of field area drained through the 5 field margin points of greatest flow accumulation area was used as a proxy for flow concentration. The lowest value of the topographic index was -14713.7 and corresponded to a field where ~59% of the field area is drained through 5 points along the field's margin. The highest value of the topographic index was -799.042 and corresponded to a field where ~69% of the field area is drained through 5 points along the field's margin. The median value of the topographic index was -5787.06 and the mean value was -6306.18. The topographic index displayed a positive correlation with flow concentration that was not statistically significant with $R^2 = 0.0137$ (*Fig. 14*).

Water Retention Index

The mean value of the water retention index for each field was compared to flow concentration on each field (*Fig. 15*). Again, the percentage of field area drained through the 5 field margin points of greatest flow accumulation area was used as a proxy for flow

concentration. The lowest value of the water retention index was -0.190 and corresponded to a field where ~60% of the field area is drained through 5 points along the field's margin. The highest value of the water retention index was 0.121 and corresponded to a field where ~59% of the field area is drained through 5 points along the field's margin. The median value of the water retention index was 0.012 and the mean value was 0.002. The water retention index displayed a positive correlation with flow concentration that was not statistically significant with $R^2 = 0.00721$ (*Fig. 15*).

Sediment Transport Index

The mean value of the sediment transport index for each field was compared to flow concentration on each field (*Fig. 16*). Again, the percentage of field area drained through the 5 field margin points of greatest flow accumulation area was used as a proxy for flow concentration. The lowest value of the sediment transport index was 0.028 and corresponded to a field where ~89% of the field area is drained through 5 points along the field's margin. The highest value of the sediment transport index was 0.797 and corresponded to a field where ~29% of the field area is drained through 5 points along the field's margin. The median value of the sediment transport index was 0.221 and the mean value was 0.261. The sediment transport index displayed a negative correlation with flow concentration that was statistically significant with $R^2 = 0.211$ (*Fig. 16*).

Principle Component Analysis

The mean values of each of the six input variables for the above-analyzed indexes for each field were tested for normality. The mean slope values of the 74 fields studied

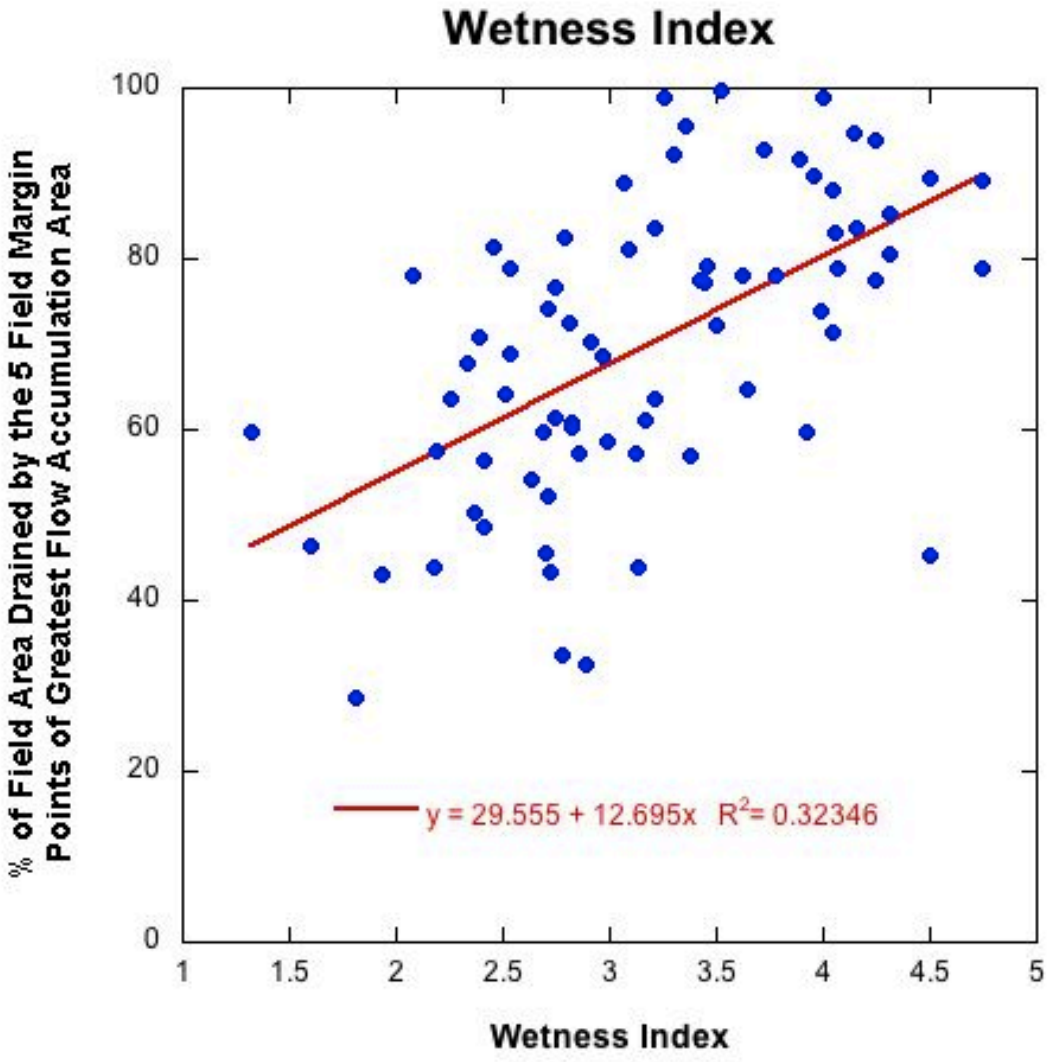

Figure 13. Wetness Index. Each point represents the average value of the wetness index for each of the 74 fields. The average value of the wetness index on each field is plotted against the % of field area drained by the 5 field margin points of greatest flow accumulation area (proxy for flow concentration). ($p = 0.000$)

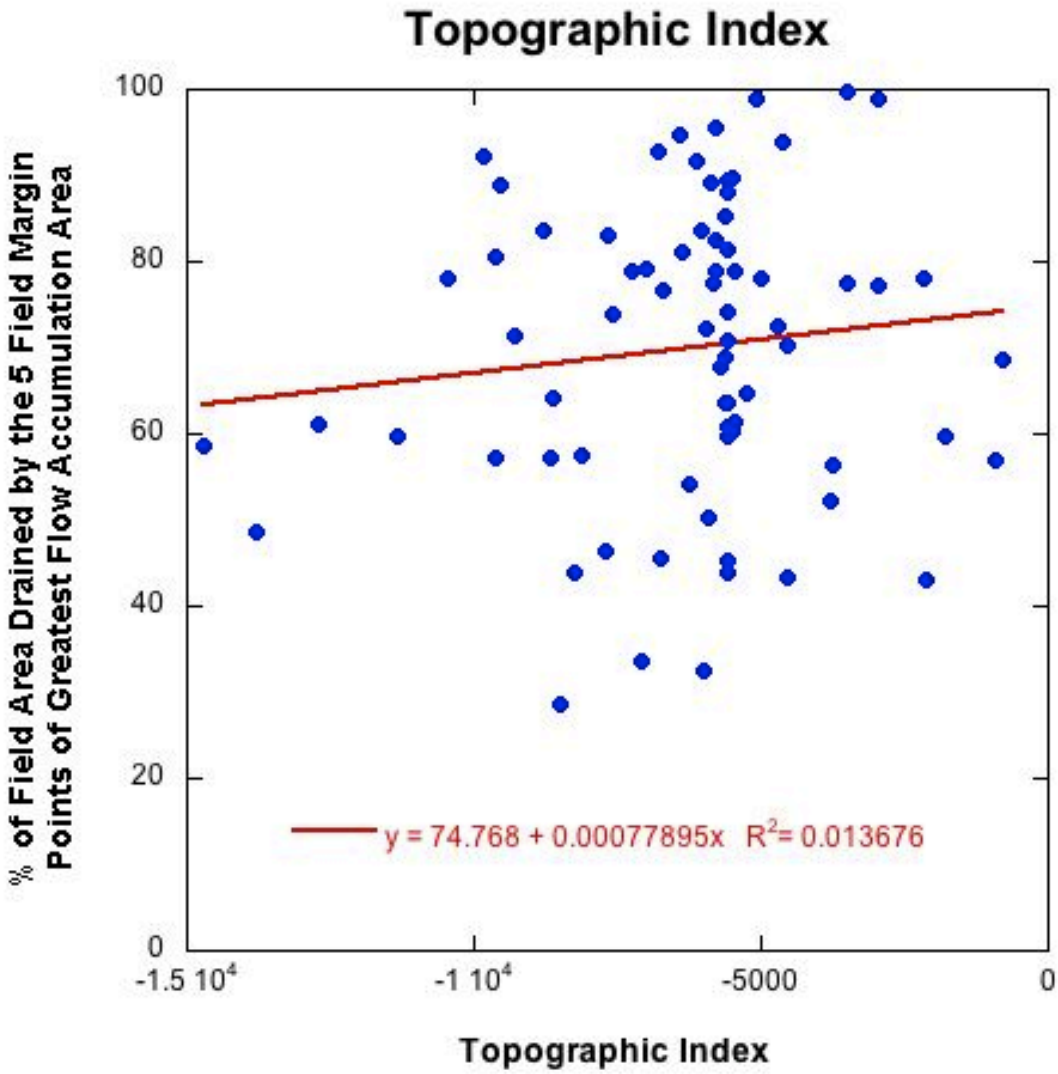

Figure 14. Topographic Index. Each point represents the average value of the topographic index for each of the 74 fields. The average value of the topographic index on each field is plotted against the % of field area drained by the 5 field margin points of greatest flow accumulation area (proxy for flow concentration). ($p = 0.401$)

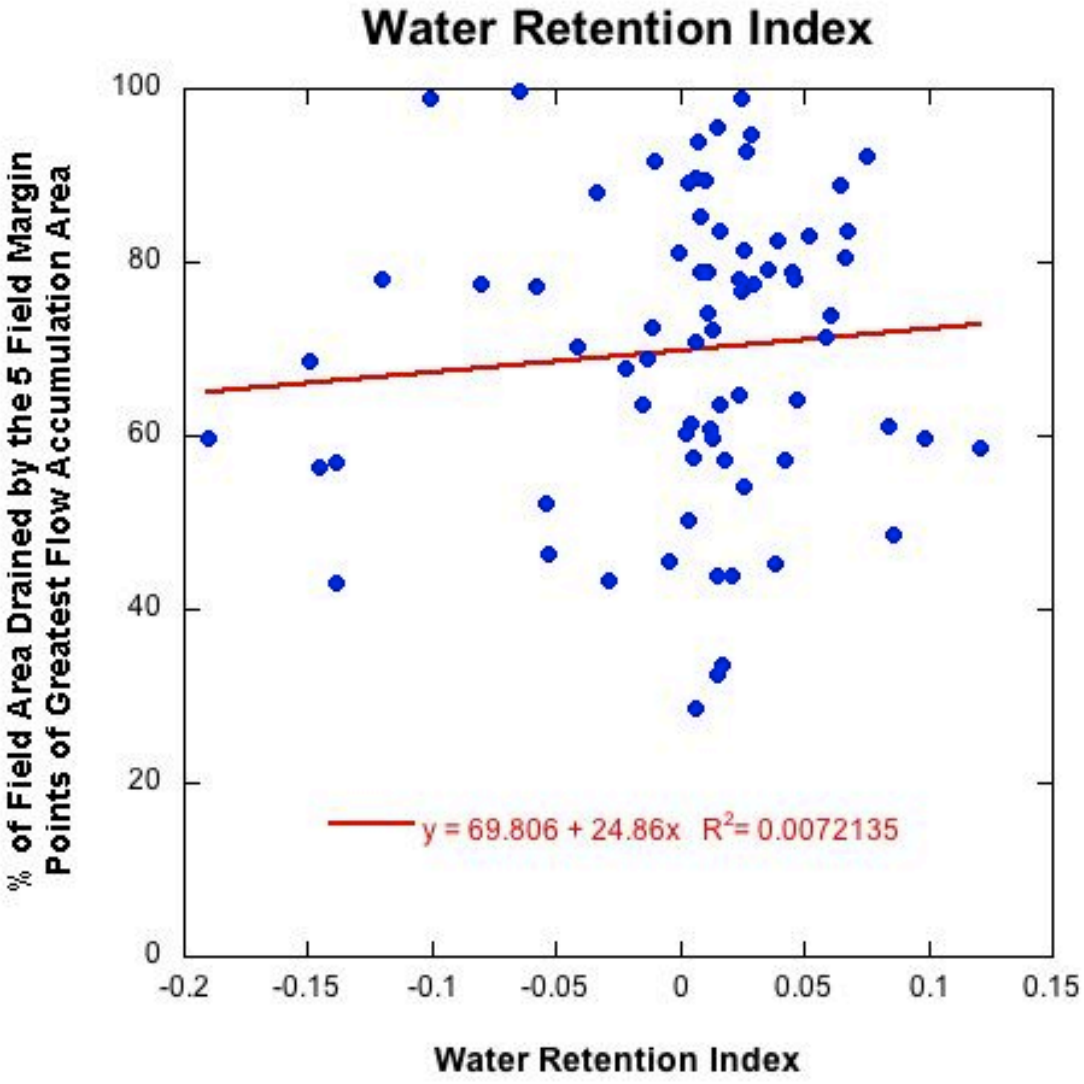

Figure 15. Water Retention Index. Each point represents the average value of the water retention index for each of the 74 fields. The average value of the water retention index on each field is plotted against the % of field area drained by the 5 field margin points of greatest flow accumulation area (proxy for flow concentration). ($p = 0.472$)

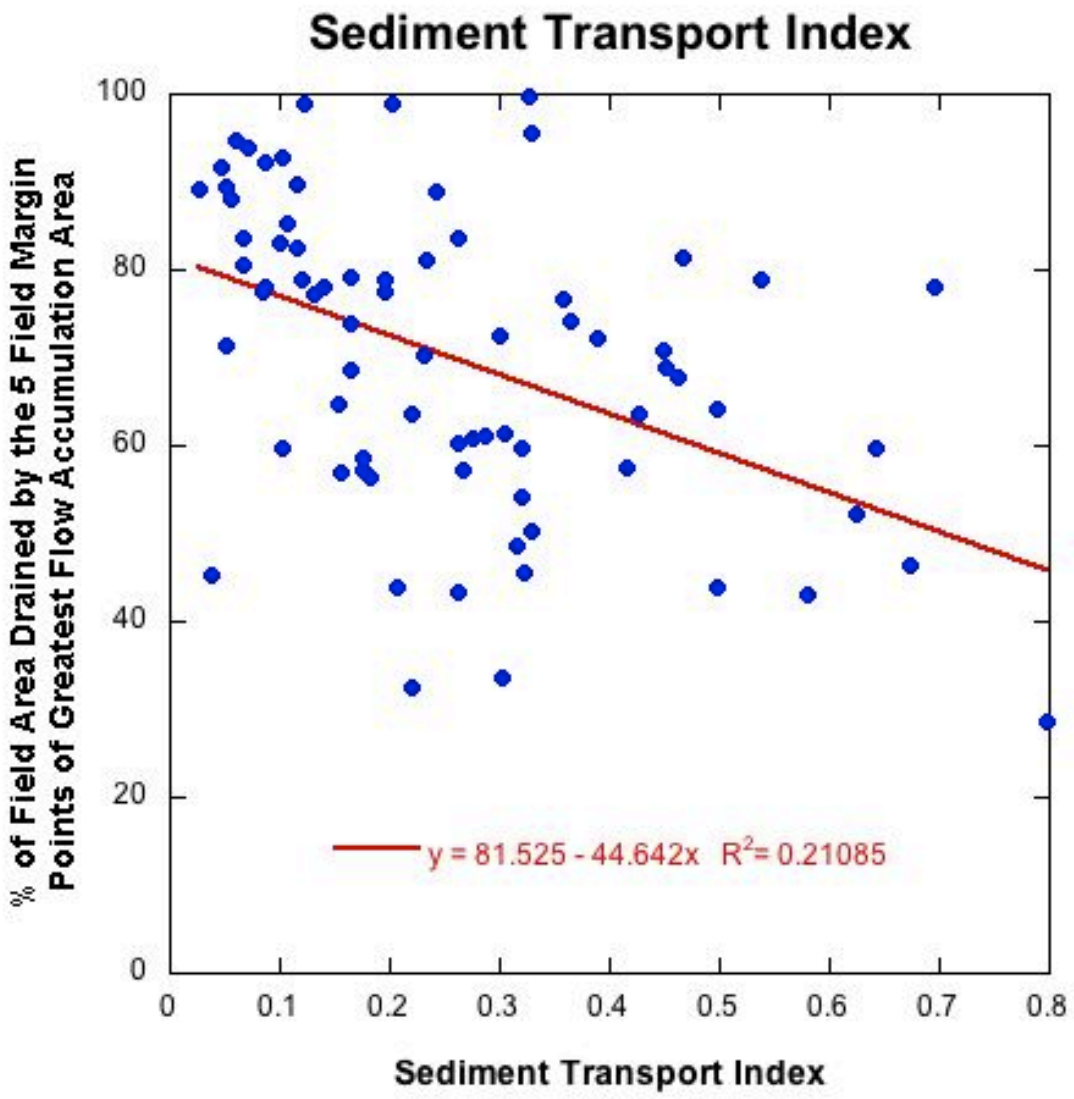

Figure 16. Sediment Transport Index. Each point represents the average value of the sediment transport index for each of the 74 fields. The average value of the sediment transport index on each field is plotted against the % of field area drained by the 5 field margin points of greatest flow accumulation area (proxy for flow concentration). ($p = 0.000$)

were normally distributed with a mean of 0.02 degrees, and a standard deviation of 0.015 degrees. The mean specific catchment area (the average specific catchment area of the cells on a field), mean runoff source area (the average runoff source area of the cells on a field), mean saturated hydraulic conductivity (K_{sat}), mean depth above impermeable subsurface layer (D), and mean rainfall erosivity (R) values on the 74 fields were non-parametrically distributed. For these non-parametrically distributed variables the following transformations were used to attempt to transform the data to be normally distributed: sqrt(X) for variables moderately skewed to the right, log10(X) for variables heavily skewed to the right, sqrt(K-X) for variables moderately skewed to the left, and log10(K-X) for variables heavily skewed to the left, where K is a constant from which each value of a variable is subtracted so that the smallest score is 1 (Howell, 2007; Tabachnick and Fidell, 2007). The proxy values for flow concentration (% of field area drained by the 5 field margin points of greatest flow accumulation area) on each the 74 study fields analyzed were normally distributed with a mean of 69.86% and a standard deviation of 17.33%. Graphs from these tests of normality are shown in Appendix G.

Linear regression tests were run to compare each of the individual variables used in the field indexes to flow concentration on the study fields. The R^2 values for each were as follows: mean specific catchment area, 0.160; mean runoff source area, 0.160; mean slope, 0.270; mean K_{sat}, 0.010; mean D, 0.004; and mean R, 0.081. These relationships are shown in *Figures 17-22*. The mean specific catchment area, mean runoff source area, mean slope, and mean R relationships were statistically significant. The mean K_{sat} and Mean D relationships were not statistically significant.

Principle component analysis was then run on the six variables listed above (*Tab. 1*). Transformations of the mean specific catchment area (log10(X)) and the mean runoff source area (log10(X)) were used in place of the untransformed variables in this analysis because these transformations increased the normality of these variables (Appendix G). A Scree plot (*Fig. 23*) was created and 2 components were extracted (*Tab. 2*). Component 1 had a positive relationship with flow concentration (*Fig. 24*) that was statistically significant with an R^2 value of 0.403. Component 2 showed little correlation with flow concentration (*Fig. 25*) that was not statically significant with an R^2 value of 0.001.

Discussion

The results of this study suggest that flow accumulation is highly concentrated at a few points along agricultural field margins. The model used in this study indicates that flow concentration is likely to occur on all 74 of the fields analyzed. These results suggest that flow concentration is both common on agricultural fields and prevalent over a widespread area of the Virginia Coastal Plain. Previous studies, for example Dosskey *et al*. (2002), have noted that flow concentration through riparian buffers reduces buffer effectiveness, but few studies have analyzed this over a large geographic area, such as done in this study across the Coastal Plain of Virginia. The prevalence of flow concentration on agricultural fields throughout the Coastal Plain of Virginia may be one reason why the goals of the CBA of 1987 have not been met. Flow convergence can lead to channelization. When runoff is channelized through buffers its velocity is not slowed,

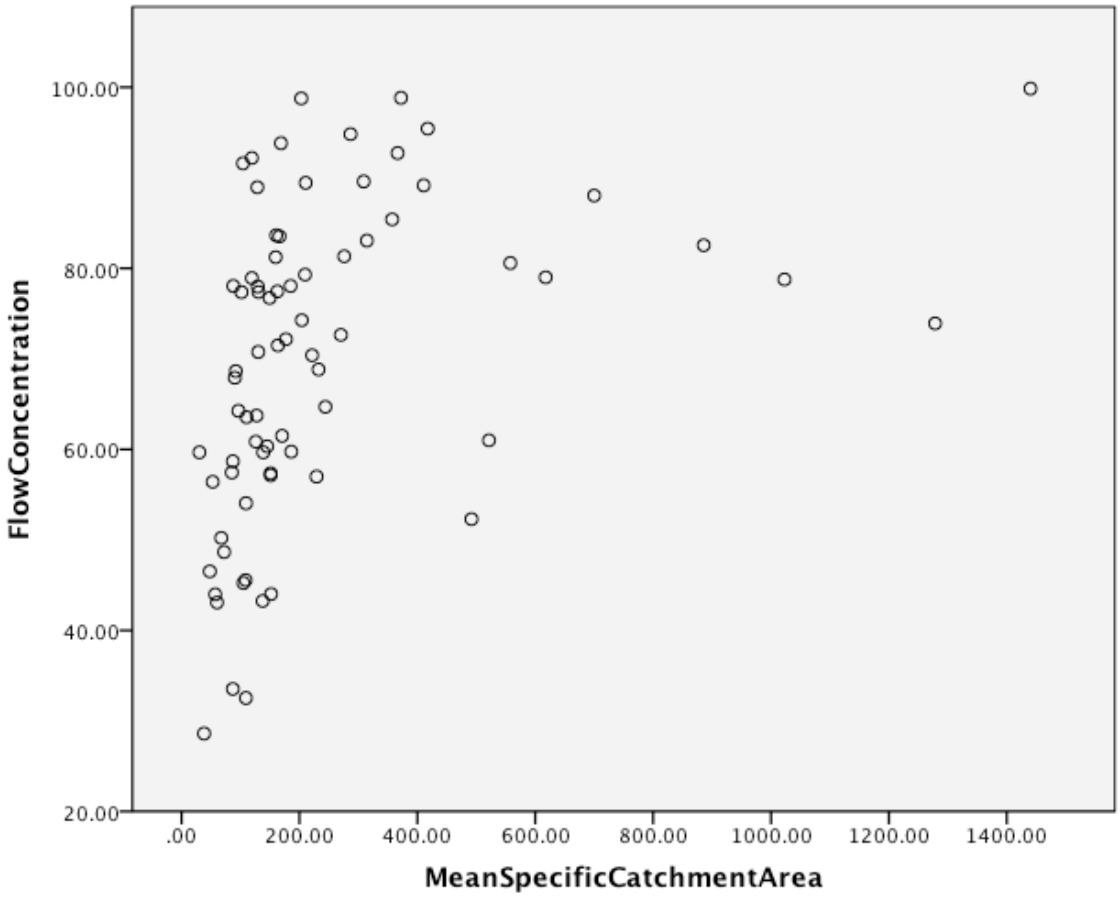

Figure 17. Relationship between mean specific catchment area (in m^2) and flow concentration on each field, where flow concentration is defined as the percentage of field area drained through the 5 field margin points of greatest flow accumulation area. ($R^2 = 0.160$; $p = 0.000$)

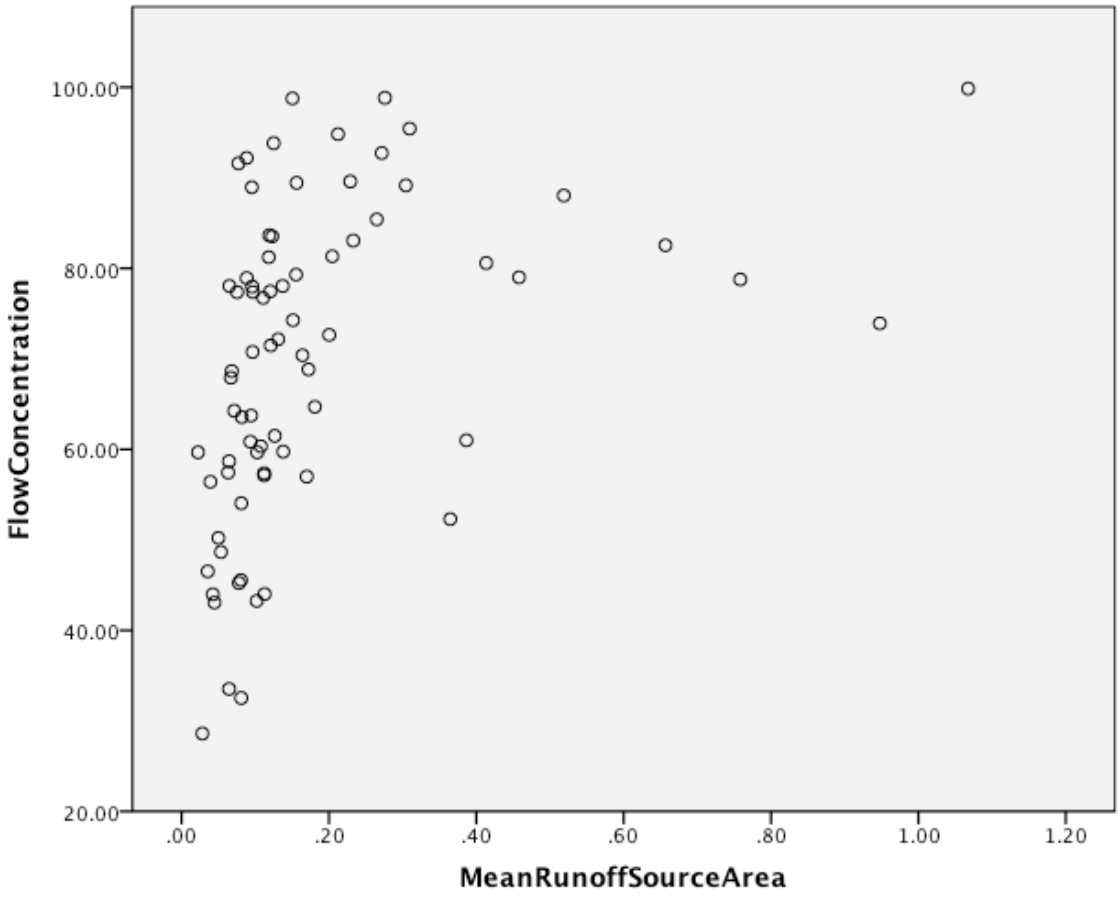

Figure 18. Relationship between mean runoff source area (in m^2) and flow concentration on each field, where flow concentration is defined as the percentage of field area drained through the 5 field margin points of greatest flow accumulation area. ($R^2 = 0.160$; $p = 0.000$)

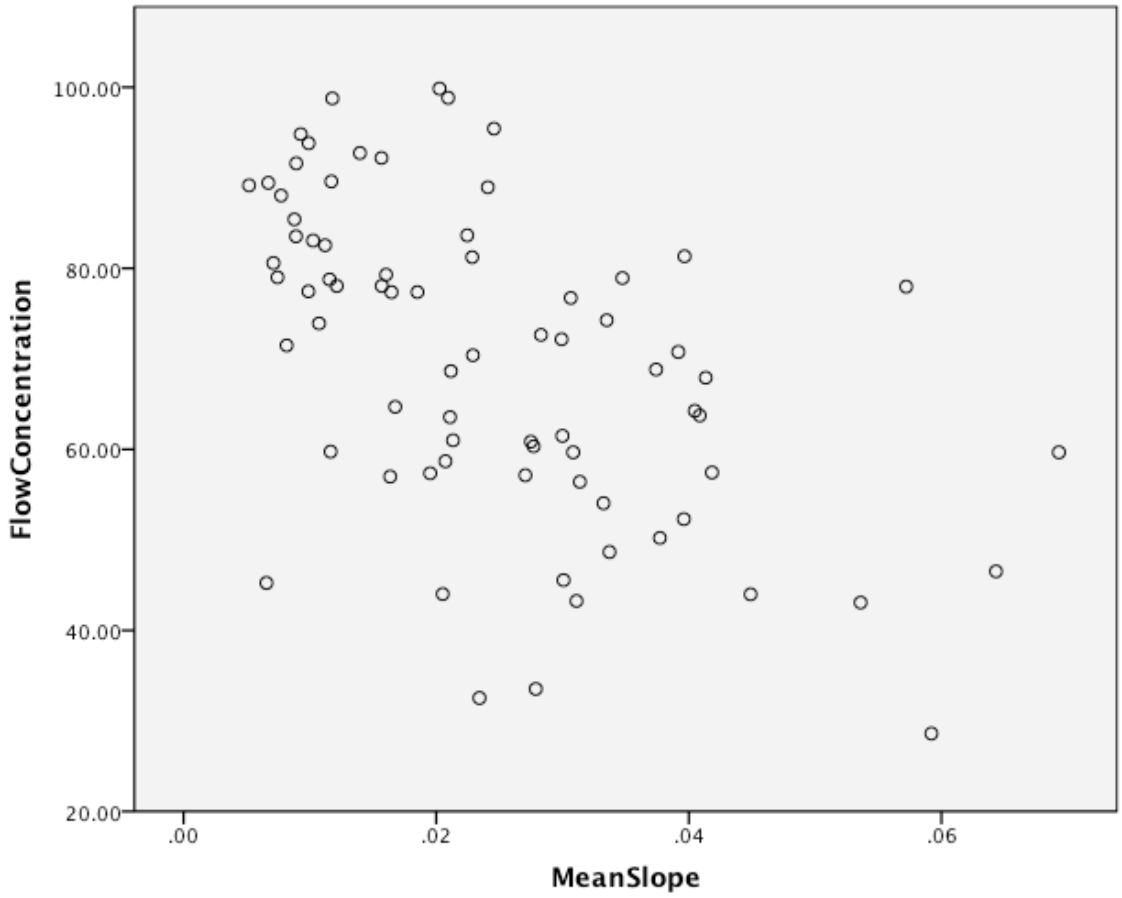

Figure 19. Relationship between mean slope (in degrees) and flow concentration on each field, where flow concentration is defined as the percentage of field area drained through the 5 field margin points of greatest flow accumulation area. ($R^2 = 0.270$; $p = 0.000$)

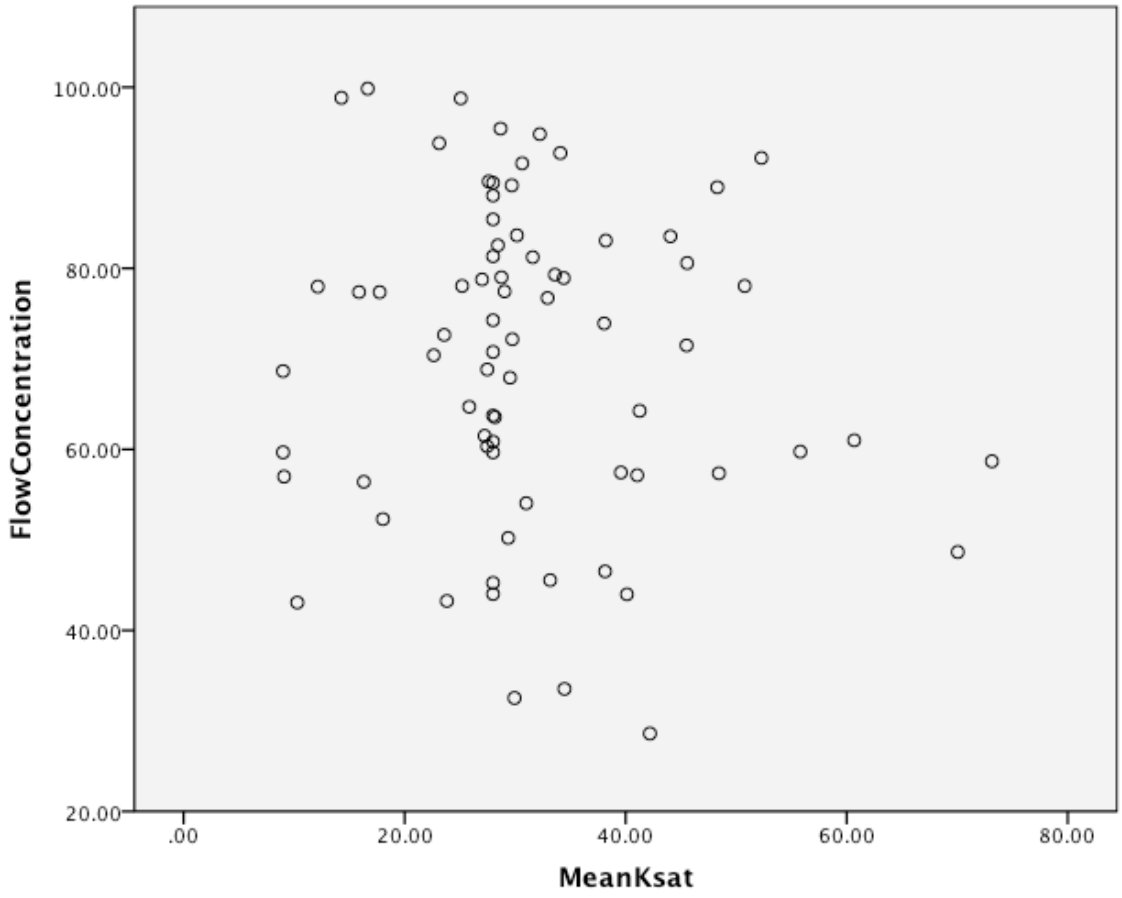

Figure 20. Relationship between mean Ksat (in µm/s) and flow concentration on each field, where flow concentration is defined as the percentage of field area drained through the 5 field margin points of greatest flow accumulation area. ($R^2 = 0.013$; $p = 0.332$)

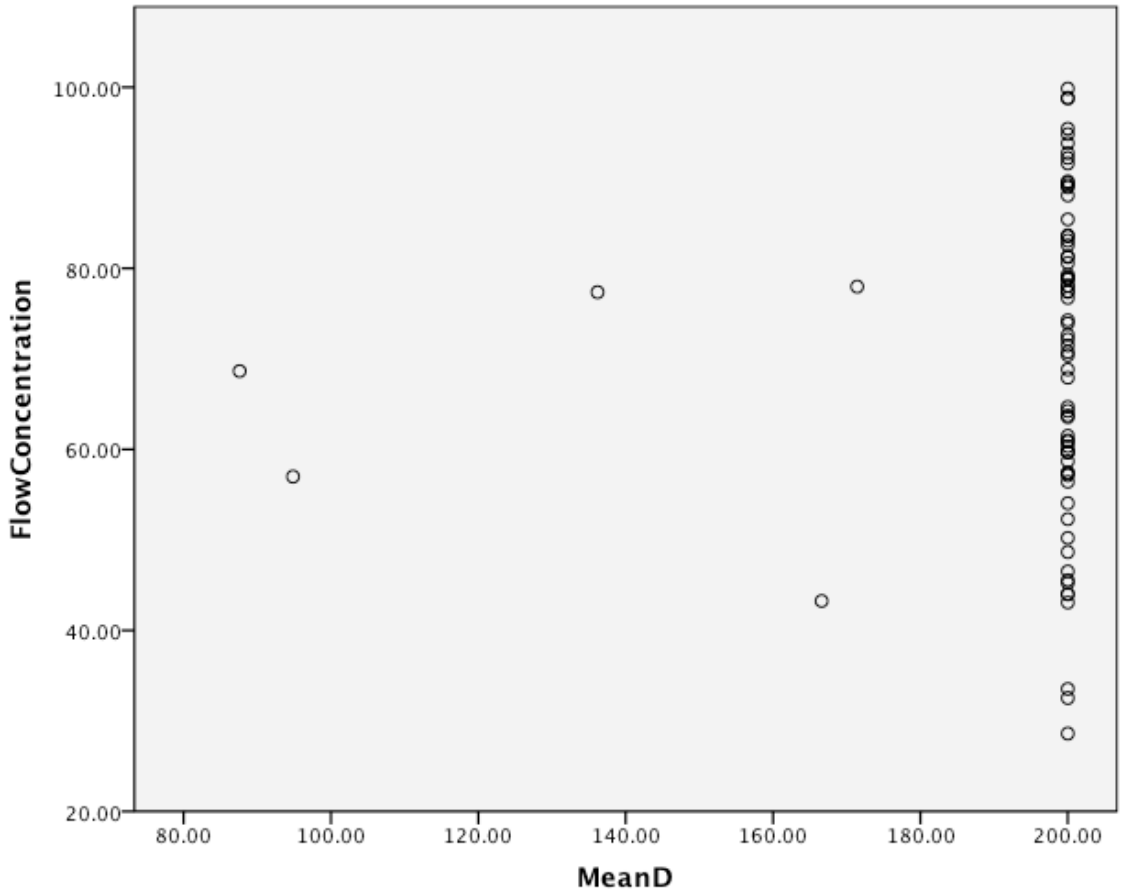

Figure 21. Relationship between mean D (in cm) and flow concentration on each field, where flow concentration is defined as the percentage of field area drained through the 5 field margin points of greatest flow accumulation area. ($R^2 = 0.004$; $p = 0.570$)

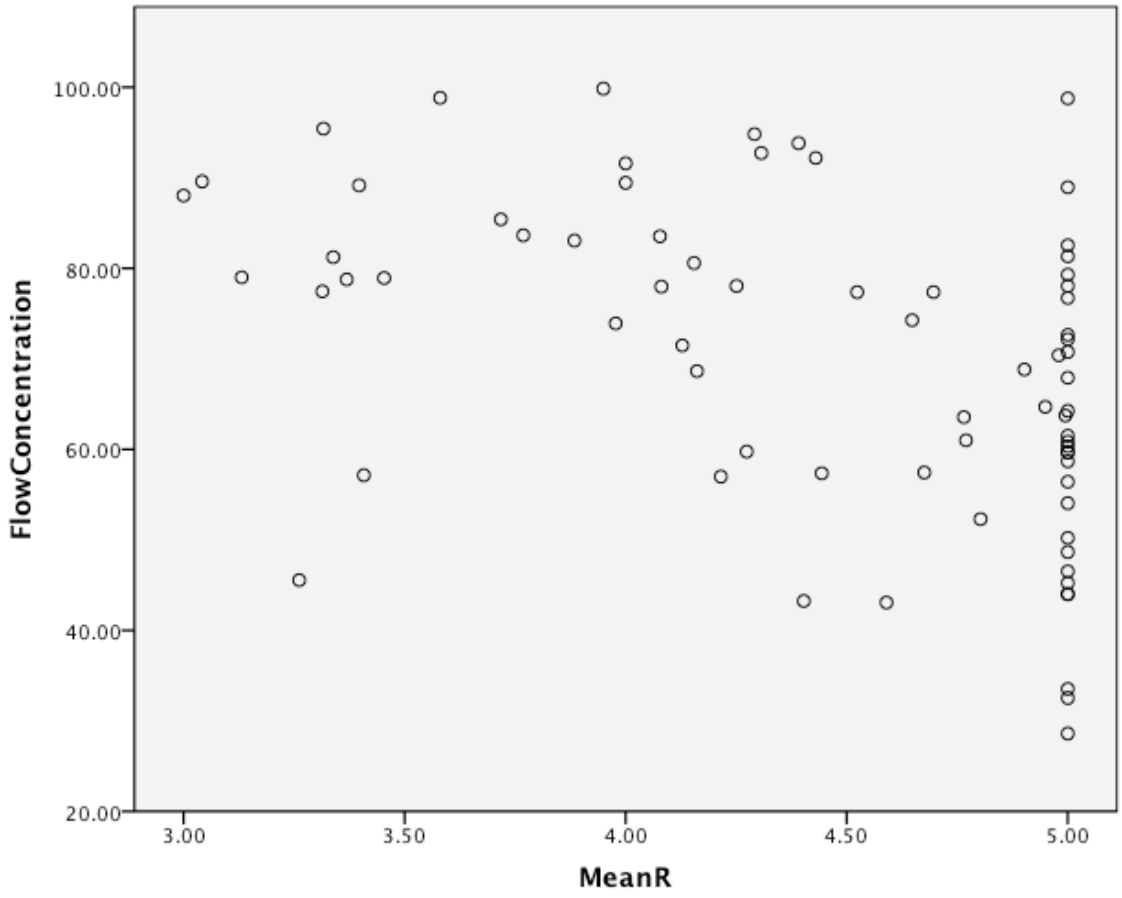

Figure 22. Relationship between mean R (in tons/acre/year) and flow concentration on each field, where flow concentration is defined as the percentage of field area drained through the 5 field margin points of greatest flow accumulation area. ($R^2 = 0.218$; $p = 0.000$)

Total Variance Explained

Component	Initial Eigenvalues			Extraction Sums of Squared Loadings		
	Total	% of Variance	Cumulative %	Total	% of Variance	Cumulative %
1	2.796	46.602	46.602	2.796	46.602	46.602
2	1.383	23.057	69.660	1.383	23.057	69.660
3	.813	13.545	83.204			
4	.627	10.453	93.657			
5	.381	6.343	100.000			
6	-5.233E-16	-8.721E-15	100.000			

Extraction Method: Principal Component Analysis.

Table 1. Principle Component Analysis. This table describes the total variance between the 6 input variables: log10(mean specific catchment area), log10(mean runoff source area), mean slope, mean Ksat, mean D, and mean R.

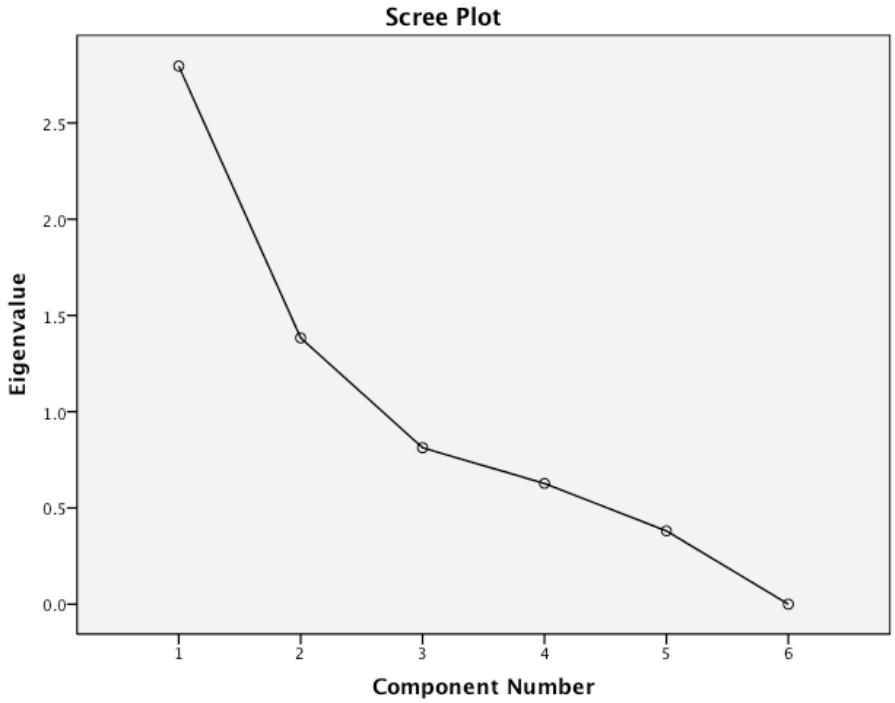

Figure 23. Scree Plot for the principle component analysis of the 3 topographic and 3 soil property characteristics analyzed.

Component Matrix[a]

	Component	
	1	2
Log10MSCA	.941	.006
Log10MRSA	.941	.006
MeanSlope	-.767	-.105
MeanKsat	-.030	.832
MeanD	.043	.810
MeanR	-.659	.153

Extraction Method: Principal Component Analysis.

a. 2 components extracted.

Table 2. Relationships between Component 1 and Component 2 and the 3 topographic and 3 soil property characteristics analyzed. Positive numbers indicate positive relationships and negative numbers indicate negative relationships.

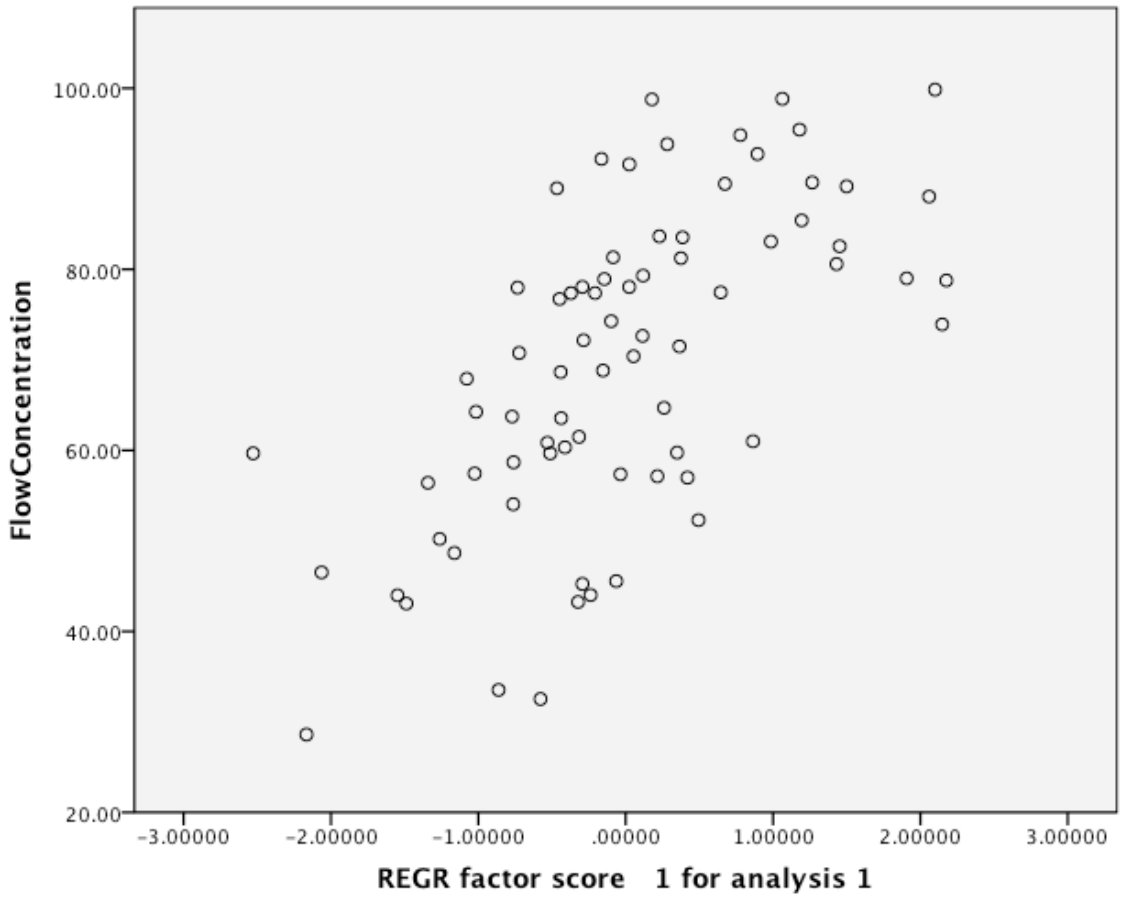

Figure 24. Relationship between Component 1 (and flow concentration on each field, where flow concentration is defined as the percentage of field area drained through the 5 field margin points of greatest flow accumulation area. ($R^2 = 0.403$; $p = 0.000$)

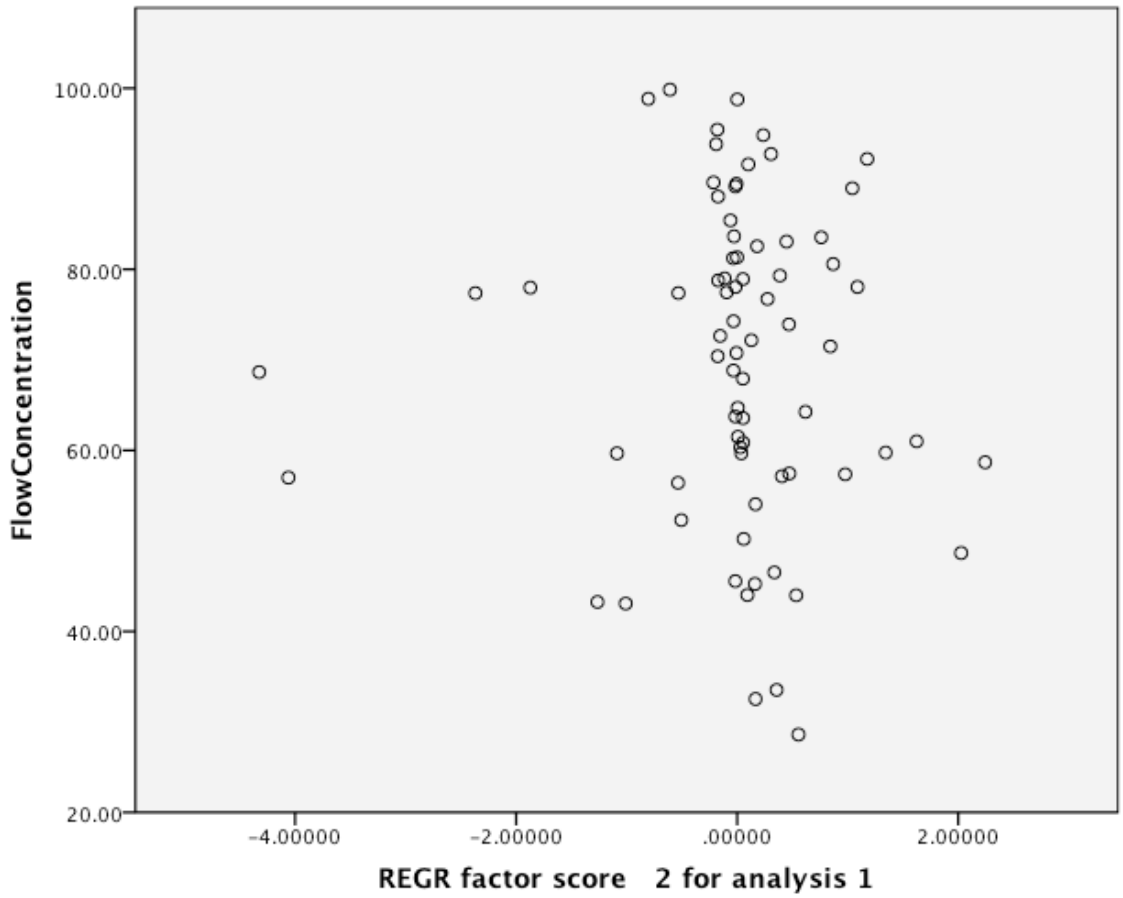

Figure 25. Relationship between Component 2 and flow concentration on each field, where flow concentration is defined as the percentage of field area drained through the 5 field margin points of greatest flow accumulation area. ($R^2 = 0.001$; $p = 0.758$)

so less sediment is allowed to settle out, and less infiltration into the subsurface occurs, where nutrients are absorbed by riparian vegetation (Dosskey *et al*., 2002; Knight *et al*., 2010). The estimates made by Lowrance *et al*. (1997) that forested riparian buffers may accomplish nitrogen, phosphorous, and sediment reductions of ~75%, ~77%, and ~96% respectively, were dependent on a contributing area:buffer area ratio of ~2:1 (Lowrance *et al*., 1984). If channelization of runoff leaving agricultural fields is widespread in the Coastal Plain region of Virginia, which the model in this study strongly suggests, the buffer area in Lowrance *et al*.'s (1984) ratio is reduced to the effective buffer area (*Fig. 3*), and the ratio is increased. It is likely that flow concentration is leading to high contributing area:buffer area ratios in the Coastal Plain region of Virginia. This may explain why the riparian buffers required by the CBPA have not been as effective as predicted.

The wetness index, topographic index, water retention index, and sediment transport index are well-known field indexes that are used to describe the relationships between topography, soil, and water on agricultural fields. The wetness index showed the best correlation with flow concentration ($R^2 = 0.32$) on the fields analyzed in this study (*Fig. 12*). While the 4 field indexes examined in this study have uses in predicting the propensity for soil saturation and water table rising, the volume of water able to be retained in riparian buffers, and the ability of water to transport sediment (Burkart *et al*., 2004; Dosskey *et al*., 2011a; Dosskey *et al*., 2011b), none are good predictors of flow concentration across agricultural fields in the Coastal Plain region of Virginia. For any given value of one of these indexes, there is a large variance in the possible extent of flow concentration that could be found on a field. For example, a wetness index value of 3

could represent a field where from ~30% to ~90% of the field area might be drained by the 5 field margin points of greatest flow accumulation area (*Fig. 12*).

Specific catchment area, runoff source area, slope, saturated hydraulic conductivity, depth above an impermeable subsurface layer, and rainfall erosivity are also not good predictors of areas where flow concentration is likely to occur. Of these, the field slope had the greatest correlation with flow concentration ($R^2 = 0.270$) (*Fig. 19*). The highest correlation was seen between component 1, an index of these 6 variables from the principle component analysis run on them, and flow concentration ($R^2 = 0.403$) (*Fig. 24*). However, for any single value of component 1, flow concentration has a large variance. A component 1 value of 0 could represent a field where from ~45% to ~100% of the field area might be drained by the 5 field margin points of greatest flow accumulation area (*Fig. 24*), thus component 1 would not be a good predictor of flow concentration. Rather than being attributable to differences in any single topographic characteristic, soil property characteristic, or field index value, flow concentration seems to occur across the Coastal Plain region of Virginia as a whole. Thus, it does not matter where riparian buffers are required throughout the Coastal Plain region of Virginia, as the widespread phenomenon of flow concentration likely renders them ineffective at removing nutrients and sediment from agricultural runoff on most fields.

The primary limitations of this study exist in the calculation of the field indexes and the analysis of the relationship between soil property characteristics and flow concentration. When calculating the Wetness Index ($w = \ln(A_s / B)$, where A_s is the specific catchment area, and B is the slope), the natural log could not be taken if A_s was equal to 0 m, and the function was undefined if B was equal to 0 degrees. This was also

true when calculating the Topographic Index ($TI = \ln(A_s / B) – (K_{sat}D)$, where A_s is the specific catchment area, B is the slope, K_{sat} is the saturated hydraulic conductivity, and D is the depth above an impermeable subsurface layer). Data cells on fields where this occurred were given no data value and were not accounted for in the average w and TI for the field. When calculating the Water Retention Index ($WRI = 0.2805 * \log(AR^{0.5}K_{sat})$, where A is the runoff source area, R is the rainfall erosivity, and K_{sat} is the saturated hydraulic conductivity), the log could not be taken if A, R, or K_{sat} were equal to 0. Data cells on fields where this occurred were also given no data value and were not accounted for in the average WRI for the field. Further, the saturated hydraulic conductivity (K_{sat}) and rainfall erosivity (R) were unknown for a few soil types. Cells on fields with unknown values for K_{sat} and/or R were given no data value and not used in the index calculations, the linear regression analyses between K_{sat} and/or R and flow concentration, or the principle component analysis. However, this only occurred in very small areas on only 10 fields. Additionally, if the depth to impermeable subsurface layer (D) was greater than 200 cm, the vertical extent of the Web Soil Survey, 200 cm was assigned to a cell as the value of D in order to be able to calculate the Topographic Index.

This study sought to find a metric that was correlated with concentrated flow and that would be easy to calculate for a large geographic area so that areas where flow concentration might be likely to reduce the effectiveness of riparian buffers could be located without having to analyze agricultural fields individually. While no such metric was found, the results of this study suggest that flow concentration occurs throughout the Coastal Plain of Virginia. Future research should focus on ways to reduce concentrated flow on agricultural fields, and subsequently to increase the effectiveness of riparian

buffers at absorbing nutrients and trapping sediment in agricultural runoff. Three potential alterations that might increase the effectiveness of riparian buffers in the Coastal Plain of Virginia are discussed below.

Changing the constant-width, 100-foot, riparian buffer design that is currently mandated by law along perennial streams and RPAs in the Coastal Plain of Virginia to a variable-width buffer design may increase the effectiveness of these buffers. This design increases the width of riparian buffers in areas with more runoff, and decreases their widths in areas with little runoff (*Fig. 26*). Dosskey *et al*. (2005) suggests that the width of current riparian buffers be assessed to determine the contributing area to buffer area ratio along the sections of agricultural field margins where riparian buffers are required by law; then, in areas where this ratio is greater than 2:1, the buffer should be widened until the 2:1 ratio is achieved (Dosskey *et al*., 2005). However, this method is difficult to implement in a large geographical area, like the Coastal Plain of Virginia, because it requires analysis of every individual field. Future research might include performing a GIS-based analysis on the contributing area to buffer area ratio for riparian buffers in the Coastal Plain region of Virginia. Such an analysis could provide the widths needed to achieve the 2:1 ratio for all Coastal Plain riparian buffers. With the variable-width buffer design, the effectiveness of riparian buffers should increase, allowing for improvement in both the ecological health of the Bay and its fisheries and tourism industry. Also, only being required to have wide buffers in a few discrete locations along their agricultural field margins where runoff drains, would allow farmers more land on which to grow additional crops.

A second alteration to the current riparian buffer legislation that may help to

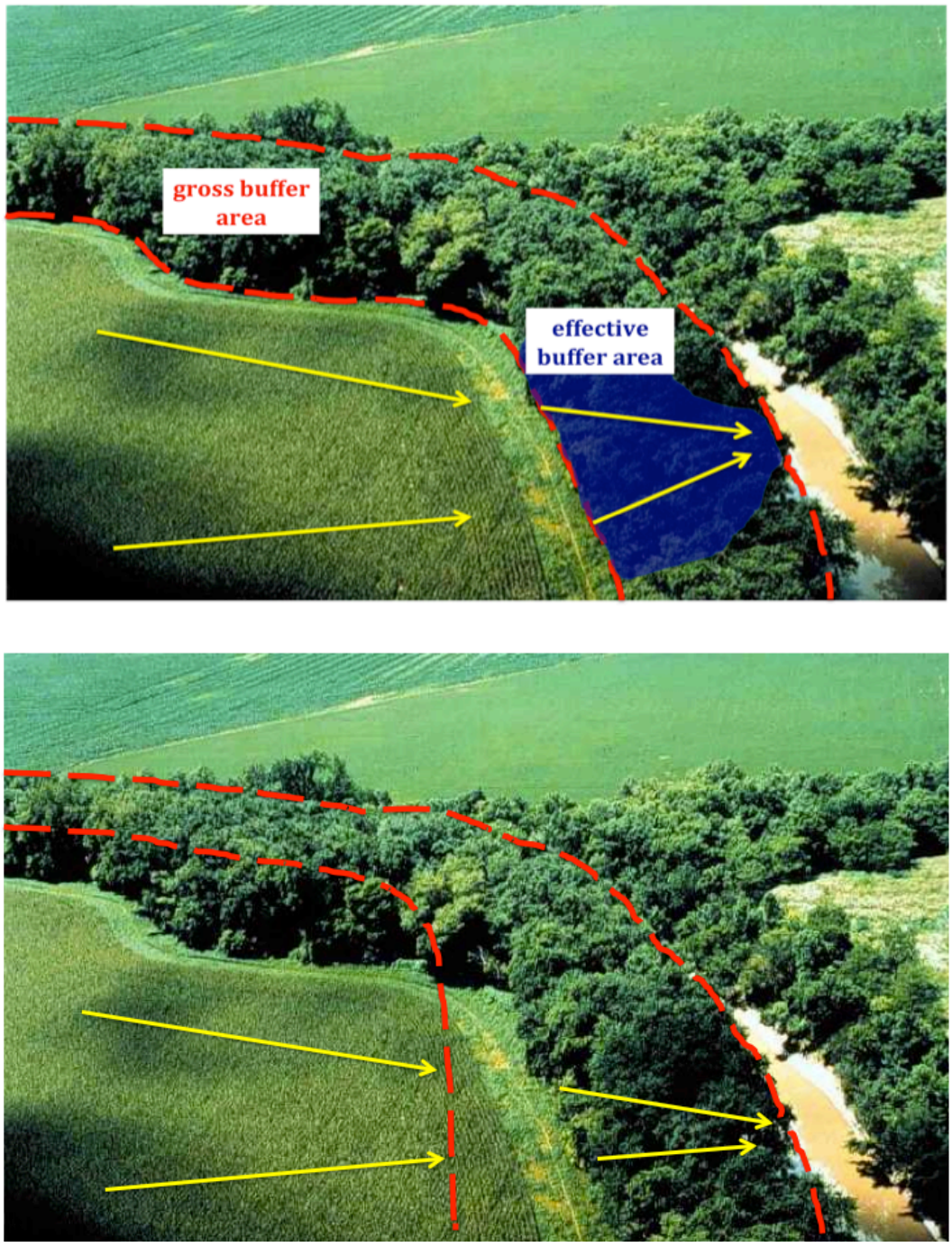

Figure 26. Variable-width Buffer Design. Current legislation requires 100-foot riparian buffers between agricultural fields and perennial streams (top diagram). A variable-width buffer would be thinner in areas with little to no runoff and thicker in areas with more runoff (bottom diagram). Red dashed lines represent the boundaries of the buffer, while yellow arrows depict runoff patterns.

decrease the amounts of nutrients and sediments being delivered to Chesapeake Bay is to require riparian buffers on agricultural fields in areas with high flow accumulation area in addition to lands adjacent to perennial streams and RPAs (*Fig. 27*). Future research would be needed to determine a threshold flow accumulation area level, above which a riparian buffer would be required (e.g. areas on agricultural fields with flow accumulation area > 50 m^2 must be a forested riparian buffer). This requirement would allow runoff to be intercepted further away from a perennial stream than 100 m, and may help to reduce flow concentration and channelization. Further, with more buffer along the pathways of water flow on agricultural fields, runoff would spend more time in buffer root systems, potentially allowing for increased absorption of nutrients and trapping of sediment. The drawback to this alternative is that it would be hard to implement; individual farmers would have to be told which areas of their fields exceed the threshold flow accumulation level and must be converted to buffer.

A third alternative would be to require farmers to alter their field drainage system so that runoff exists their fields more uniformly. This would involve requiring farmers to have a specified number of drainage ditches per area of riparian buffer (*Fig. 28*). Future research would need to be conducted to determine how many drainage ditches per area of riparian buffer in the Coastal Plain of Virginia could reduce flow concentration levels such that channelization does not occur in buffers. More drainage ditches could help to disperse flow through riparian buffers and increase the contributing area to effective buffer area ratio. However, runoff volume differs with locality due to precipitation, soil type, and surface cover differences, and thus an area with more runoff might need more drainage ditches per area of riparian buffer than one with less runoff. Implementation of

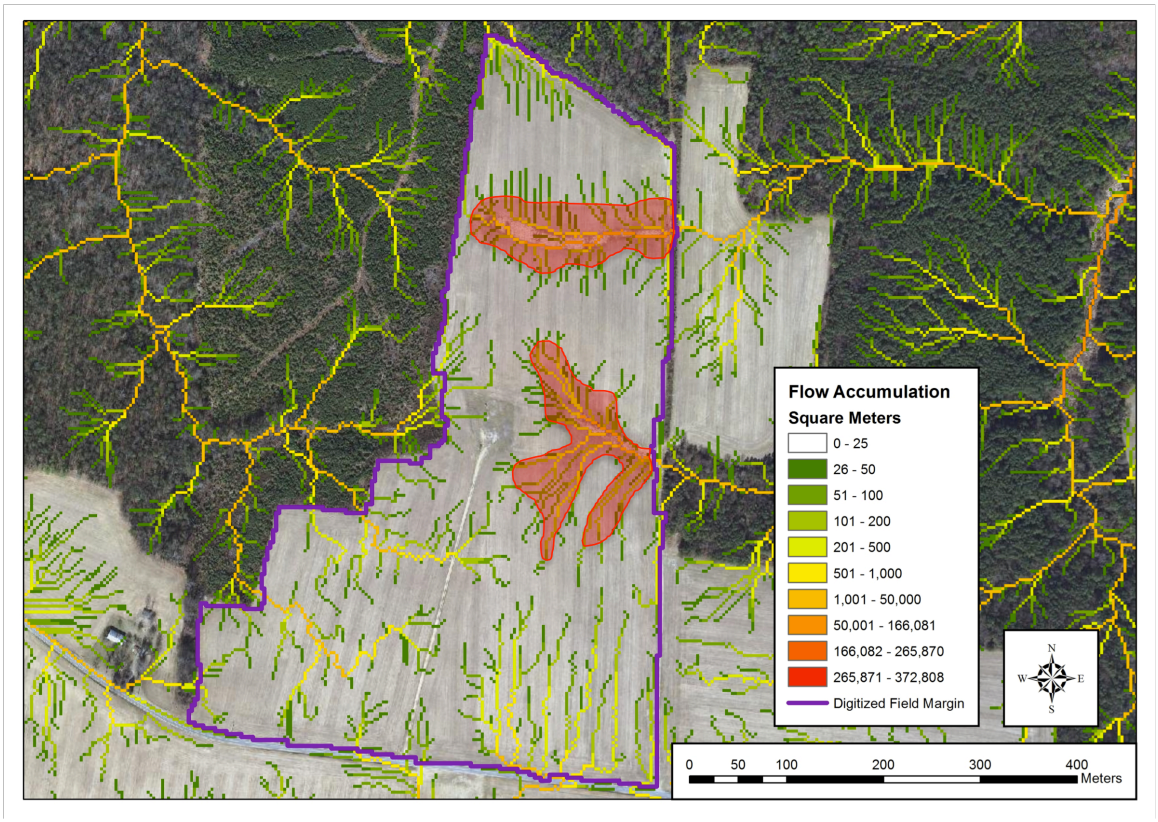

Figure 27. Areas of concentrated flow on an example field that might be required to have a buffer. The perennial stream nearby this field is on the right. In this example, buffers are required in areas with flow accumulation > 50 m^2 that drain into the perennial stream; these areas are shaded in red.

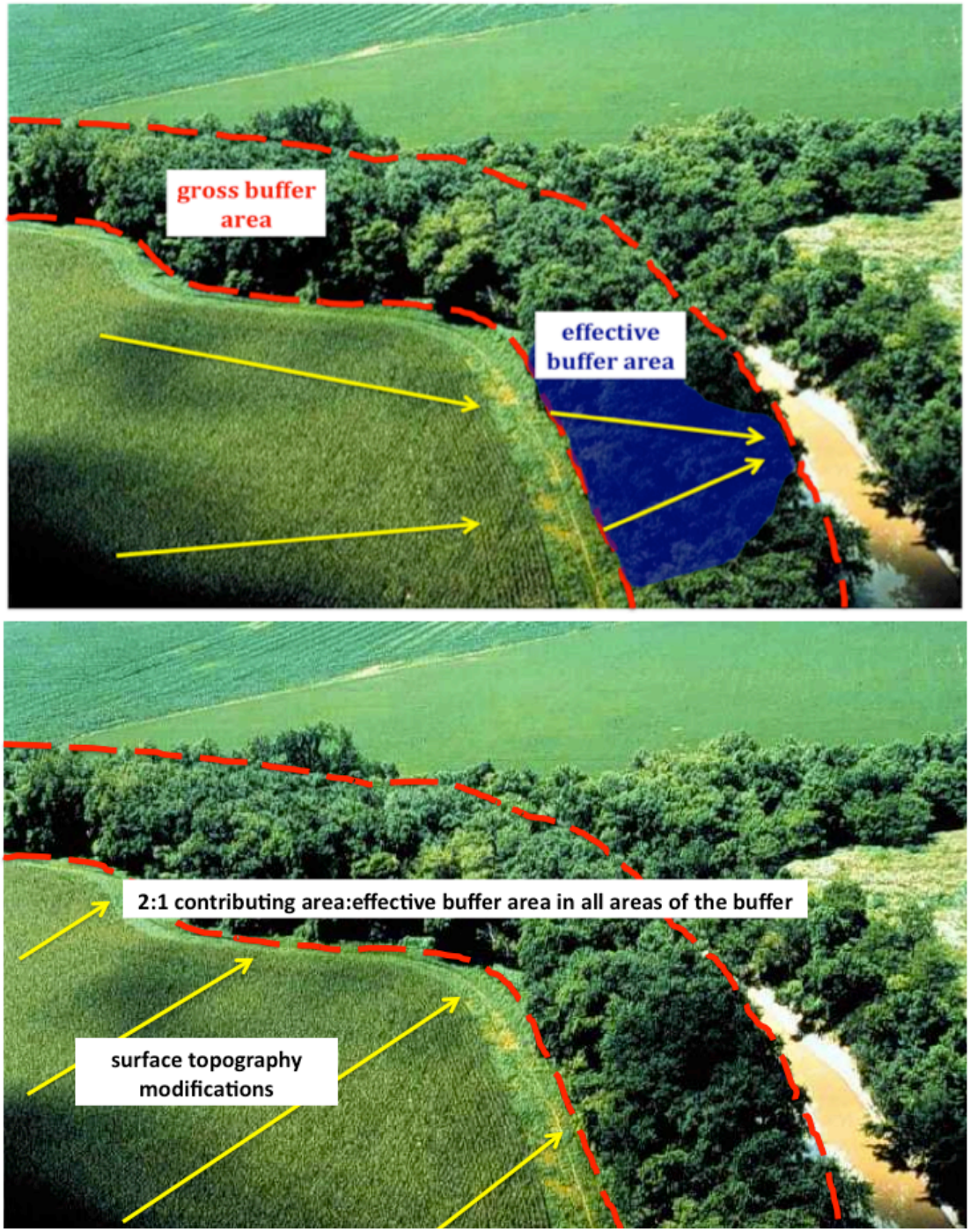

Figure 28. Example modification of flow patterns on a field. This diagram depicts how modifying the topography of this field by adding drainage ditches (bottom diagram) may help increase the 2:1 contributing area to effective buffer area that leads to flow concentration (as shown in the top diagram). Red dashed lines represent the boundaries of the buffer, while yellow arrows depict runoff patterns.

this throughout the whole of the Coastal Plain of Virginia might be difficult because different localities would have different drainage ditch to riparian buffer area requirements, which would be hard to incorporate into legislation for this large geographic area.

I propose that the requirement of a 100-foot riparian buffer between agricultural fields and perennial water bodies that drain to Chesapeake Bay, as required by the Chesapeake Bay Protection Act, be amended. I advocate amending the law to require that farmers maintain riparian buffers on their land yearly, in order to prevent the formation of channels through the buffers that reduce their effectiveness at removing nutrients and sediment from agricultural runoff. This would require farmers to fill-in any channels that form in riparian buffers on their land and to re-vegetate any areas that are cleared by runoff. Additionally, I recommend that a GIS-based analysis be performed on the Coastal Plain region of Virginia to determine how the widths of riparian buffers could be altered to achieve maximum nutrient absorption and sediment trapping efficiencies. While all three proposed alterations to Coastal Plain riparian buffers in Virginia would be hard to implement, I believe that the variable-width buffer design has the greatest potential to be successful. A GIS-modeling technique could be used to determine how wide buffers need to be throughout the entire Coastal Plain region of Virginia to achieve the 2:1 contributing area to effective buffer area ratio. All three alternative designs would require riparian buffer regulations to be different based on locality. However, this design is the one that would both help improve the ecological health of the Bay and be beneficial to farmers, who could plant more crops in areas where buffers could be thinner.

Conclusions

Chesapeake Bay has been receiving increased amounts of nutrients and sediment over the last century that has both hurt the Bay's ecosystem stability, as well as Virginia's fisheries and tourism industry (Boesch *et al*., 2001; Kemp *et al*., 2005). Agricultural runoff is the largest contributor of nitrogen, phosphorous, and sediment delivered to Chesapeake Bay (Chesapeake Bay Program, 2012). GIS analyses of flow accumulation patterns across the Coastal Plain region of Virginia indicate that flow concentration is widespread across this area of the Bay's watershed. This may partially explain the lack of reduction in nutrient and sediment loads being delivered to the Bay in recent years. A metric was sought in this study that could be used to easily predict where concentrated flow would be likely to occur in a large geographic area without having to analyze individual agricultural fields. The wetness index, the topographic index, the water retention index, and the sediment transport index were all poor predictors of flow concentration, as well as the 3 topographic and 3 soil property characteristics that are used to calculate these indexes. Instead, flow concentration seems to be a phenomenon that occurs throughout the Coastal Plain region of Virginia in all topographies and soil types. Chesapeake Bay is important ecologically, its health impacts Virginia's economy, and it is a valuable aesthetic. I recommend requiring farmers to maintain riparian buffers on their land yearly. Further, I advocate for future research on determining the buffer widths needed to implement a variable-width buffer design in the Coastal Plain region of Virginia. Amending the riparian buffer regulations in the Coastal Plain of Virginia, so that riparian buffers can be more effective at removing nutrients and sediment from agricultural runoff, may help to better protect Virginia's most valuable natural resource.

References

Boesch, D.F., Brinsfield, R.B., and Magnien, R.E., 2001, Chesapeake Bay eutrophication: Scientific understanding, ecosystem restoration, and challenges for agriculture: Journal of Environmental Quality, v. 30, p. 303-320.

Burkart, M.R., James, O.E., and Tomer, M.D., 2004, Hydrologic and terrain variables to aid strategic location of riparian buffers: Journal of Soil and Water Conservation, v. 59, no. 5, p. 216– 223.

Chesapeake Bay Preservation Area Designation and Management Regulations (CBPADMR), 1990, Resource Protected Areas: Virginia Administrative Code, 4VAC50-90-80 http://www.dcr.virginia.gov/stormwater_management/theregs.shtml.

Chesapeake Bay Program, 2012, Chesapeake Bay Program: Restoration and Protection Efforts: http://www.chesapeakebay.net/track/restoration (accessed November 2013).

Chesapeake Bay Program, n.d., Chesapeake Bay Program: Learn the issues: http://www.chesapeakebay.net/issues/ (accessed October 2013).

Dosskey, M.G., Eisenhauer, D.E., and Helmers, M.J., 2005, Establishing conservation buffers using precision information: Journal of Soil and Water Conservation, v. 60, no. 6, p. 349–354.

Dosskey, M.G., Helmers, M.J., Eisenhauer, D.E., Franti, T.G., and Hoagland, K.D., 2002, Assessment of concentrated flow through riparian buffers: Journal of Soil and Water Conservation, v. 57, no. 6, p. 336–343.

Dosskey, M.G., and Qiu, Z., 2011a, Comparison of indexes for prioritizing placement of water quality buffers in agricultural watersheds: Journal of the American Water Resources Association, vol. 47, no. 4, p. 662-671.

Dosskey, M.G., Qiu, Z., Helmers, M.J., and Eisenhauer, D.E., 2011b, Improved indexes for targeting placement of buffers of Hortonian runoff: Journal of Soil and Water Conservation, v. 66, no. 6, p. 362–372.

Dosskey, M.G., Vidon, P., Gurwick, N.P., Allan, C.J., Duval, T.P., and Lowrance, R., 2010, The role of riparian vegetation in protecting and improving chemical water quality in streams: Journal of the American Water Resources Association, v. 46, no. 2, p. 261-277.

Funkhouser, L., 2011, Using GIS to quantify riparian buffer bypassing in the Coastal Plain of Virginia within the Chesapeake Bay watershed [B.S. thesis]: Williamsburg, The College of William and Mary, 96 p.

Howell, D.C., 2007, Statistical methods for psychology (6th ed.): Belmont, CA: Thomson Wadsworth.

Jenson, S.K., and Domingue, J.O., 1988, Extracting topographic structure from digital elevation data for geographic information-system analysis: Photogrammetric Engineering and Remote Sensing, v. 54, no. 11, p. 593-1600.

Kemp, W.M., Boynton, W.R., Adolf, J.E., Boesch, D.F., Boicourt, W.C., Brush, G., Cornwell, J.C., Fisher, T.R., Glibert, P.M., Hagy, J.D., Harding, L.W., Houde, E.D., Kimmel, D.G., Miller, W.D., Newell, R.I.E., Roman, M.R., Smith, E.M., and Stevenson, J.C., 2005, Eutrophication of Chesapeake Bay: historical trends and ecological interactions: Marine Ecolology Progress Series, v. 303, p. 1–29.

Kleinman, P.J.A., Sharpley, A.N., McDowell, R.W., Flaten, D.N., Buda, A.R., Tao, L., Bergstrom, L., and Zhu, Q., 2011, Managing agricultural phosphorous for water quality protection: Principles for progress: Plant Soil, DOI 10.1007/s11104-011-0832-9.

Knight, K.W., Schultz, R.C., Mabry, C.M., and Isenhart, T.M., 2010, Ability of remnant riparian forests, with and without grass filters, to buffer concentrated surface runoff: Journal of the American Water Resources Association, v. 46, no. 2, p. 311-322.

Leh, M.D., and Chaubey, I., 2009, GIS-based predictive models of hillslope runoff generation processes: Journal of the American Water Resources Association, v. 45, no. 4, p. 844-856.

Lowrance, R., Altier, L.S., Newbold, J.D., Schnabel, R.R., Groffman, P.M., Denver, J.M., Correll, D.L., Gilliam, J.W., Robinson, J.L., Brinsfield, R.B., Staver, K.W., Lucas, W., and Todd, A.H., 1997, Water quality functions of riparian forest buffers in Chesapeake Bay watersheds: Environmental Management, v. 21, no. 5, p. 687–712.

Lowrance, R., Todd, R., Fail, Jr., J., Hendrickson, Jr., O.H., Leonard, R., and Asmussen, L., 1984, Riparian forests and nutrient filters in agricultural watersheds: Bioscience, v. 34, no. 6, p. 374-377.

National Research Council (NRC), 2011, Achieving nutrient and sediment reduction goals in the Chesapeake Bay: An evaluation of program strategies and implementation: The National Academies Press, 258 p.

Tabackhnick, B.G., and Fidell, L.S., 2007, Using multivariate statistics (5th ed.): Boston: Allyn and Bacon.

Tomer, M.D., Dosskey, M.G., Burkart, M.R., James, D.E., Helmers, M.J., and Eisenhauer, D.E., 2009, Methods to prioritize placement of riparian buffers for

improved water quality: Agroforest Systems, v. 75, no. 1, p. 17–25.

Verstraeten, G., Poesen, J., Gillijns, K., and Govers, G., 2006, The use of riparian vegetated filter strips to reduce river sediment loads: an overestimated control measure?: Hydrological Processes, v. 20, p. 4259-4267.

Young, S., 2013, Utilizing GIS to study concentrated flow from agricultural fields in the Virginia Chesapeake Bay watershed [B.S. thesis]: Williamsburg, The College of William and Mary, 90 p.

Zhang, W., and Montgomery, D.R., 1994, Digital elevation model grid size, landscape representation, and hydrologic simulations: Water Resources Research, v. 30, no. 4, p.1019-1028.

Appendix A: Using the Agricultural Runoff Flow Concentration ArcGIS Toolbox Models

In this appendix the operation of the Agricultural Runoff Flow Concentration ArcGIS Toolbox models are described step-by-step. The Agricultural Runoff Flow Concentration Toolbox accompanies this report, and can be found on the included CD.

Computer and Data Requirements

The models described in this paper are designed to run in ArcGIS 10.0. The Spatial Analyst extension must be activated and the user must download and activate the ET GeoWizard extension and toolbar. All data should be saved into file geodatabases and should be represented in a projected coordinate system.

An agricultural field in Lancaster County, VA (located in the Virginia Coastal Plain) is used as an example. This field is named a1092324, and this name is carried out in all file names throughout the toolbox.

Overview

The agricultural runoff model operates in two parts with user intervention at the beginning and between the two model segments. LIDAR data was obtained from the VA LIDAR database housed at the William & Mary Center for Geospatial Analysis site, www.wm.edu/cga.

Downloading Data

1.) Download the Lancaster County Field example data zip file from gisfiles.wm.edu. Extract all files from the zip file and import the DEM files to ArcMap.

This data was obtained using VA Lidar data hosted at the College of William and Mary. If more than one DEM raster is required to represent the study area, the model accounts for all mosaicking of rasters. Elevation data should be obtained for the study area and all area within 500 m of the edge of the field of interest in order to maintain data integrity. All data should be used in the best available resolution, 3x3 m DEM in this case. As the purpose of this toolbox is to analyze micotopography on relatively small areas (<100 hectares), DEMs larger than 10m resolution should be avoided. Projected data should be used in order to maintain grid dimensions in all calculations throughout the model. The model reprojects all data into NAD 83 UTM Zone 18N.

The Center for Geospatial Analysis at the College of William and Mary hosts publicly available lidar data for Virginia. The lidar point cloud data are stored as .laz files and bare earth DEMs as .img files.

In order to access these data, navigate to www.wm.edu/cga and select VA Lidar in the menu on the left-hand side of the page.

Locate the lidar file that corresponds with the study area counties. Each lidar flight file contains a metadata document with all pertinent information about the data (projection, extent, dates, etc.). When working in ArcGIS, download the shapefile for the lidar flight by following the link on the VA Lidar page. This will provide the user with a tiled file indicating each .laz or .img file available for download (*A1*).

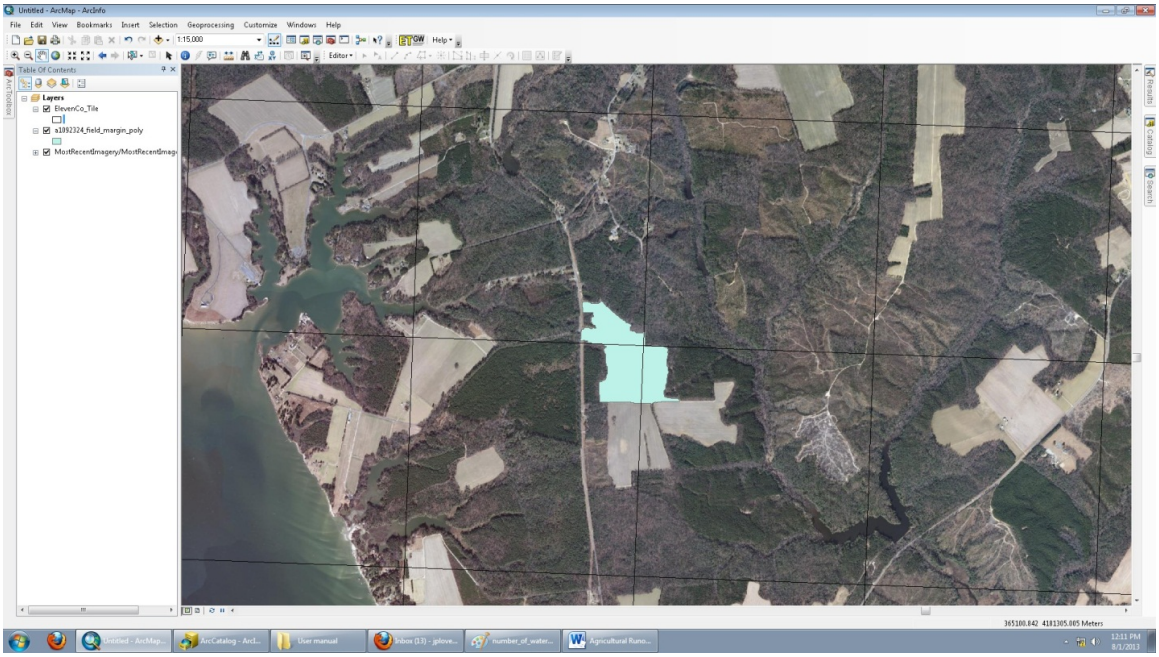

A1. Example field shapefile and tiled file for the area in ArcMap.

By using the Identify tool, the downloadable .img and .laz files can be accessed directly from ArcMap. By clicking on the lightning bolt link next to either DEM_URL or LAS_URL, the file will be downloaded from the hosting site (*A2*).

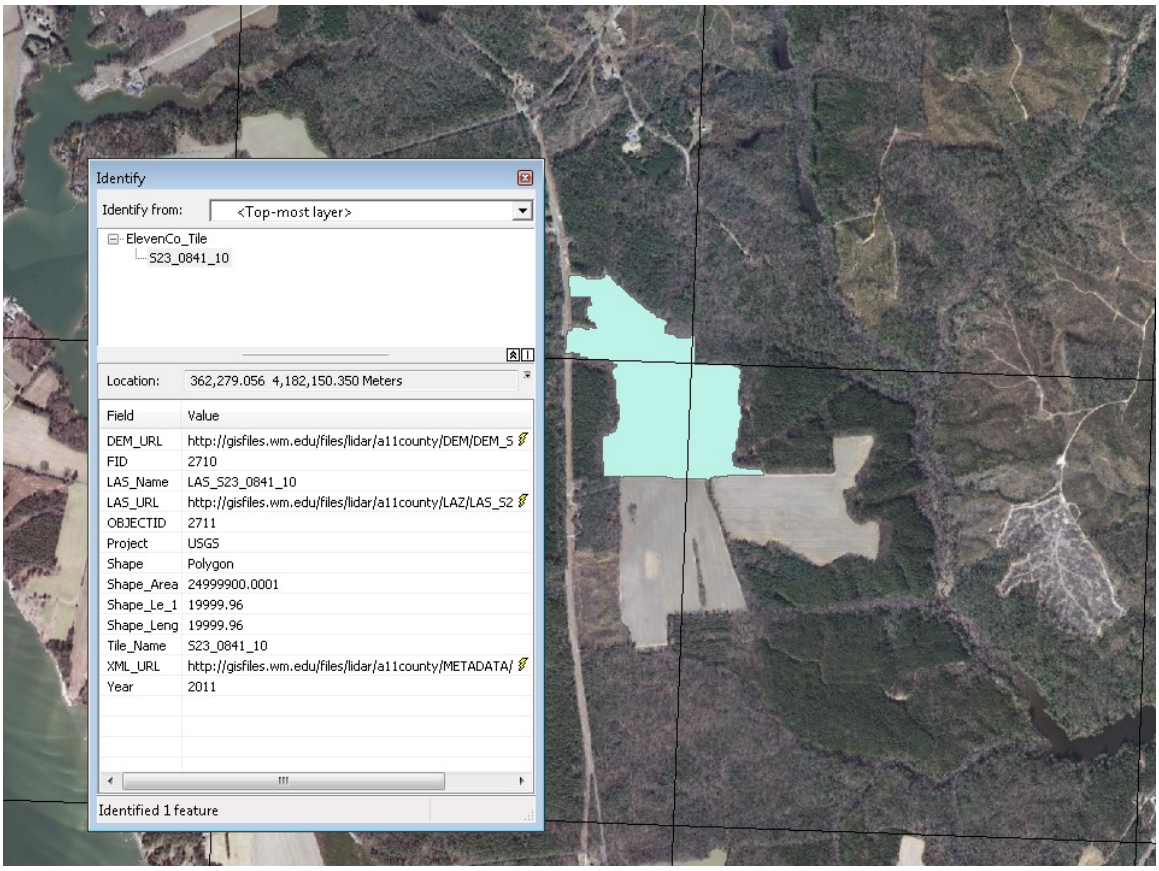

A2. Example use of the Identify tool to download the DEMs for the tiles this field occupies.

When using these files in model Part_1, it is important to note the projection listed in the metadata. This projection should be input in the Mosaic to New Raster tool within the model to maintain data integrity.

At the conclusion of this step, DEM files covering the field area should be added to the ArcMap document (*A3*).

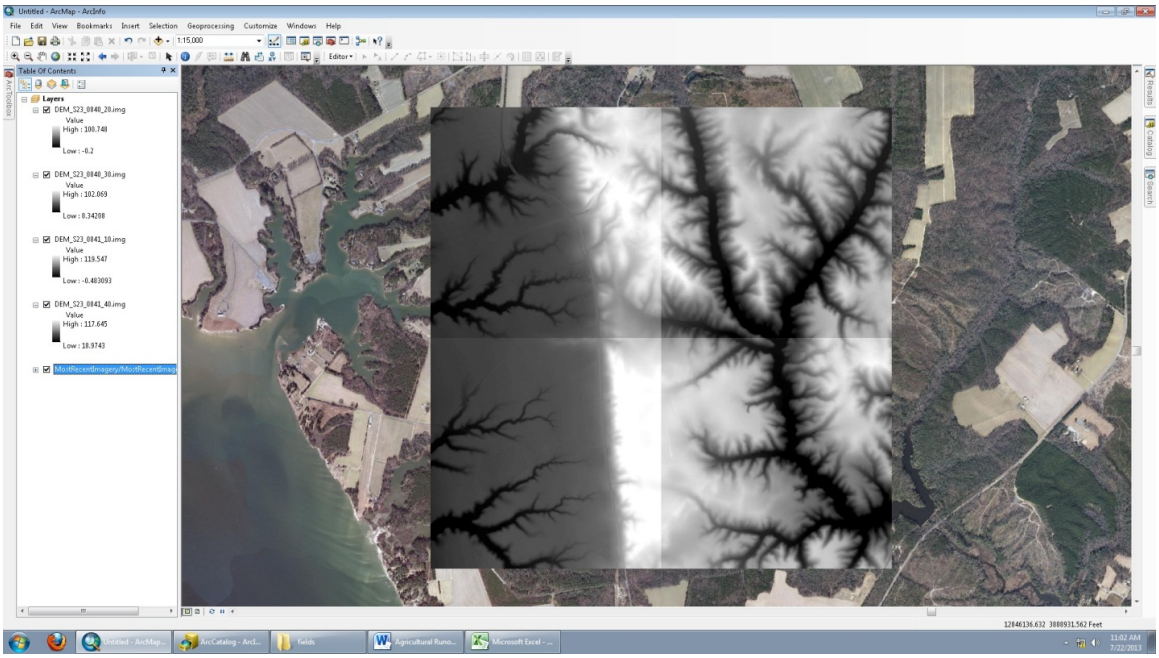

A3. Downloaded DEMs for field a1092324 in ArcMap.

2.) Using ArcCatalog (or the Catalog window nested within ArcMap), create two file geodatabases. Do this by right clicking within the catalog window and selecting New->File Geodatabase (*A4*).

The first (fields.gdb) will be utilized to store output files pertinent to data analysis and further operations of the model. The second (fields_archive.gdb) stores background files and acts as a temporary location to store intermediate data. In order for the extensions to operate properly and for the models to run quickly and efficiently, the two geodatabases should be housed on a local drive rather than one on the network.

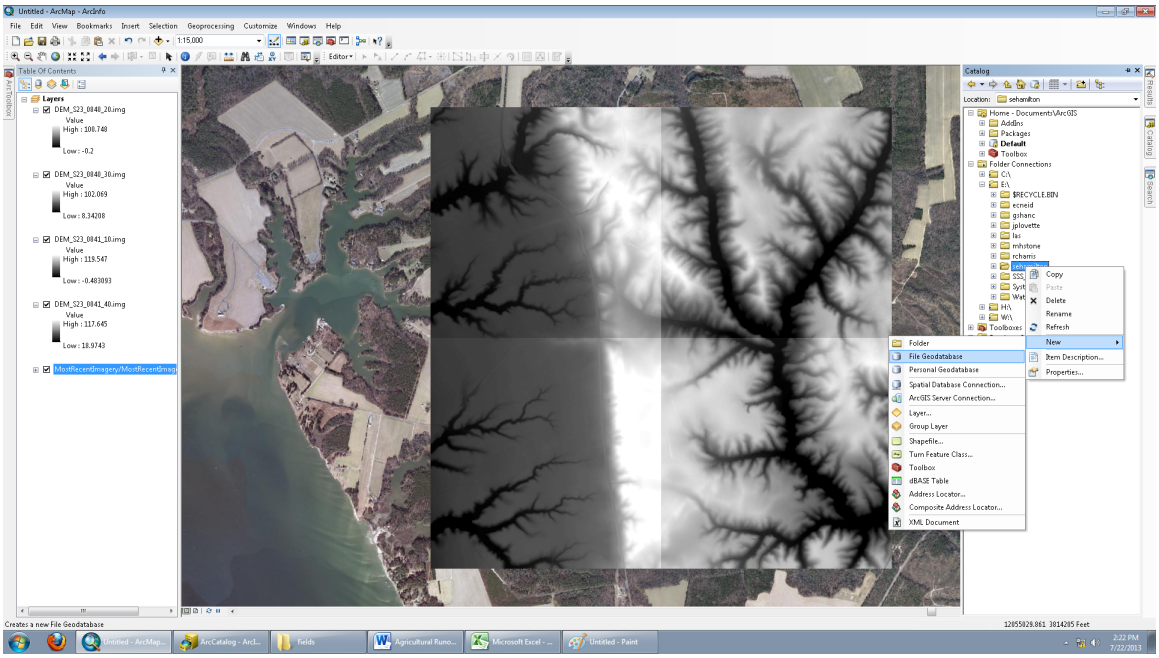

A4. Creating file geodatabases in ArcMap.

Agricultural Runoff Flow Concentration Model Part 1

The first model (Part_1) (*A6*) works to mosaic and reproject the study area DEMs and utilizes the hydrology tool set to create hydrology output files. The only input is the set of DEMs, and working environments are defined (*A5*). As the model uses many relative path names, it is important to maintain consistency with input and output file names.

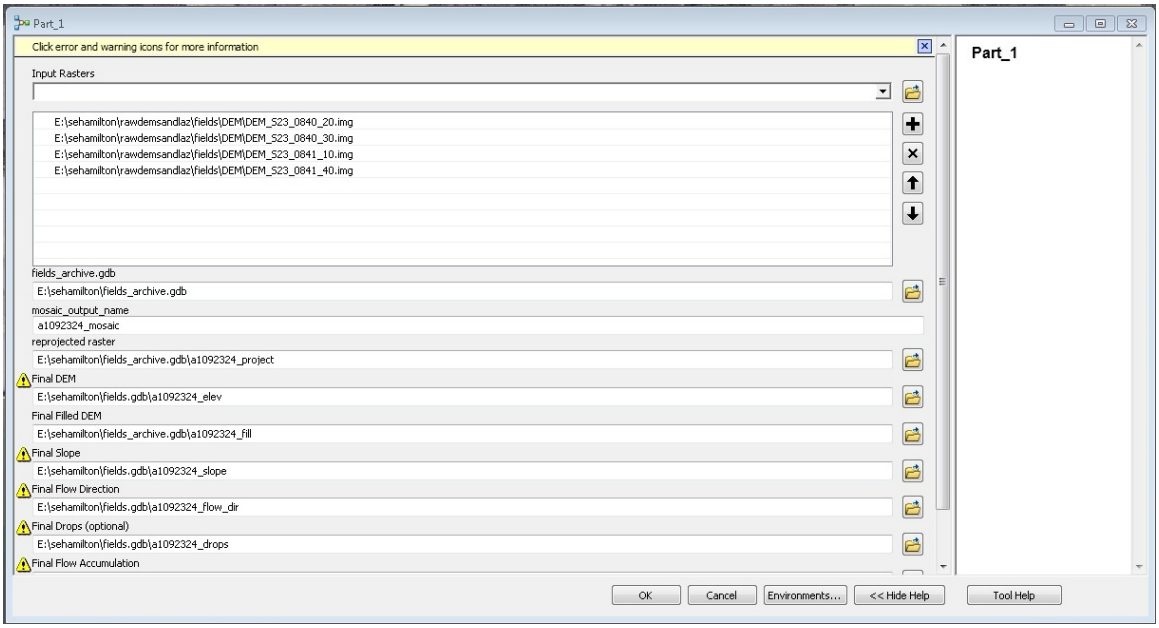

A5. Part 1 of the Agricultural Runoff Flow Concentration Model input-output specification window.

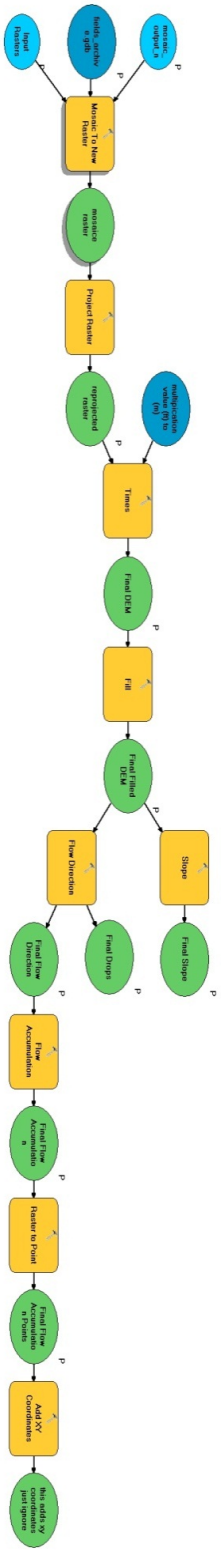

A6. Schematic of Part 1 of the Agricultural Runoff Flow Concentration Model

The first section of Part_1 mosaics and reprojects the DEM to NAD 83 UTM Zone 18N (*A7*). The Times function also acts to convert all elevation data to meters. The default projection before mosaicking is NAD 83 HARN and the reprojection is based on this. If other projections are present or desired, these inputs can be changed within the model.

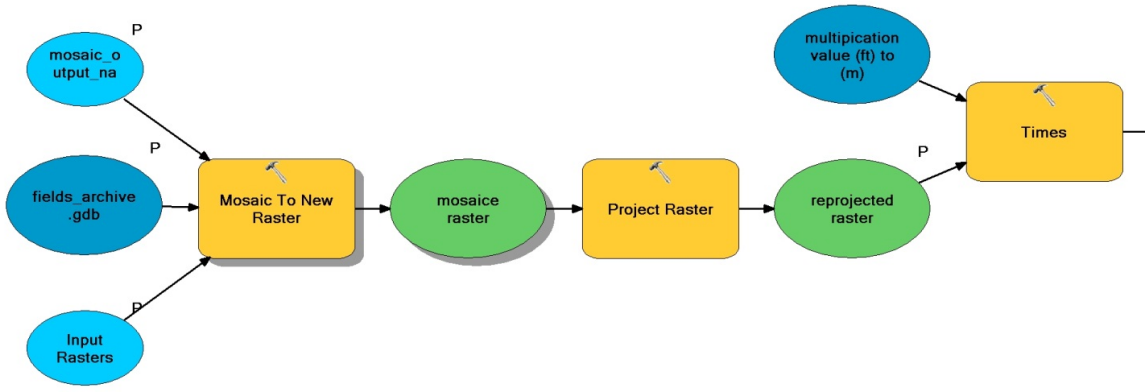

A7. Section of Part 1 of the Agricultural Runoff Flow Concentration Model showing the mosaic, reprojection, and conversion of elevation data to meters steps.

The model then uses the hydrology toolset to create slope, drops, flow direction, and flow accumulation rasters for the study area. Finally, the tool converts the flow accumulation raster to points and adds XY data to each point to be used for field margin digitization (*A8*).

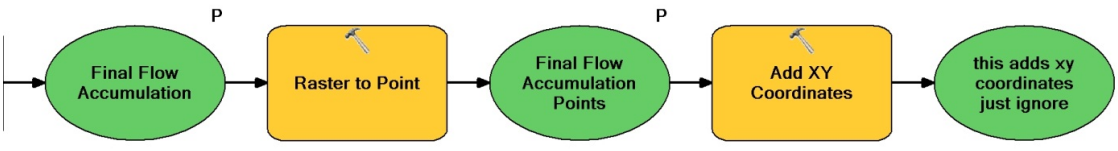

A8. Section of Part 1 of the Agricultural Runoff Flow Concentration Model showing the raster to point, and adding XY data steps.

If changes to background operations within the model are desired, this can be accomplished by right clicking the model and selecting Edit. Double click on the desired tool to change parameters.

Field Digitization

1.) In order to maintain the proper projections through the rest of the model operations, close the current window of ArcMap and open a new ArcMap document, making sure to import the accumulation and accumulation points layers first. After these layers are added to the map, the base map layer can be added again. Check the projection for the data frame by selecting View->Data Frame Properties->Coordinate System. This should note that NAD 83 UTM Zone 18N as the projected coordinate system (*A9*).

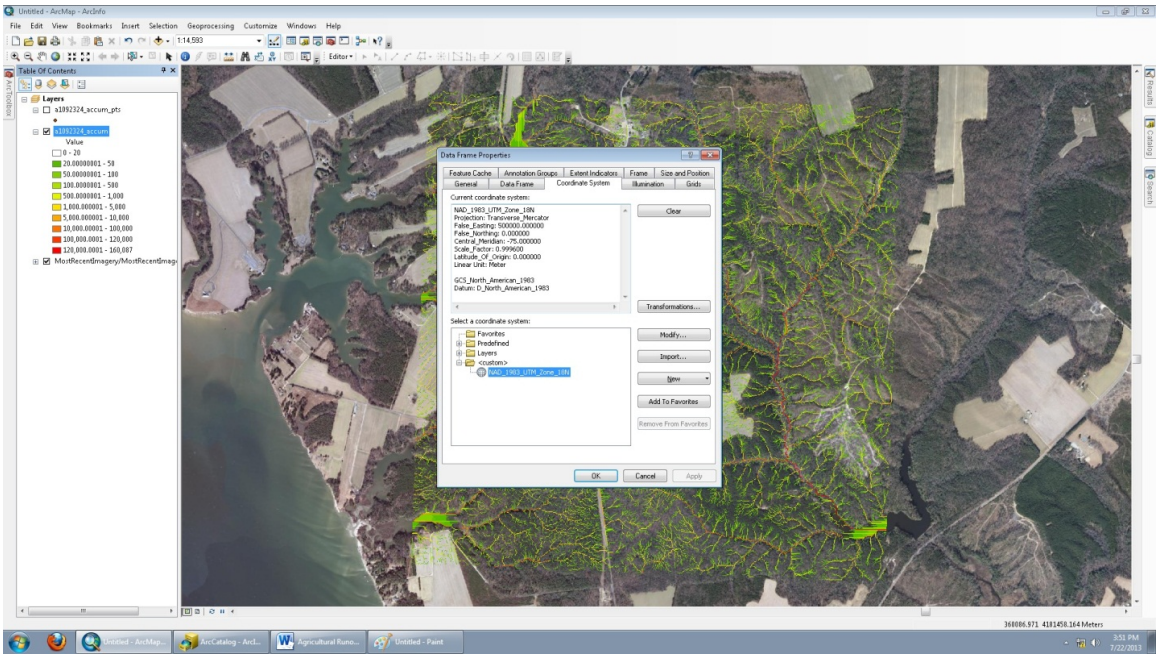

A9. Checking the projection in ArcMap.

2.) Create the field margin layer by opening the fields file geodatabase and right-clicking, selecting New->Feature Class (*A10*). This line layer should be named with the field name, followed by _field_margin_1 (ex. a1092324_field_margin_1).

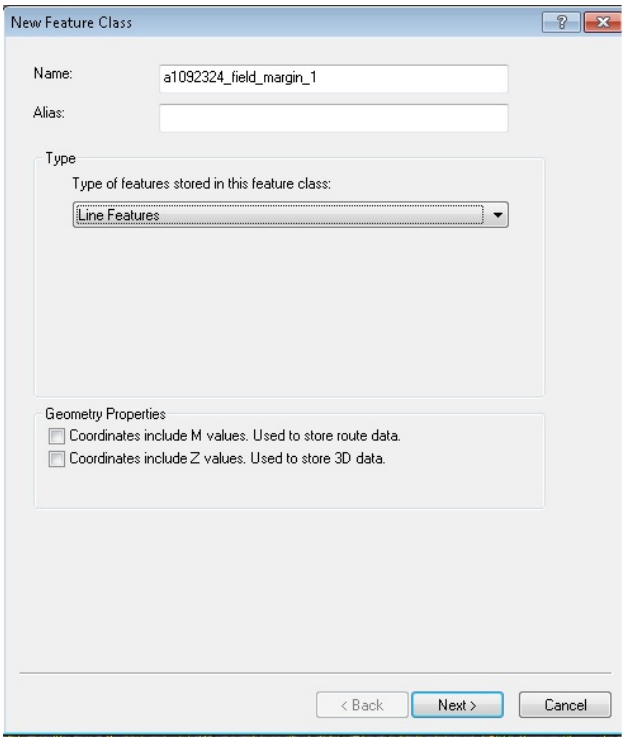

A10. Creating the field margin layer.

The coordinate system should be imported from that of the accumulation layer in order to maintain consistency (*A11*).

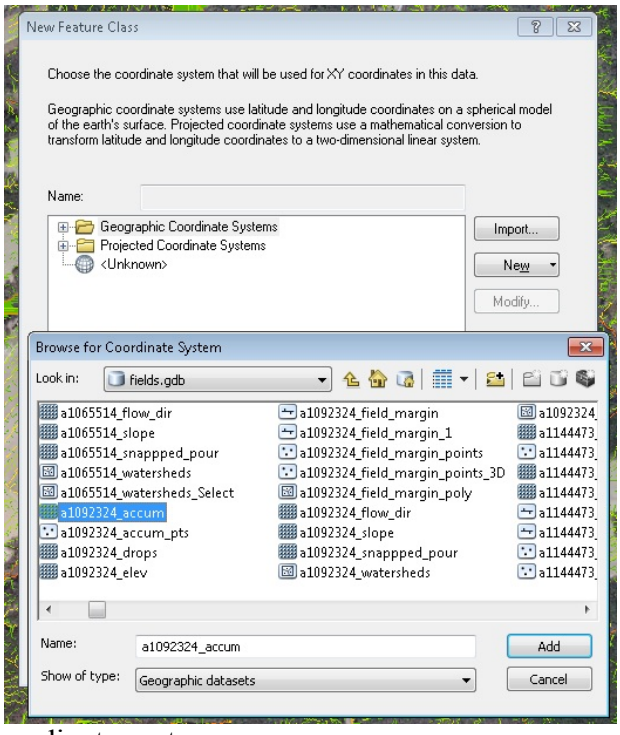

A11. Importing the coordinate system.

All other parameters can be left in their default positions for the layer creation. This created layer (field_margin_1) should then be added to the ArcMap document.

3.) The symbology of the flow accumulation layer should be changed in order to accommodate field digitization and simplify the viewing window. Open the layer properties and change the symbology from stretched to classified. Select 10 classes and then classify the symbology. For the breaks, select a series of low values in order to denote the microtopography of the landscape. For the sample field, the values of 20, 50, 100, 500, 1000, 5000, 10000, and 100000 were selected and breaks over this value were calculated automatically (*A12*).

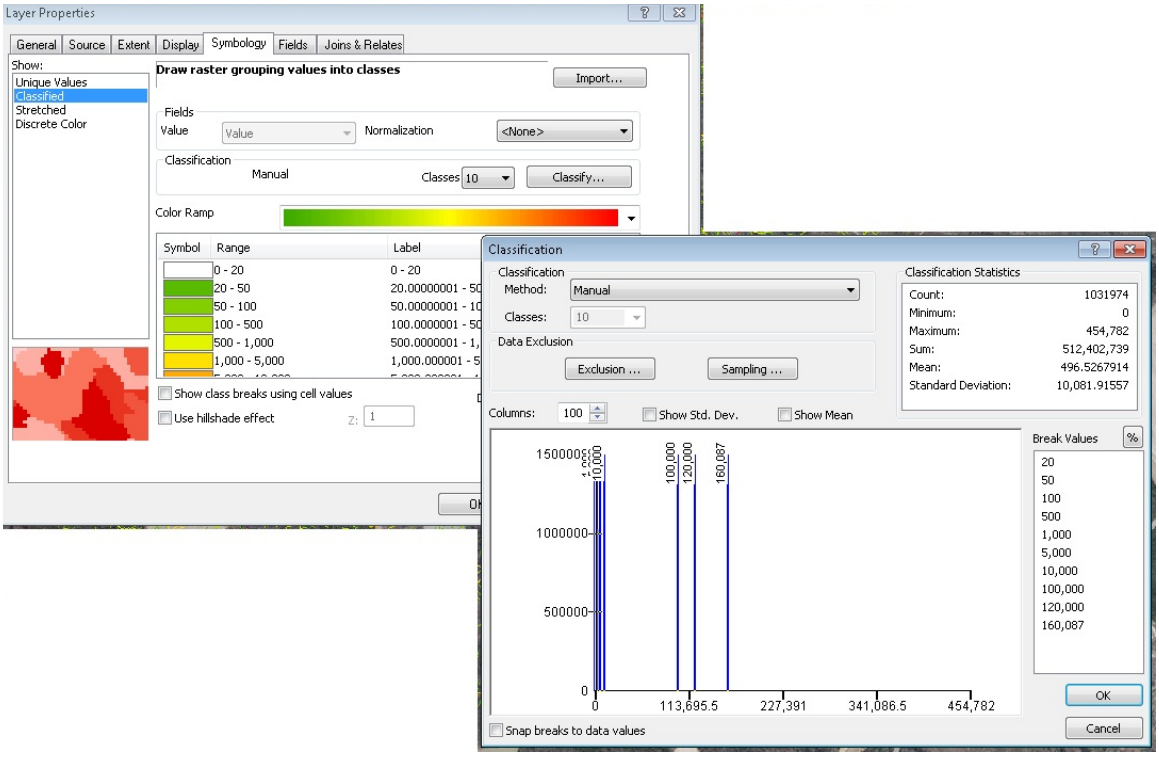

A12. Setting the symbology for the flow accumulation layer.

4.) Select a color ramp that allows for easy distinguishable value ranges (i.e. green to red). The lowest value range should also be changed to "No Color" by double-clicking the color box next to the range. This clear value range allows the user to view the base map through the flow accumulation layer.

5.) The field can now be digitized using the flow accumulation points, flow accumulation, and base map. During digitization, the creation of the field margin should have each segment snap to a flow accumulation point. By snapping the field margin to the flow accumulation points, the value at each of these points can be attributed to the line segments, as well as the values from other rasters of the same resolution. Begin editing the field margin by opening the Editor toolbar, selecting Start Editing, and selecting the a1092324_field_margin_1 layer to edit.

6.) Field digitization should begin at the southernmost point on the field. When multiple points lie along a southern line on the field, the easternmost point acts as a tiebreaker. Verify that the Straight Segment button is selected on the Editor toolbar. Begin by clicking on the most southern (and secondly, most eastern) point and proceed in a clockwise direction, clicking from one flow accumulation point to the next along the field margin. A 1:600 or 1:800 zoom should be adequate for digitization (*A13*).

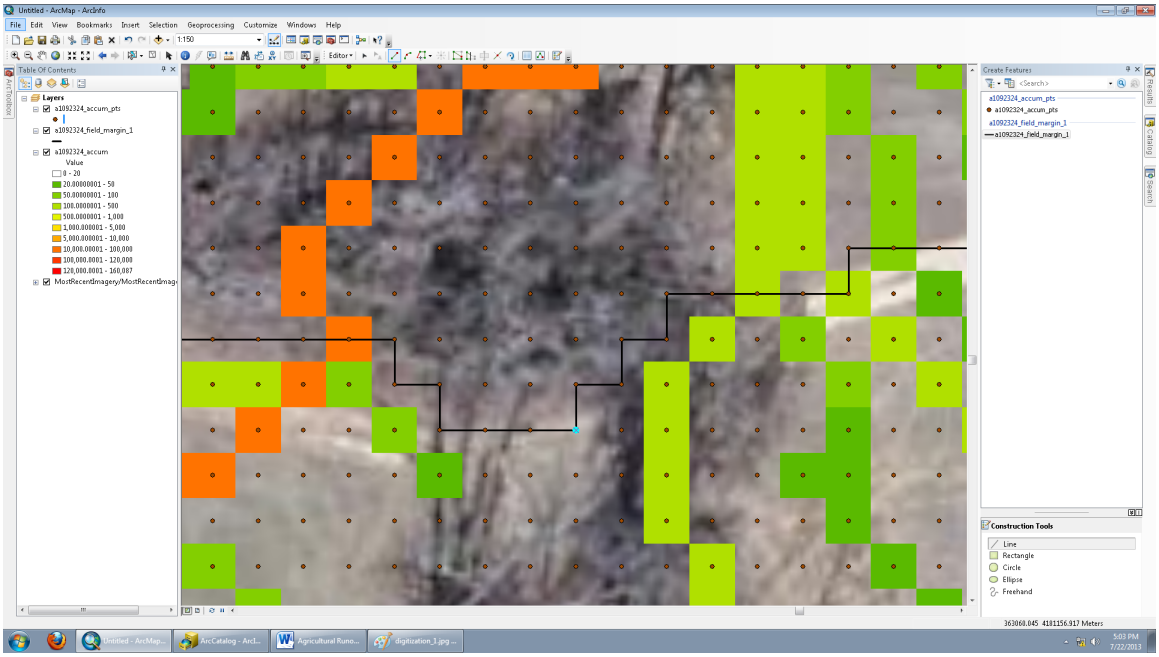

A13. Field digitization example. The blue dot indicates where field digitization on this field should occur.

The following rules should be followed while digitizing fields:

- Segments should not be longer than the cell size (3 m at this resolution)
- Segments should only proceed in orthogonal directions
- Field margin should not follow along within visible flow lines*
- Flow should not be "double-counted", meaning that if flow is counted on to or off of the field at one location, the same flow line should not be counted in that same direction without having flowed through the margin in the opposite direction first (even this "snaking" should be avoided)
- Field margin digitization can deviate slightly from the base map field margin in order to accommodate digitization rules

When issues arise or flow is difficult to determine, the flow direction raster can be beneficial in following flow lines.

*Example. In the following image (*A14*), it appears as though the field margin runs through three consecutive visible accumulation cells (which would violate the third rule above). However, if the flow direction layer is analyzed, all three of these cells have flow direction values of "32" indicating a flow to the northwest and therefore verifying that none of these three cells flow in to each other.

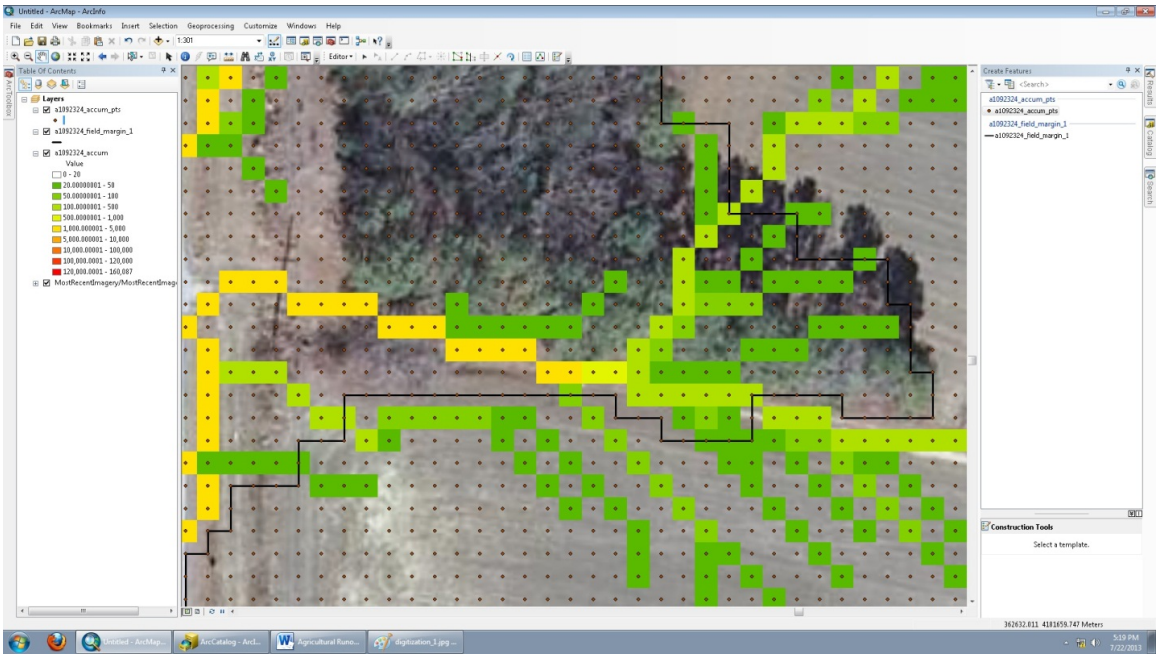

A14. Example of correct field digitization.

7.) Finish the field margin sketch by returning back to the beginning point and double-clicking on that point, thus closing the field margin. Make sure that the points at the end of the field margin sketch do not violate the rules surrounding the selection of the beginning point of the sketch.

8.) When the field margin (a1092324_field_margin_1) is correct and complete, copy and paste the feature in the same file geodatabase in ArcCatalog. This file will paste as a1092324_field_margin_1_1.

9.) Rename this file a1092324_field_margin and import it to the ArcMap document. At this point, there will be two identical files in the map document, a1092324_field_margin_1 and a1092324_field_margin.

10). Open the Editor toolbar again and select the new layer, a1092324_field_margin, to edit. Using the selection tool, highlight the layer and locate the starting point of the line. First drag the beginning point down and away from the flow accumulation point to which it is snapped. Then do the same with the end point which is snapped to the same accumulation point, thereby separating these overlaying points. Delete this end point by right-clicking on the point and selecting Delete Vertex (*A15*). Snap the beginning point back to the original starting flow accumulation point and select the Finish Sketch button on the Editing toolbar. Save the edits and finish editing.

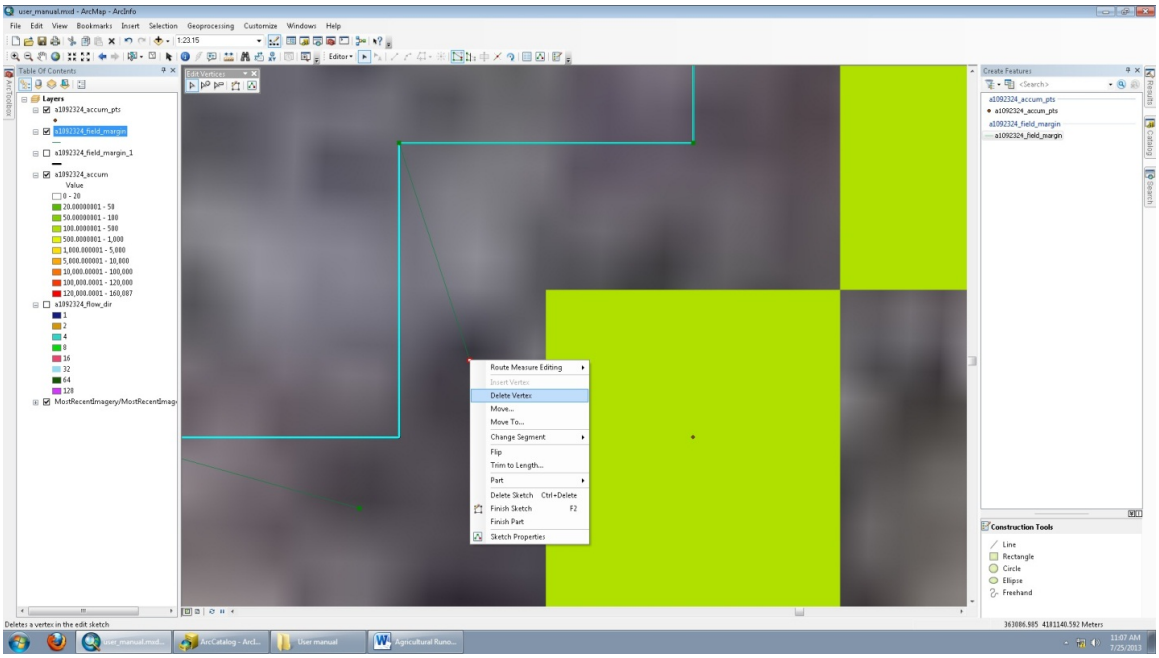

A15. Example showing the deletion of one vertex at the starting point of digitization.

11.) At this point, the following files should be in the file geodatabase:

- a1092324_accum
- a1092324_accum_pts
- a1092324_drops
- a1092324_elev
- a1092324_field_margin
- a1092324_field_margin_1
- a1092324_flow_dir
- a1092324_slope

<u>Agricultural Runoff Flow Concentration Model Part 2</u>

Activate the ET GeoWizards toolbar in order to operate model Part_2.

ET GeoWizards is an external toolbar that enables extensive data manipulation in addition to what is already available in the ArcGIS toolboxes. Within this described toolbox, ET GeoWizards works to convert the field margin polyline to points while adding a variety of attributes to each point depending on the spatial location.

In order to download this toolbar, navigate to http://www.ian-ko.com/ and click on the ET GeoWizards tab in the left hand column. Then select download and select the ET GeoWizards version that is compatible with your current version of ArcGIS. As the website states, all downloads from different servers are identical.

In ArcMap, the ET GeoWizards toolbar must be activated before use. Click Customize→ Toolbars→ET GeoWizards. Then click on the ET GW button next to the "help" button on the box and enter your License Server and TCP Port information, and finally select

"Test License Server". After the toolbar is registered, it should run within Model Part_2 without incident.

Model Part_2 (*A17*) uses all of the above layers to sample values from the created rasters to each point along the field margin. Input the appropriate layers to create field margin polygon, field margin 3D point, and watershed outputs (*A16*).

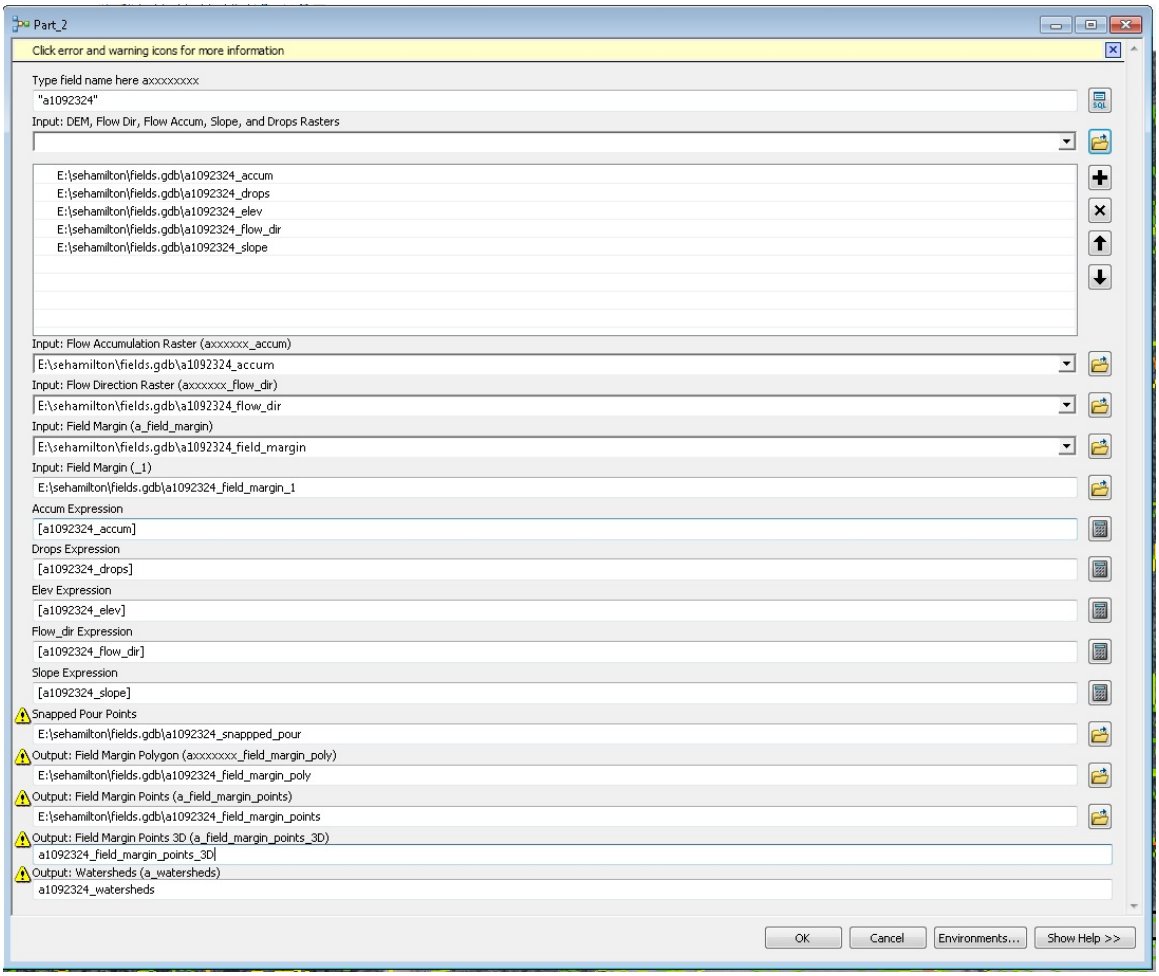

A16. Part 2 of the Agricultural Runoff Flow Concentration Model input-output specification window.

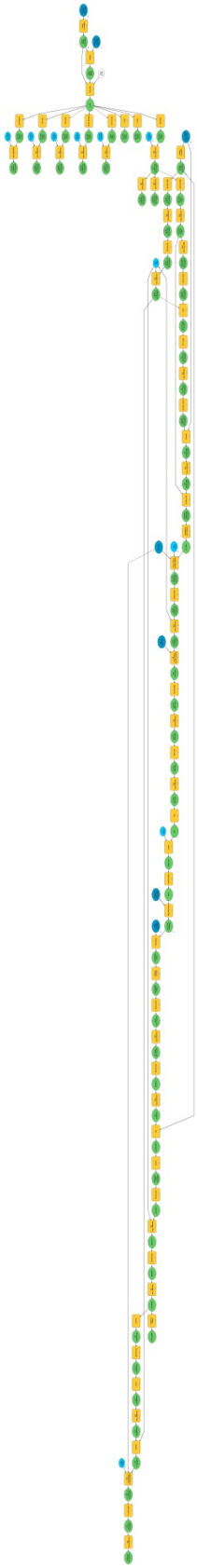

A17. Schematic of Part 2 of the Agricultural Runoff Flow Concentration Model

The ET GeoWizards toolbar allows for the assignment of field margin distance and angle to each field margin point using the Polyline to Point tool. This tool also removes any duplicate points within the field margin. With the sampling of all of the raster layers to the nearest point along the margin, a variety of details can then be determined from these points (*A18*).

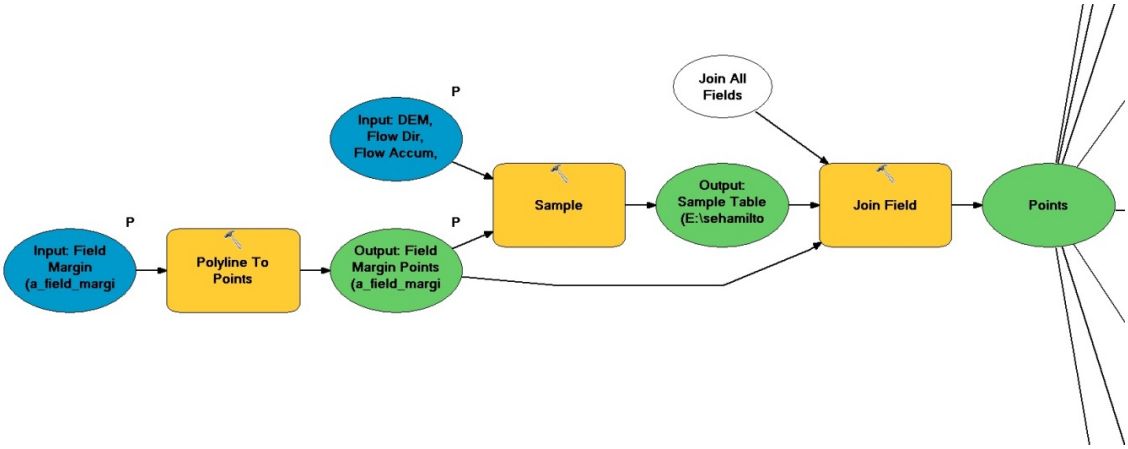

A18. Section of Part 2 of the Agricultural Runoff Flow Concentration Model showing the polyline to point and sampling steps.

If the user is interested in adding other raster layers to the sampling process, the layer must be added to the Sample tool inputs and then the field from that new raster must be joined in a similar fashion to the other layers already included in the model.

A series of new fields and temporary files are then created in order to determine the direction of each flow line, either on to or off of the field. This is done by creating a shadow point down slope of each point along the field margin through the use of the flow direction layer. Based on whether or not this point falls inside the field polygon, flow direction as it relates to the field is determined. Through this process, flow lines and pour points can also be determined from the field margin points.

The model calculates the flow accumulation at each of the outflow points along the margin and ranks them to create pour points. The top ten points by accumulation are extracted, converted to pour points, and utilized to create watersheds. If the user desires more or less watersheds to be created, this ranking number can be altered within the model.

Finally, the model clips these watersheds to the field margin (*A19*). Because the watershed size and rank is determined before the clip step, some of the low rank watersheds are not represented properly on the field. Because of this inherent error, a general rule is to create 25-50% more watersheds than are needed for analysis (i.e. analyze 5-7 watersheds when creating 10).

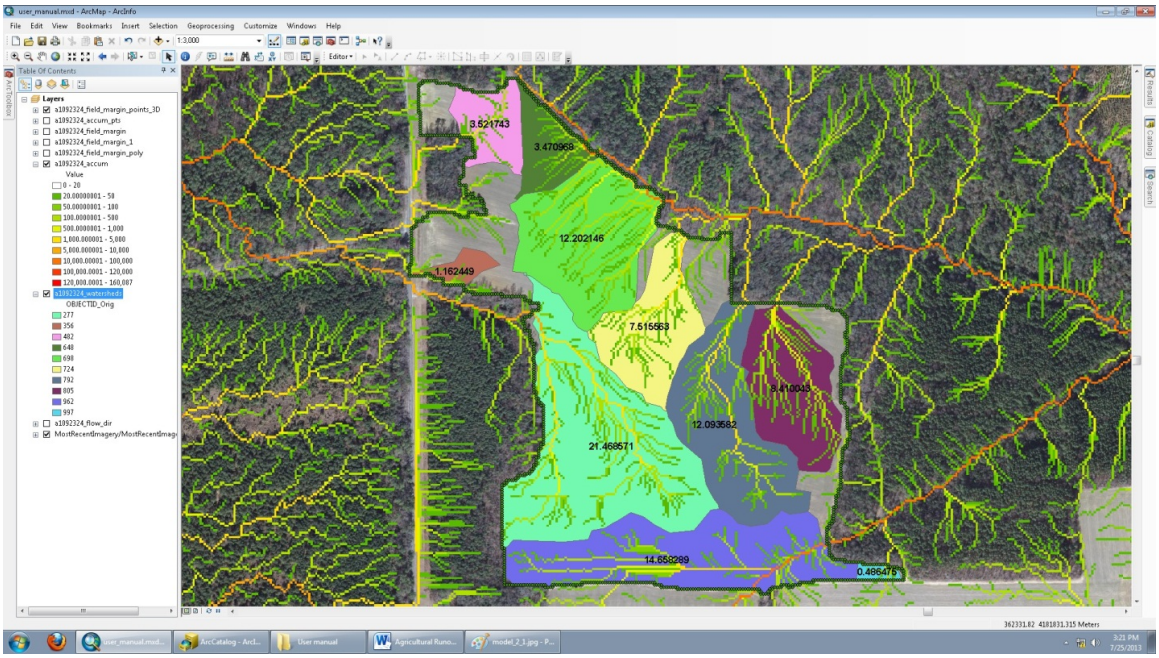

A19. Clipped field-level watersheds for an example field in ArcMap.

Appendix B: Wetness Index Model

The following methodology was used to calculate the mean value of the Wetness Index for each of the 74 fields analyzed. Steps 1-3 were completed using the model shown in *B1*, and Step 4 was run separately following the model. The "batch" function was used to run both this model and Step 4 74 consecutive times.

Model Steps

1.) *Raster Calculator*
Input: flow accumulation raster
Map Algebra Expression: (flow accumulation raster * raster cell area in meters) / raster cell width in meters
Intermediate Output: specific catchment area raster

2.) *Raster Calculator 2*
Input: slope (in percent rise) raster
Map Algebra Expression: (ATan (slope raster / 100) * (360 / (2 * 3.14))
Intermediate Output: slope (in degrees) raster

3.) *Raster Calculator 3*
Inputs: flow accumulation raster, slope (in degrees) raster
Map Algebra Expression: Ln (specific catchment area raster / slope (in degrees) raster)
Extent: field polygon shapefile
Output: wetness index raster

Statistics Steps

4.) *Zonal Statistics*
Input Raster or Feature Zone Data: field polygon shapefile
Zone Field: FIELD_ID
Input Value Raster: wetness index raster
Output Raster: mean wetness index raster
Statistics Type: MEAN
Ignore No Data in Calculations: true

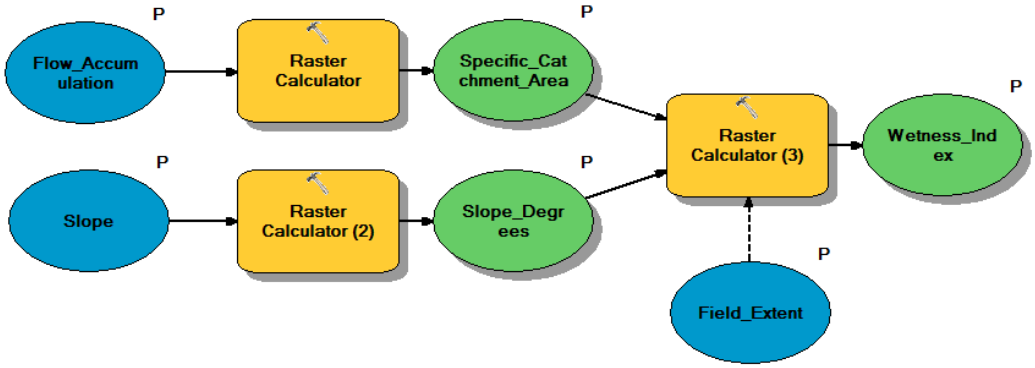

B1. Wetness Index Model

Appendix C: Topographic Index Model

The following methodology was used to calculate the mean value of the Topographic Index for each of the 74 fields analyzed. The Web Soil Survey was used to determine the Ksat and D values for each field (Steps 1-9). Steps 10-14 were completed using the model shown in *C1*, and Step 15 was run separately following the model. The "batch" function was used to run both this model and Step 15 74 consecutive times.

Determining Ksat & D Steps

1.) Import the field polygon shapefile as the AOI on the Web Soil Survey (http://websoilsurvey.sc.egov.usda.gov/App/WebSoilSurvey.aspx).

2.) Click on the "Download Soils Data" tab and download the spatial data for the AOI uploaded.

3.) Open the "soilmu_a_aoi" spatial data file in ArcMap.

4.) Open the attributes table of the "soilmu_a_aoi" spatial data file. Add 2 fields (named: Ksat and D) to the attributes table and select float as the data type for each.

5.) Using the Editor toolbar, start an editing session. Returning to the Web Soil Survey with the field AOI uploaded, click on the "Soil Data Explorer" tab. Click on the "Soil Properties and Qualities" subtab. Expand "Soil Physical Properties" and click on "Saturated Hydraulic Conductivity (Ksat)." Select "Surface Layer" under "Advanced Options" and then click "View Rating." Enter the values of Ksat into the attributes table for each soil type (distinguished by unique map unit symbols). Next, expand "Soil Qualities and Features" and click on "Depth to Any Soil Restrictive Layer." Select "Higher" under "Advanced Options" and then click "View Rating." Enter the values of D into the attributes tab for each soil type (again distinguished by unique map unit symbols). Stop the editing session in ArcMap and click yes to "Save Edits."

6.) *Polygon to Raster*
Input: soilmu_a_aoi polygon shapefile
Value Field: Ksat
Cell Assignment Type: CELL_CENTER
Priority Field: NONE
Cellsize: leave as default
Output: Ksat raster

7.) *Polygon to Raster 2*
Input: soilmu_a_aoi polygon shapefile
Value Field: D

Cell Assignment Type: CELL_CENTER
Priority Field: NONE
Cellsize: leave as default
Output: D raster

8.) *Project Raster*
Input: Ksat raster
Cell Assignment Type: this is automatically filled in by the tool
Output Coordinate System: import coordinate system of the field polygon shapefile
Geographic Transformation: this is automatically filled in by the tool
Resampling Technique: NEAREST
Output Cellsize: 3
Registration Point: leave these two boxes blank
Output: projected Ksat raster

9.) *Project Raster 2*
Input: D raster
Cell Assignment Type: this is automatically filled in by the tool
Output Coordinate System: import coordinate system of the field polygon shapefile
Geographic Transformation: this is automatically filled in by the tool
Resampling Technique: NEAREST
Output Cellsize: 3
Registration Point: leave these two boxes blank
Output: projected D raster

Model Steps
10.) *Raster Calculator*
Input: slope (in percent rise) raster
Map Algebra Expression: Tan ((slope raster / 100) * (3.14 / 180))
Intermediate Output: tangent of slope raster

11.) *Raster Calculator 2*
Inputs: tangent of slope raster, flow accumulation raster
Map Algebra Expression: ((flow accumulation raster * raster cell area in meters) / raster cell width in meters) / tangent of slope raster
Intermediate Output: topographic index intermediate raster output #1

12.) *Raster Calculator 3*
Inputs: projected Ksat raster, D raster
Map Algebra Expression: Ksat raster * D raster
Intermediate Output: topographic index intermediate raster output #3

13.) *Raster Calculator 5*
Input: topographic index intermediate raster output #1
Map Algebra Expression: Ln (topographic index intermediate raster output #1)
Intermediate Output: topographic index intermediate raster output #2

14.) *Raster Calculator 4*
Inputs: topographic index intermediate raster output #2, topographic index intermediate raster output #3
Map Algebra Expression: (topographic index intermediate raster output #2 – topographic index intermediate raster output #3)
Extent: projected Ksat raster
Output: topographic index raster

Statistics Steps
15.) *Zonal Statistics*
Input Raster or Feature Zone Data: field polygon shapefile
Zone Field: FIELD_ID
Input Value Raster: topographic index raster
Output Raster: mean topographic index raster
Statistics Type: MEAN
Ignore No Data in Calculations: true

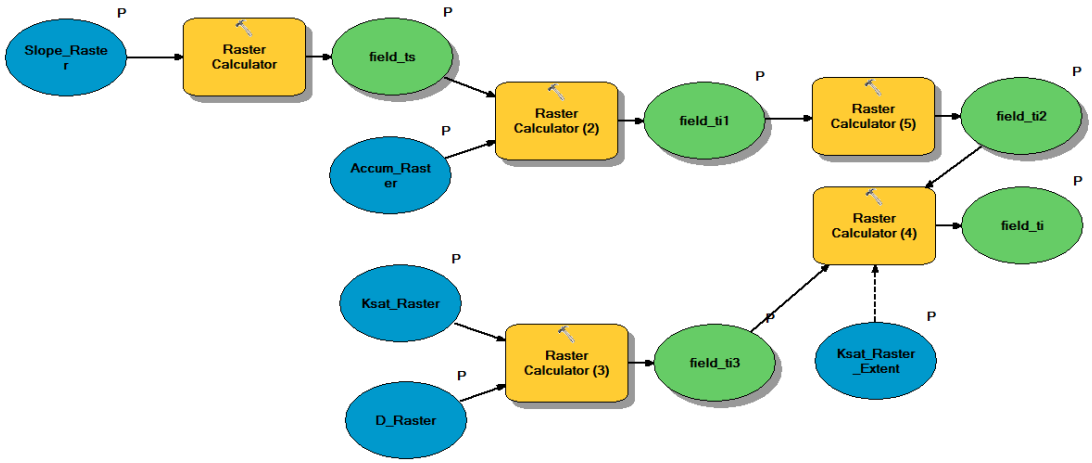

C1. Topographic Index Model

Appendix D: Water Retention Index Model

The following methodology was used to calculate the mean value of the Water Retention Index for each of the 74 fields analyzed. The Web Soil Survey was used to determine the Ksat and R values for each field (Steps 1-9). Steps 10-12 were completed using the model shown in *D1*, and Step 13 was run separately following the model. The "batch" function was used to run both this model and Step 13 74 consecutive times.

Determining Ksat & R Steps

1.) Import the field polygon shapefile as the AOI on the Web Soil Survey (http://websoilsurvey.sc.egov.usda.gov/App/WebSoilSurvey.aspx).

2.) Click on the "Download Soils Data" tab and download the spatial data for the AOI uploaded.

3.) Open the "soilmu_a_aoi" spatial data file in ArcMap.

4.) Open the attributes table of the "soilmu_a_aoi" spatial data file. Add 2 fields (named: Ksat and R) to the attributes table and select float as the data type for each.

5.) Using the Editor toolbar, start an editing session. Returning to the Web Soil Survey with the field AOI uploaded, click on the "Soil Data Explorer" tab. Click on the "Soil Properties and Qualities" subtab. Expand "Soil Physical Properties" and click on "Saturated Hydraulic Conductivity (Ksat)." Select "Surface Layer" under "Advanced Options" and then click "View Rating." Enter the values of Ksat into the attributes table for each soil type (distinguished by unique map unit symbols). Next, expand "Soil Erosion Factors" and click on "T Factor." Click "View Rating." Enter the values of R (the T Factor) into the attributes tab for each soil type (again distinguished by unique map unit symbols). Stop the editing session in ArcMap and click yes to "Save Edits."

6.) *Polygon to Raster*
Input: soilmu_a_aoi polygon shapefile
Value Field: Ksat
Cell Assignment Type: CELL_CENTER
Priority Field: NONE
Cellsize: leave as default
Output: Ksat raster

7.) *Polygon to Raster 2*
Input: soilmu_a_aoi polygon shapefile
Value Field: R
Cell Assignment Type: CELL_CENTER

Priority Field: NONE
Cellsize: leave as default
Output: R raster

8.) *Project Raster*
Input: Ksat raster
Cell Assignment Type: this is automatically filled in by the tool
Output Coordinate System: import coordinate system of the field polygon shapefile
Geographic Transformation: this is automatically filled in by the tool
Resampling Technique: NEAREST
Output Cellsize: 3
Registration Point: leave these two boxes blank
Output: projected Ksat raster

9.) *Project Raster 2*
Input: R raster
Cell Assignment Type: this is automatically filled in by the tool
Output Coordinate System: import coordinate system of the field polygon shapefile
Geographic Transformation: this is automatically filled in by the tool
Resampling Technique: NEAREST
Output Cellsize: 3
Registration Point: leave these two boxes blank
Output: projected R raster

Model Steps
10.) *Raster Calculator*
Input: flow accumulation raster
Map Algebra Expression: (flow accumulation raster * area of raster cell in meters) * (1 / 4046.86)
Intermediate Output: runoff source area raster

11.) *Raster Calculator 2*
Input: projected R raster
Map Algebra Expression: Power (projected R raster, 0.5)
Intermediate Output: power function R raster

12.) *Raster Calculator 3*
Input: projected Ksat raster, runoff source area raster, power function R raster
Map Algebra Expression: 0.2805 * (Log10 (runoff source area raster * power function R raster * projected Ksat raster
Output: water retention index raster

Statistics Steps
13.) *Zonal Statistics*
Input Raster or Feature Zone Data: field polygon shapefile
Zone Field: FIELD_ID

Input Value Raster: water retention index raster
Output Raster: mean water retention index raster
Statistics Type: MEAN
Ignore No Data in Calculations: true

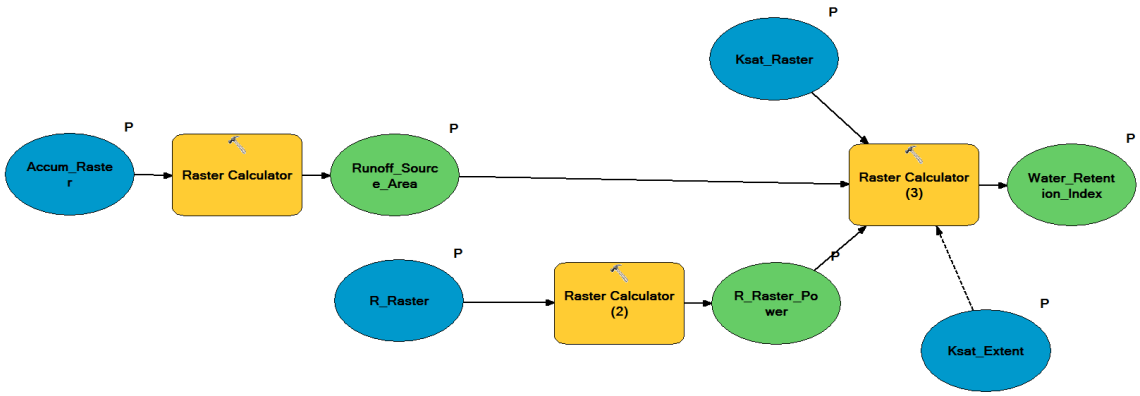

D1. Water Retention Index Model

Appendix E: Sediment Transport Index Model

The following methodology was used to calculate the mean value of the Sediment Transport Index for each of the 74 fields analyzed. Steps 1-4 were completed using the model shown in *E1*, and Step 5 was run separately following the model. The "batch" function was used to run both this model and Step 5 74 consecutive times.

Model Steps

1.) *Raster Calculator*
Input: specific catchment area raster
Map Algebra Expression: Power ((specific catchment area raster / 22.13), 0.6)
Intermediate Output: sediment transport index intermediate raster output #1

2.) *Raster Calculator 2*
Input: slope (in degrees) raster
Map Algebra Expression: Sin ((slope raster * ((2 * 3.14) / 360)))
Intermediate Output: sediment transport index intermediate raster output #2

3.) *Raster Calculator 3*
Input: sediment transport index intermediate raster output #2
Map Algebra Expression: Power ((sediment transport intermediate raster output #2 / 0.0896), 1.3)
Intermediate Output: sediment transport index intermediate raster output #3

4.) *Raster Calculator 4*
Inputs: sediment transport index intermediate raster output #1, sediment transport index intermediate raster output #3
Map Algebra Expression: sediment transport index intermediate raster output #1 * sediment transport index intermediate output #3
Extent: field polygon shapefile
Output: sediment transport index raster

Statistics Steps

5.) *Zonal Statistics*
Input Raster or Feature Zone Data: field polygon shapefile
Zone Field: FIELD_ID
Input Value Raster: sediment transport index raster
Output Raster: mean sediment transport index raster
Statistics Type: MEAN
Ignore No Data in Calculations: true

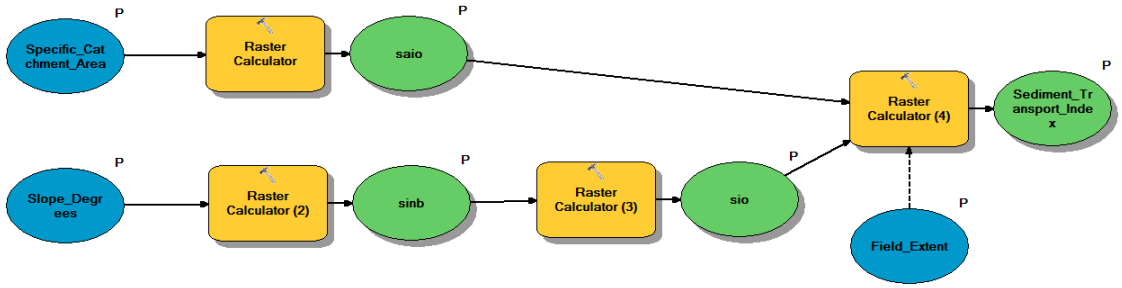

E1. Sediment Transport Index Model

Appendix F: Principle Component Analysis Methodology

SPSS was used to determine the normality of the 6 topographic and soil property variables analyzed in this study, run linear regressions to determine how these variables relate to flow concentration, and to perform a principle component analysis. In the Data View spreadsheet in SPSS the field names were entered in the first column, and then the following variables were entered into subsequent columns for each field: mean specific catchment area, mean runoff source area, mean slope, mean Ksat, mean D, and mean R. In the Variable View, these 6 variables were changed so that "Type" was set to "Numeric" and that "Measure" was set to "Scale."

Testing for Normality

1.) Under the Analyze Menu, select "Descriptive Statistics," and then "Explore." Put all 6 variables in the "Dependent" box. Select "Plots" and check "Normality Plots" and "Histogram." Click "Okay" to both the Plots Submenu and then the Explore Tool.

2.) If the Komogorov-Smirnov number is >0.05, the data values for the given index are normally distributed. If the Komogorov-Smirnov number is <0.05, the data values for the given index are non-parametric. For the non-parametric variables use the following equations to transform the data:

- if the data are moderately skewed to the right: sqrt(X)
- if the data are heavily skewed to the right: log10(X)
- if the data are moderately skewed to the left: sqrt(K-X)
- if the data are heavily skewed to the left: log10(K-X)

where K is a constant from which each value of a variable is subtracted so that the smallest score is 1 (Howell, 2007; Tabachnick and Fidell, 2007). Add these new transformed values of any non-parametric variables to the Data View spreadsheet, in the Variable View change the "Type" to be "Numeric" and the "Measure" to be "Scale," and then repeat step 1.

Linear Regression

1.) Under the Analyze Menu, select "Regression," and then "Linear." In the "Dependent" box put the flow concentration. In the "Independent" box put the mean specific catchment area (or transformation of this variable if applicable). Click "Okay."

The program will output a linear regression that gives an R^2 value for the relationship between the 2 input variables.

2.) Under the Graph Menu, select "Chart Builder." Highlight the "scatter plot" option. Drag and drop the mean specific catchment area (or transformation of this variable if applicable) onto the x-axis. Drag and drop the flow concentration onto the y-axis. Click "Okay." The program will output a scatter plot showing the relationship between these 2 variables.

3.) Repeat steps 1 and 2 with the mean runoff source area, mean slope, mean Ksat, mean D, and mean R instead of the mean specific catchment area.

Principle Component Analysis

1.) Under the Analyze Menu, select "Dimensional Reduction," and then "Factor." In the "Variables" box put the mean specific catchment area, mean runoff source area, mean slope, mean Ksat, mean D, and mean R (or any transformations that were made on these variables). Select "Extraction" and check "Scree Plot." Click "Okay" to close the Extraction Submenu. Select "Score" and check "Save as Variables." Click "Okay" to both the Score Submenu and the Principle Component Analysis Tool. The program will output an Eigen Table that describes the percentage of variance in the data that can be explained by each of the principle components. The program also outputs a Scree plot that depicts how the Eigen values change with increasing components. The program analyzes 6 principle components, but extracts just components 1 and 2. The values of component 1 and component 2 for each of the fields will automatically be added to the Data View spreadsheet in two additional columns. Lastly, the program outputs a Component Matrix, which describes how each of the variables is related to principle component 1 and principle component 2.

2.) Under the Analyze Menu, select "Regression," and then "Linear." In the "Dependent" box put the flow concentration. In the "Independent" box put principle component 1. Click "Okay." The program will output a linear regression that gives an R^2 value for the relationship between principle component 1 (i.e. a new "index") and flow concentration.

3.) Under the Graph Menu, select "Chart Builder." Highlight the "scatter plot" option. Drag and drop component 1 onto the x-axis. Drag and drop the flow concentration onto the y-axis. Click "Okay." The program will output a scatter plot showing the relationship between component 1 and flow concentration.

4.) Repeat steps 2 and 3 using component 2 instead of component 1.

Appendix G: Tests of Normality for Index Variables

Mean Specific Catchment Area

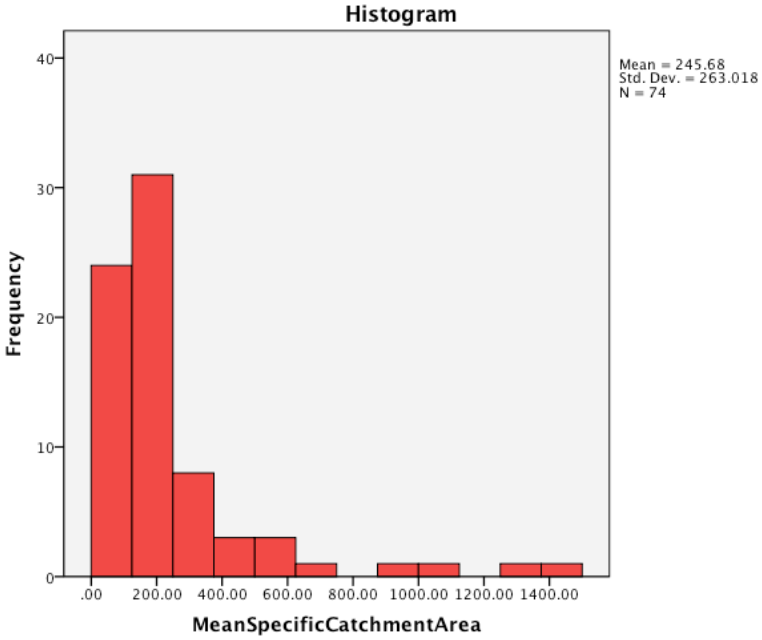

G1. Distribution of values of the mean specific catchment area across the 74 study fields. Kolmogorov-Smirnov = 0.000.

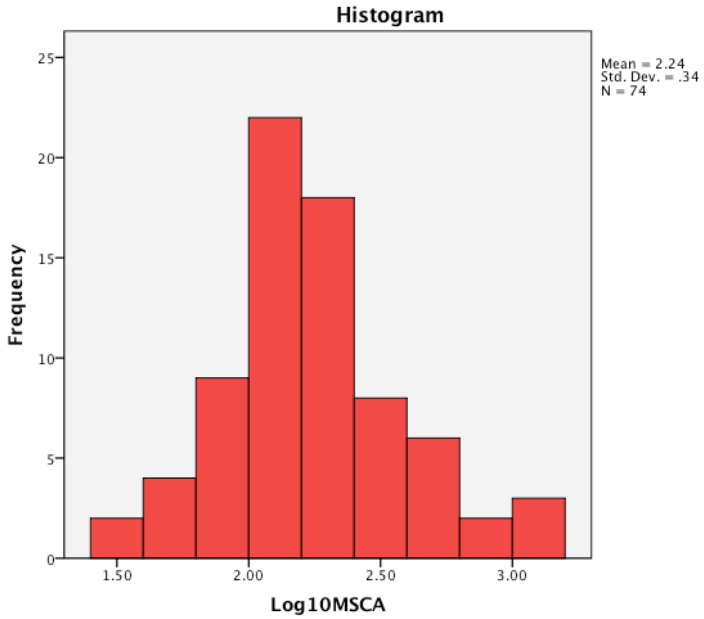

G2. Distribution of values of the mean specific catchment area across the 74 study fields under a log10(X) transformation. Komogorov-Smirnov = 0.044.

Mean Runoff Source Area

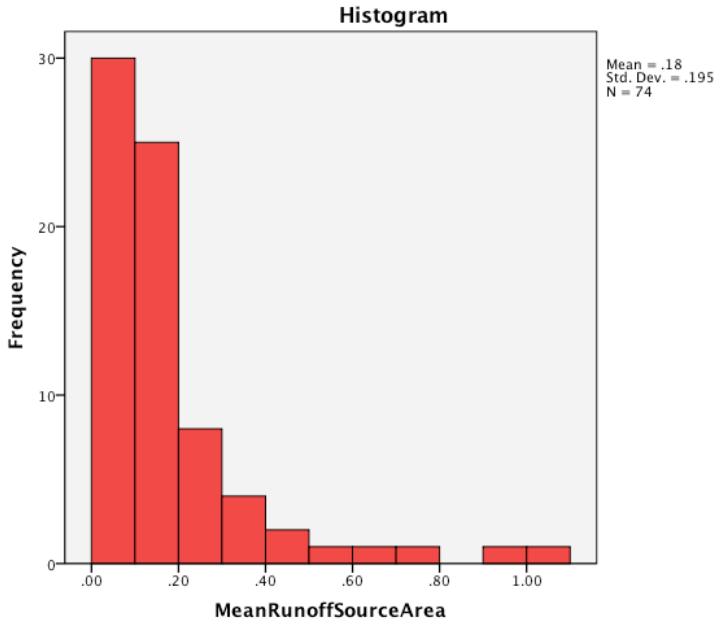

G3. Distribution of values of the mean runoff source area across the 74 study fields. Kolmogorov-Smirnov = 0.000.

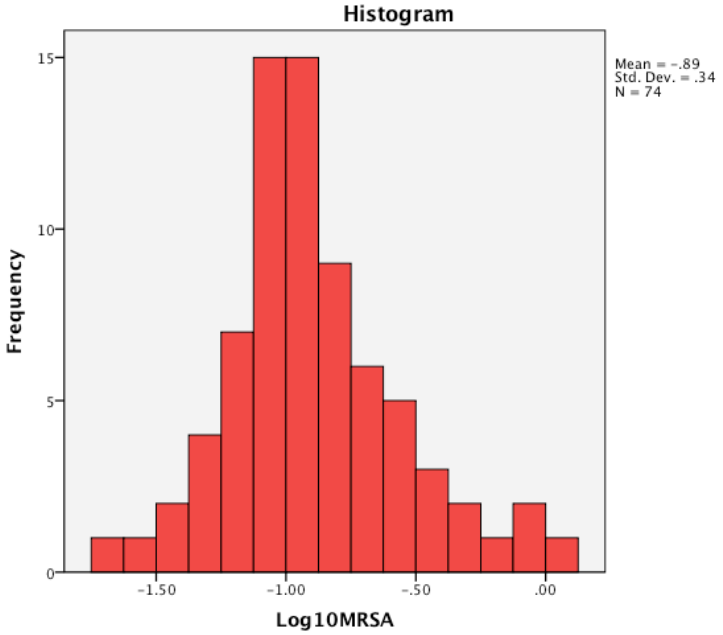

G4. Distribution of values of the mean runoff source area across the 74 study fields under a log10(X) transformation. Komogorov-Smirnov = 0.044.

Mean Slope

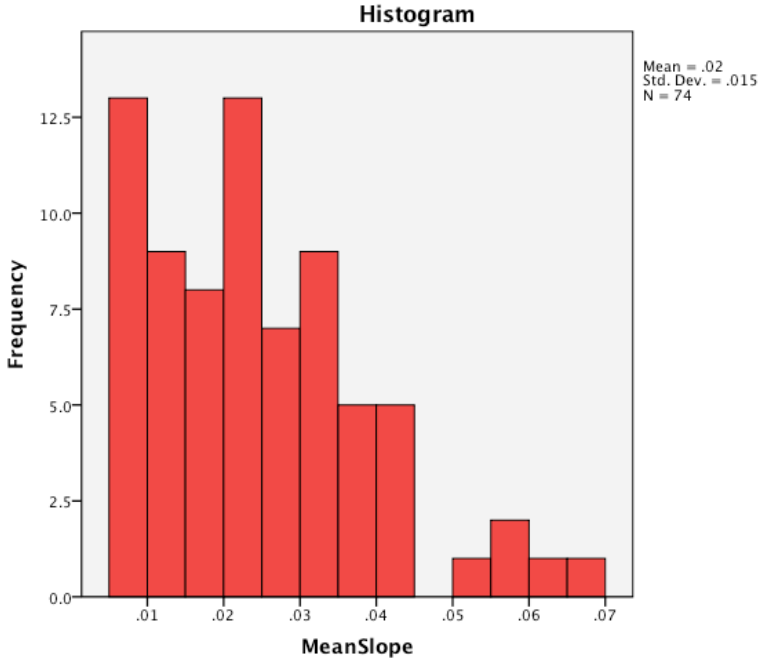

G5. Distribution of values of the mean slope across the 74 study fields. Kolmogorov-Smirnov = 0.174.

Mean Ksat

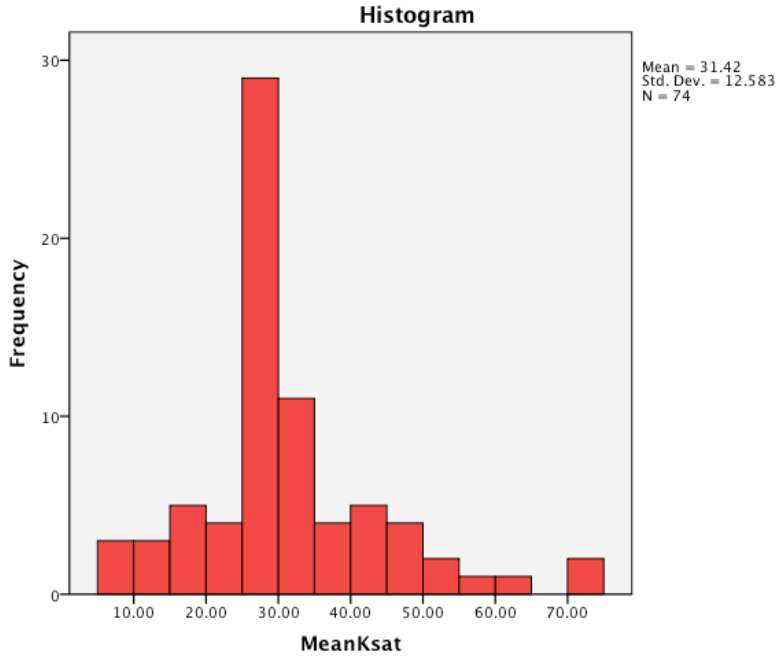

G6. Distribution of values of the mean Ksat across the 74 study fields. Kolmogorov-Smirnov = 0.000.

Mean D

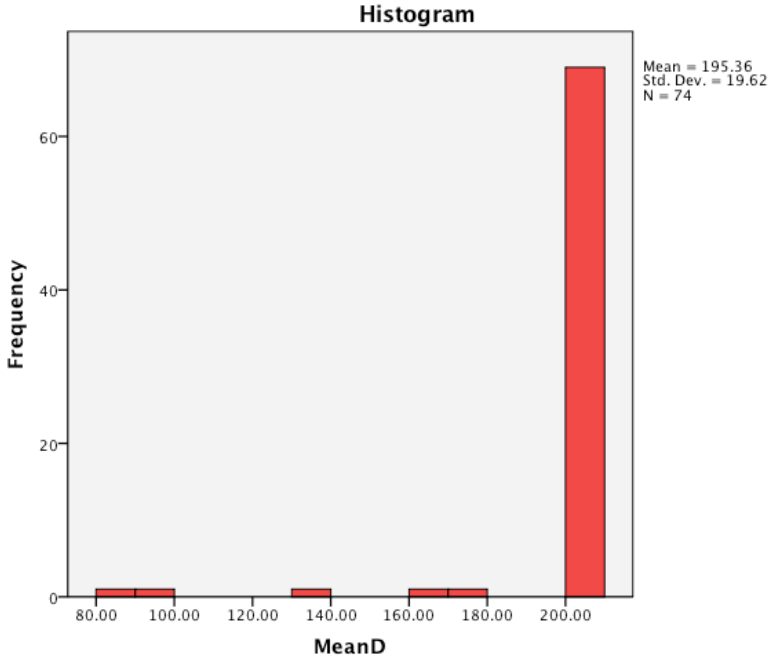

G7. Distribution of values of the mean D across the 74 study fields. Kolmogorov-Smirnov = 0.000.

Mean R

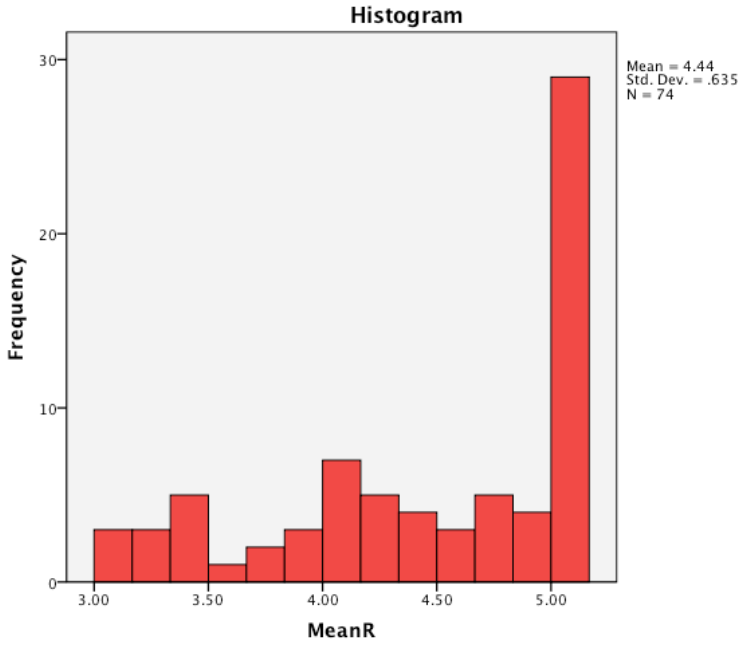

G8. Distribution of values of the mean R across the 74 study fields. Kolmogorov-Smirnov = 0.000.